12-18-2020

Transitions Between Radial and Bipolar Liquid Crystal Drops in the Presence of Novel Surfactants

Jake Shechter
University of Massachusetts Amherst

TRANSITIONS BETWEEN RADIAL AND BIPOLAR LIQUID CRYSTAL DROPS IN THE PRESENCE OF NOVEL SURFACTANTS

A Dissertation Presented

by

JAKE SHECHTER

Submitted to the Graduate School of the
University of Massachusetts Amherst in partial fulfillment
of the requirements for the degree of

DOCTOR OF PHILOSOPHY

September 2020

Physics Department

TRANSITIONS BETWEEN RADIAL AND BIPOLAR LIQUID CRYSTAL DROPS IN THE PRESENCE OF NOVEL SURFACTANTS

A Dissertation Presented

by

JAKE SHECHTER

Approved as to style and content by:

Jennifer L. Ross, Chair

Christian Santangelo, Member

Anthony Dinsmore, Member

S. Thayumanavan, Member

Narayanan Menon, Department Chair
Physics Department

ACKNOWLEDGMENTS

I am not good at this, so I apologize for the awkwardness here.

First, I have to thank my family for their love and support. Their encouragement and excitement have reminded so many times that I can do this. I wouldn't have made it this far without them. Specifically, I thank Sara for her unwavering love and support on a daily basis. I must also thank my friends, old and new, who have helped keep me sane during the last six years when things got intense.

Taki Stanhope was the lab manager when I joined the Ross lab. She trained me in the most basic of lab skills, like how to use a pipette, from day 1 and was a great mentor.

Vikrant Yadav and Peker Milas were two post-docs in the lab when I joined. Peker trained me on how to use the microscope and taught me some more advanced optics and was a good role model for documenting lab work. Vikrant was very helpful with theoretical calculations and teaching me general cool physics things.

Ben Strain and Linda Oster were undergraduate physics majors in the lab that worked with me very closely from 2017-2020. They're both incredibly talented and hard working students and this work wouldn't have been possible without their help. Of the 4 main projects discussed later, they are each the main person for one. Those projects are mostly their work and I only mentored them as needed. Ben has already graduated and is starting graduate school at Brandeis in Fall 2020. Linda is starting her senior year at UMass Amherst in the fall.

Jessica Sleator was a post-bac student from Springfield University who worked in the lab for the summer of 2018. Jess was absolutely fantastic at organizational

management and made the first version of our data organization method that we still use.

Kelsey Weeden was a high school student who also worked in the lab during the summer of 2018. She designed and 3D printed a very specific tool that could be used to make the experimental chamber construction much easier. This tool has been a great time saver and also saved my eyes and shoulders from getting sore.

This work was funded through a MURI grant and I've had lots of help and support from that whole team. In particular, Noe Canas, Ali Mozaffari, and Rui Zhang were post-docs in Juan de Pablo's group from University of Chicago that did almost all of the theory work in this dissertation. Their work is shown in Chapter 4 (project 1) which was published in our paper. I also thank Manisha Chahar, Uma Sridhar, and Thameez Mohammed Koyasseril Yehiya from the Thayumanavan lab in the University of Massachusetts Amherst Chemistry department for their work synthesizing the novel surfactants used in this dissertation and managing orders of lab supplies.

Special thanks to my committee members, Dr. Thayumanavan, Dr. Dinsmore, and Dr. Santangelo, for their advice and knowledge these past several years. Their suggestions for experiments to try and techniques to use have made this work possible.

Lastly, but certainly not least, thank you to Dr. Ross for everything. Dr. Ross has provided excellent guidance, support, mentoring, and has been an amazing role model. I can't describe how thankful I am that I was lucky enough to be part of her lab. She is truly inspirational.

ABSTRACT

TRANSITIONS BETWEEN RADIAL AND BIPOLAR LIQUID CRYSTAL DROPS IN THE PRESENCE OF NOVEL SURFACTANTS

SEPTEMBER 2020

JAKE SHECHTER

B.Sc., ROCHESTER INSTITUTE OF TECHNOLOGY

Ph.D., UNIVERSITY OF MASSACHUSETTS AMHERST

Directed by: Professor Jennifer L. Ross

Liquid crystals (LCs) are a class of molecules that form a variety of configurations easily influenced by external interactions. Of particular interest are rod-like LC molecules confined to a spherical geometry, which have a competition between interfacial tension and elastic deformations. The configuration of the liquid crystal inside a droplet can be controlled using surfactants, influencing the boundary conditions, in an oil-in-water emulsion. I tested the effects of novel surfactants on the configuration of the LC droplets. These novel surfactant molecules, synthesized by collaborators, are oligomers with either a variable length hydrophobic domain or protein sensitive hydrophilic domain. I tested the equilibrium configuration and dynamics of configurational changes, comparing experimental results to simulations performed by collaborators. We find that configuration transitions can be triggered by the addition of a control surfactant, sodium dodecyl sulfate (SDS), but not the novel surfactants. The SDS concentration at which the phase transition occurs appears to depend on the

droplet diameter and I observed a hysteresis in the SDS concentration of the phase transition, both of which depend on the novel surfactant present.

CONTENTS

LIST OF TABLES

Table **Page**

LIST OF FIGURES

Figure **Page**

CHAPTER 1

SO YOU WANT TO STUDY LCS...

This first chapter of the book is to introduce the reader to most of the jargon that will be used in the following chapters. A "jargon" term is a term that has a very specific meaning that everyone in the field would understand, but those outside the field would not. For example, if I were to ask an outsider to sketch a "radial" liquid crystal droplet, they would probably be confused. I'll introduce the terms in the way that I would for a new lab member. Since this topic is not part of a core undergraduate, or even graduate, physics curriculum I keep my assumptions of background knowledge to a minimum. Someone familiar with liquid crystals can skip this chapter and not lose anything. The traditional format for a dissertation, which starts with an introduction to the field, begins with the next chapter.

1.1 What's in a name?

Welcome! Sometimes things are named really well. For example, a "mail box" is literally a box for the mail. It is the perfect name! Liquid crystals (LCs) are another great example of something named well. Liquid crystals are a type of molecule that have both "liquid" and "crystal" properties, hence the name. Let's break it down.

The term "liquid" is exactly what you think. A liquid is something that flows. By flow we mean that the molecules that make up the liquid can move around each other freely. To say it another way, each molecule can move around in the whole volume and there is no preferred location or orientation of any individual molecule. At a macroscopic level, a liquid is something that doesn't resist a shear stress applied

to it. Instead of resisting, a liquid flows in the direction of the shear. A "shear stress" is a type of force that causes things to slide past each other parallel to the direction of the force. If you have a stack of paper, lay your hand on top and push sideways, it'll fall over as the papers slide parallel to the way you push. That is an example of shear. If you have a bucket of water, lay your hand on top of the water and move your hand sideways. The water doesn't move with your hand, because it's liquid!

When people typically think of crystals they imagine a solid object, like diamond. In physics the term "crystal" refers to a periodic order or periodic structure in something. This definition does include diamonds and other familiar crystals, but is not limited to atoms! In chemistry and solid state physics, a repeating pattern of atoms is a crystal. This is an example of crystallinity in the positional ordering of those atoms. We can extend this definition beyond point particles to objects that have approximately two dimensional shape. Examples of such extended objects include rods, disks, or banana-shaped objects. Rods aligned in the same direction (figure 1.1 a), stacked disks (figure 1.1 b), or spooning bananas (figure 1.1 c) are examples of 2-D crystalline order.

So, how do you reconcile these two terms together to define a "liquid crystal"? The key is that the 2-D crystalline order described above and the positional freedom of liquid molecules can coexist. Since all liquid crystal molecules have some sort of extended shape, they also have 2-D crystalline ordering. In my work I use a rod-like molecule called 5CB. A macroscopic analogy for a rod-like liquid crystal is a pencil. If you put many pencils in a box together, they will naturally align in the same direction (2-D crystal order) but they're still free to slide along each other or roll around (act like a liquid) without losing their 2-D crystal ordering (figure 1.3).

I would be remiss if I didn't mention briefly some other types of liquid crystal molecules. There are some cool liquid crystals that form chiral structures. Chiral means spiral and I remember that because they rhyme. Specifically, the blue phase

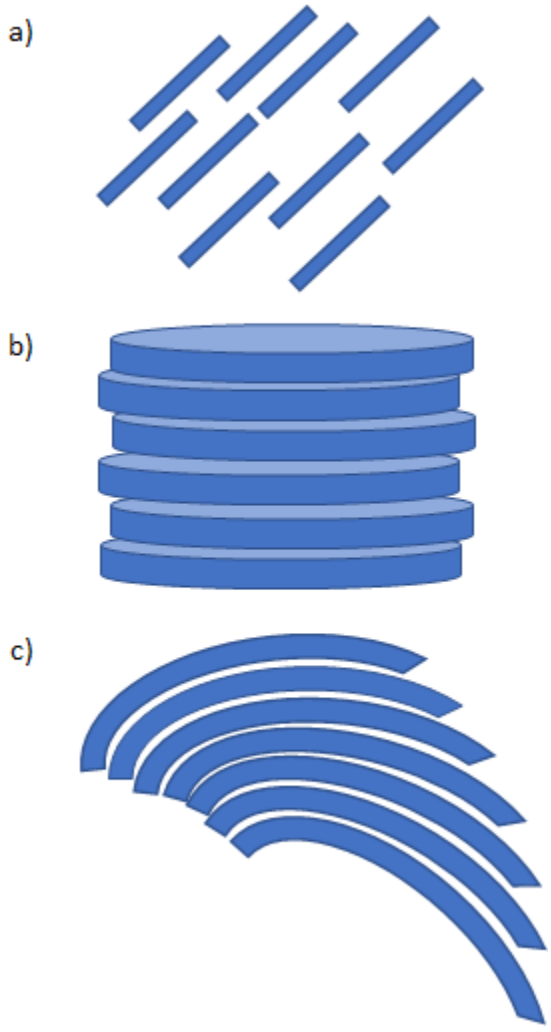

Figure 1.1. Schematic of different shaped objects that can behave like a liquid crystal. (a) rod-like, (b) disk, (c) bent core (banana).

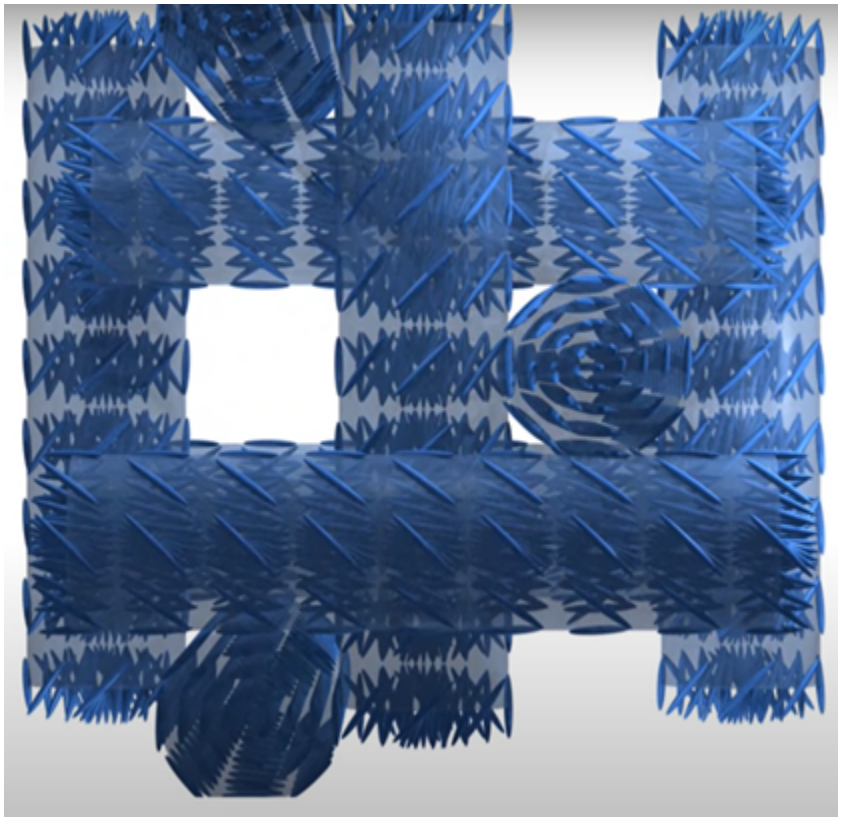

Figure 1.2. Screen shot at 0:22 seconds of Hiroyuki Yoshida's YouTube video posted April 10, 2014. https://youtu.be/NJG14FdcWkg?t=22

is beautifully confusing (figure 1.2). You can find a cool video showing the structure on youtube from Hiroyuki Yoshida on April 10, 2014 (https://www.youtube.com/watch?v=NJG14FdcWkg). Recently, some molecules that are achiral (not chiral) have been found to form chiral structures [21]! There are many different chiral liquid crystal phases. There is another classification of liquid crystal molecules that have disk-like molecular shapes. These tend to have the vectors normal to the plane of the disk align, which can result in stacks of disks (figure 1.1 b). These stacks of disks can then pack parallel to each other like piles of plates [**?**].

1.2 Phases of liquid crystal

To recap, we are focusing on rod-like molecules that have crystalline order when they're aligned with one another (figure 1.1 a) while the individual molecules have liquid mobility. In actuality, this isn't always the case for 5CB, the liquid crystal used in this work. Sorry!

What do I mean? Let's go back to the pencils in a box example. I assumed that the box was just sitting on a table (figure 1.3 a). What would happen if we put the box of pencils on a vibrating platform? We would see the pencils move around each other a little bit and stay aligned (figure 1.3 b). Ok, fine, that is consistent with everything so far. But, what if we cranked up the vibrations to simulate an earthquake? As you might imagine, the pencils will bounce around everywhere and there will be no order whatsoever (figure 1.3 c). The orientational order is gone, so does that mean that the collection of pencils are no longer a liquid crystal? Yes! The collection of pencils are no longer in their liquid crystal state of matter. This is analogous to adding lots of heat to water and turning it into a vapor. It is no longer water because it is no longer in the liquid state of matter.

This is a macroscopic analogy for what is happening at the microscopic level. If our rod-like molecules are only about 1.5 nm long, then thermal fluctuations are like our vibrating table. Recall that a nanometer is *really* small. How small? Imagine cutting a millimeter, one *thousandth* of a meter, into one thousand pieces. Take one of those pieces and cut that into another one thousand pieces. That's a nanometer, one *billionth* of a meter. At high temperature it is like an earthquake and any orientational order is lost. At low temperature we have order. What is high and low depends on the specific liquid crystal used. For the liquid crystal we use, 5CB, this transition is at 35 °C. Above 35 °C the liquid crystal is in the "isotropic" phase, meaning there is no positional or orientational order (figure 1.3 c). At room temperature, 23 °C, well below the transition point, 5CB is in the "nematic" phase and has orientational order

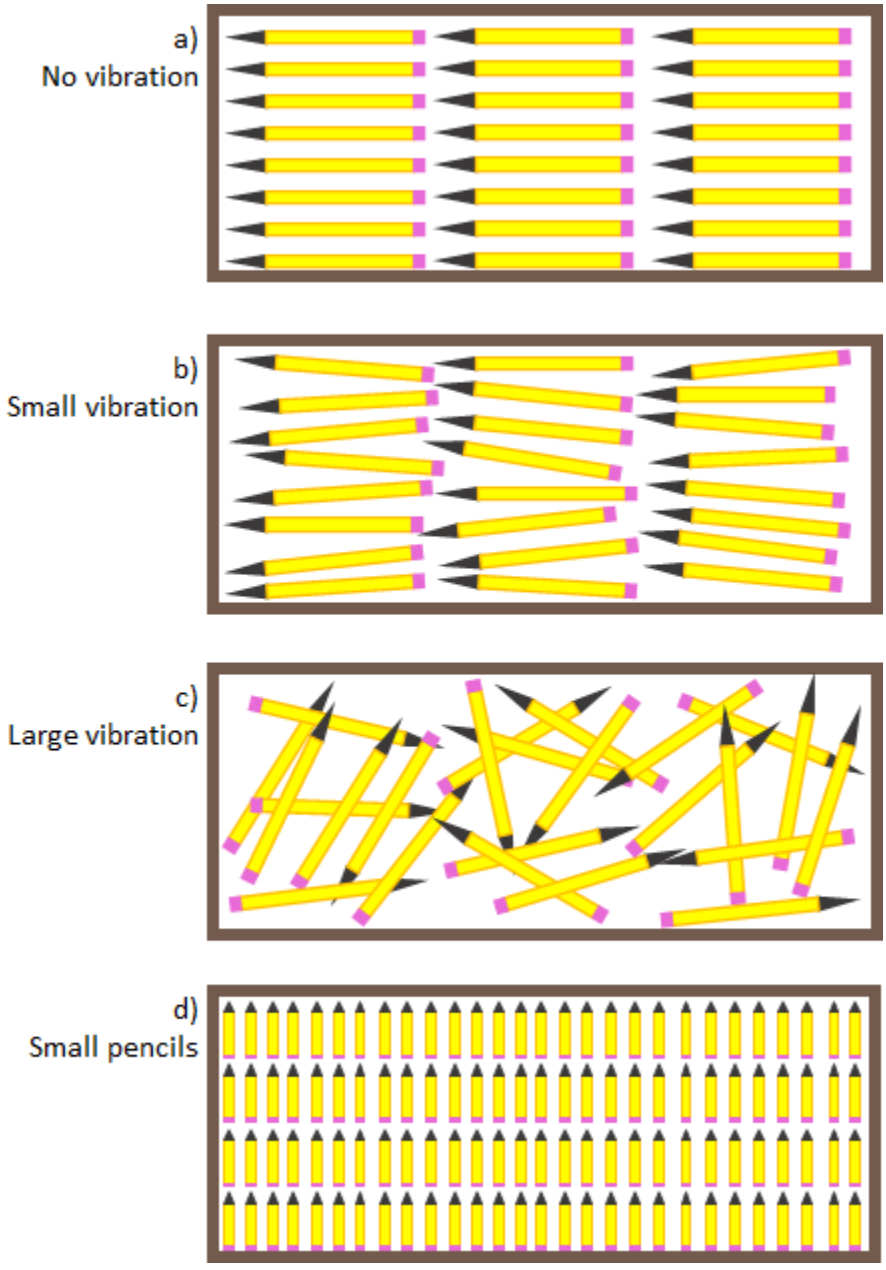

Figure 1.3. Cartoon showing ordering of pencils in a box under different conditions. (a) no vibrations, (b) small vibrations, (c) large vibrations. This is analogous to a liquid crystal system at zero temperature, room temperature, and high temperature respectively. (d) small pencils can align perpendicular to box length.

(crystalline, figure 1.3 b). The nematic phase of liquid crystals is where interesting things happen. The liquid crytal 5CB is very commonly used because it is in the nematic phase at room temperature.

Due to artistic constraints, the ordering shown in figure 1.3 a, b, and d is actually a type of *smectic* ordering. The smectic configuration is when the liquid crystals are in distinct layers. An example of true nematic ordering is in figure 1.1 a. A nematic ordering has a random distribution of the centers of each molecule.

Liquid crystals that have a phase transition as a function of temperature are called thermotropic liquid crystals. There is another type of liquid crystal, called lyotropic, that has a nematic-isotropic transition at a certain concentration (like a packing fraction) instead of temperature. The packing fraction is the volume occupied by the molecules divided by the total volume in the system, which is directly related to the molar concentration of the molecule.

Note that this temperature transition of 5CB only affects the orientational order. At 140-150 °C 5CB boils and evaporates. There is no data for the freezing temperature [1]. These are phases of matter and not crystal phases.

1.3 Geometry of the project

Up until now I've been using the pencils in a box analogy for rod like molecules. If I were to ask you how to pack pencils space-efficiently in a rectangular geometry, you would immediately align all the pencils with one wall and fill in, like in figure 1.3 a. If the pencils are much smaller than the size of the box, you don't even have to align the length of the pencil along the length of the box (figure 1.3 d)!

What if I asked you to pack pencils into a circular container? Let's start with 2D. If you were to align all the pencils in one direction and fill inwards, you'd have a lot of open space where there are no pencils because the curvature of the circle is too tight to fit another pencil. Even with smaller and smaller pencils, this "dead

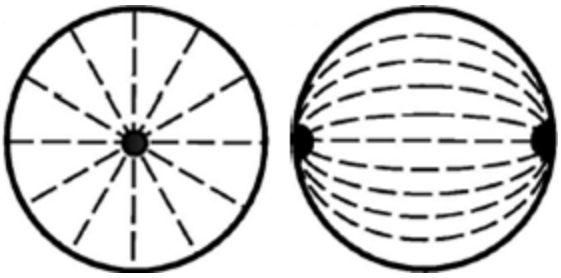

Figure 1.4. Cartoon of pencils packed into a large circular container with pencils perpendicular to the edge (left) or parallel to the edge (right). Each dashed line can be thought of as a single pencil.

space" would remain; it would just get smaller and smaller too. So what is the best strategy? There are two strong options. Just as with the rectangular box, we should consider the boundaries of our circle. What if we arrange the pencils such that each one is perpendicular to the edge? What about parallel to the edge?

If all the pencils are perpendicular to the edge, then we'll get something that looks like the spokes of a bicycle wheel (figure 1.4 left). I almost said wagon wheel, but come on, when was the last time you saw a wagon? I wonder what type of wheel people will use to describe this in 100 years. Regardless of the type of wheel you consider, this arrangement of spoke-like liquid crystal molecules is called the "radial" configuration because everything is pointing radially inward from the edge. With an appropriately sized pencil, you would only be left with a small area in the very center that is empty. This region that is left empty is called a "defect" in the liquid crystal order. A "defect" is a place where the local ordering of the liquid crystal can not be defined.

Alternatively, If you align the pencils parallel to the edge, then you get what is called the bipolar configuration. This is because there are two points on the surface, at opposite poles, where the pencils meet up and again there is a small empty space (figure 1.4 right), which is again a "defect". Both of these options are clearly better than aligning all the pencils in the same direction within a circle.

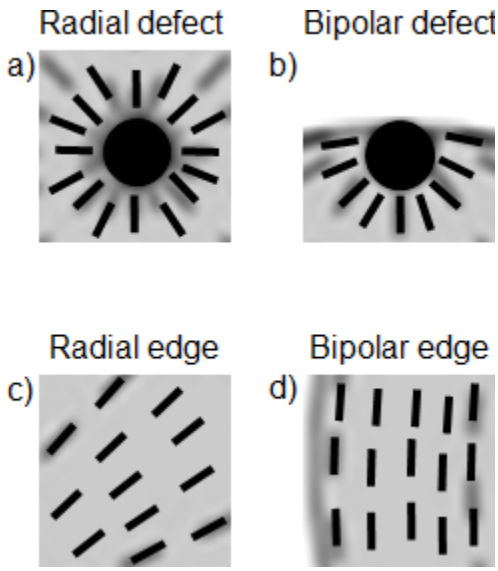

Figure 1.5. Close up of four regions from the figure 1.4 cartoon. The (a) radial defect and (b) bipolar defect are shown with extra lines for clarity. The (c) edge of the radial and (d) bipolar configurations are shown with added lines.

1.3.1 Topological defects

Let us talk more about defects. For the radial configuration, notice that at the center of the wheel, where all the pencils meet up, there is no local order. We call this a topological defect. When I say there is no local order I mean that if you were standing at any point in the circle that is not the center and looked immediately around you, everything is pointing in the same direction (figure 1.5 c). If you were to go the center and look around you, nothing is pointing in the same direction (figure 1.5 a)!

The bipolar configuration actually has two defects, one at each pole. If you zoom in on a small region of the circle that is not one of the poles, you would see local alignment just as in the radial configuration (figure 1.5 d). At either pole, however, there is no such local alignment (figure 1.5 b).

So, was there a topological defect somewhere in the rectangular box? As it turns out, there wasn't! The presence or absence of such defects is based on the geometry of the system. In a rectangular confinement, rod like LC molecules do not have to

have a defect. In a circular confinement, rod like LC molecules must have at least one defect.

These defects also have a "charge" associated with them. It is not an electrical charge, but because there are "positive" and "negative" defects and they cancel each other out if they combine, we think of it similar to charge. This is an example of a not-so-good naming, but it is not bad. The worst name of anything is the "z-scheme" of photosynthesis, which I learned about in 12th grade AP Biology. It got its name because the energy pattern looks like a sideways Z. A sideways Z is like an upright N. Why didn't they call it the "N-scheme"? Who knows. Maybe they forgot about capital letters. I digress.

These defects have charge, and they also have magnitude. The magnitude and sign of the defect is determined by considering a loop around the defect and measuring the rotation of the "director" field. The "director" is a dimensionless unit vector, $\hat{n}$, that points along the direction of an individual liquid crystal molecule. If you have an area with many liquid crystal molecules inside, you can imagine a sea of these tiny arrows filling your space. In figure 1.7 a-d the liquid crystal molecules immediately around a defect are colored. The red region of each individual molecule can be imagined as the "head" of the director vector and the blue region the "tail" of the director vector.

Imagine you walk clockwise along this loop around the defect (2π radians $= 360°$). Since we are walking around a defect, the director is going to change orientation as you walk around this small area. If the director is also rotating clockwise as you walk, the defect is "positive" (figure 1.7 a-b). If the director is rotating counterclockwise as you walk, then the defect is "negative" (figure 1.7 c-d). The magnitude comes from what fraction of a full rotation the director made when you get back to the start. So, a "+1" topological defect has the director rotate clockwise a full rotation in a complete clockwise walk (figure 1.7 a). A "-1/2" topological defect has the director rotate counterclockwise only π radians in a complete clockwise walk (figure 1.7 d).

Figure 1.6. Example fingerprint with a +1/2 defect circled in blue (left) and a -1/2 defect squared in red (right).

A macroscopic example of topological defects +1/2 and -1/2 are in your fingerprints! See if you can find some on your own fingers! A random fake fingerprint online shows an example of one +1/2 defect (figure 1.6, left) and one -1/2 defect (figure 1.6, right). Schematics of some topological defects can be seen in figure 1.7.

It is worth mentioning that topological charges have to be half or whole integers. This is because there can not be a discontinuity in the director when you complete the full loop. From the geometric symmetry of our liquid crystal, $\hat{n}$ and $-\hat{n}$ are the same. This means that a half rotation is as small as you can get. For example, suppose a "+1/4" topological charge existed. This would mean that after a 2π loop around the defect the director has rotated only $1/2\pi$ radians. This would mean the liquid crystal at the start of the loop is simultaneously vertical and horizontal, which it clearly can not be.

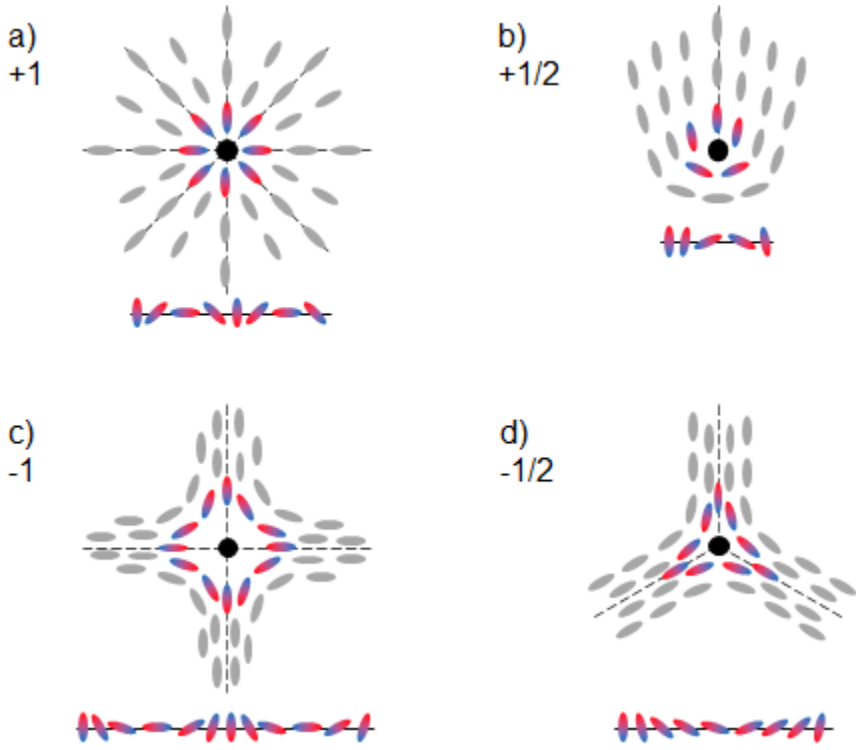

Figure 1.7. Schematics of four topological defects: (a) +1, (b) +1/2, (c) -1, and (d) -1/2. Beneath each defect is a visual aid for determining the charge of each. The first molecule is always the one directly above the defect represented by a black dot. Going clockwise around the defect, the molecules along the circular path are laid out in a line to illustrate the rotation more clearly. From one molecule to the next, the rotation is clockwise in (a) and (b), meaning it is a positive topological charge. For (c) and (d) the rotation of each step is counter clockwise, meaning it is a negative topological charge.

In the rectangular confinement, there was no defect so there is a charge of 0. Like electric charge, topological charge is conserved. In the rectangular confinement, the total charge has to be 0. What if I manually rearrange some of the pencils in the box into a "radial" formation and then try to pack the rest of the rectangle as much as I could, keeping in mind the parallel boundary conditions at the edge. Due to the conservation of topological charge, by introducing this "+1" charge (radial defect) into the box, I *must* have also created a "-1" (or two -1/2s) to balance out the positive charge and maintain a net charge of 0.

In the case of the circular confinement we have to maintain a net topological charge of +1. In the radial configuration this is satisfied by the single defect at the center. In the bipolar configuration we have two +1/2 defects. If we were to manually introduce an additional negative defect somewhere we would also have to create additional positive defects somewhere to balance the net charge back to +1.

1.4 Three dimensions

Up until now we have been confined (pun intended) to two dimensions. Let us move up to three dimensions. The ideas still apply and the two dimensional configurations easily transfer to three dimensions. There will be additional possible configurations, however.

For the two dimensional radial configuration, imagine a line through the diameter of the circle. Rotate the shape around that axis and you have a three dimensional radial droplet (figure 1.8 a).

For the two dimensional bipolar configuration, again draw a line through the diameter, but this one has to pass through both poles. Rotate around the axis through both poles and you have a three dimensional bipolar droplet (figure 1.8 b).

A third type of droplet configuration that I observed in my experiments is a monopolar structure. As the name suggests, this type of droplet has only one pole.

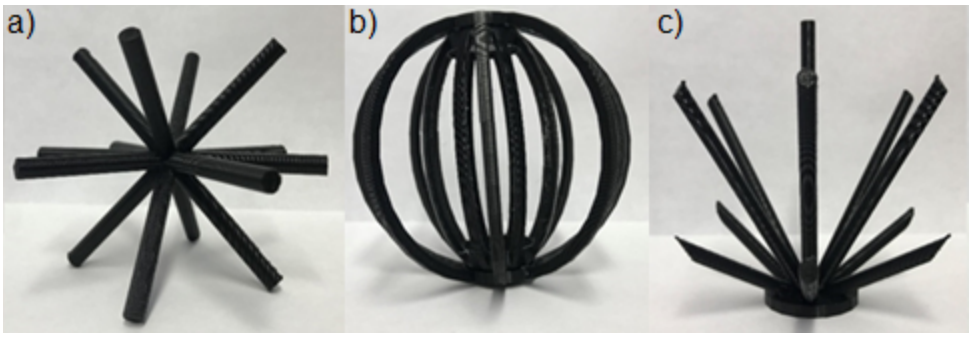

Figure 1.8. Printed models of the (a) radial, (b) bipolar, and (c) monopolar structures. The monopolar structure shown is of the "sunset" subtype.

Due to varying boundary conditions along the droplets surface a second pole does not form at the other end (figure 1.8 c). There are a few ways a monopolar structure can manifest and for my work we do not distinguish between these. I refer to all types of monopolar configurations as "monopolar".

Ben Strain, an undergraduate physics major in the lab, while working on his thesis, designed and printed 3-d models of each of these structures (figure 1.8 a-c).

1.5 Boundary conditions

What decides whether a liquid droplet will be in the bipolar, radial, or monopolar configuration? The answer is based on the surface conditions. If you add an oily liquid crystal to a water based buffer the liquid crystal will separate like oil in water. The droplets that form will be in the bipolar configuration. Without any molecule at the interface between the liquid crystal and water, the LC molecules prefer to align parallel to the interface resulting in the bipolar configuration. This is true of 5CB, but might not be true of other LCs!

1.5.1 Surfactants

To get a LC droplet to form a radial or monopolar structure you need to something that will change the boundary conditions of the droplet. Imagine you live at the end

of a street with a a cul-de-sac and invite a lot of people over but they can not park in your driveway because it is being paved. How does everyone park? A common solution is to park parallel to the edge of the cul-de-sac and form a head-to-tail chain of cars all the way around. This is like the bipolar droplet in figure 1.4, right. Now, what if some demon painted parking space lines that were *perpendicular* to the curb, so that everyone parks facing a house. This is like the radial configuration in figure 1.4, left. In our experiments we can not paint lines to tell the liquid crystal which way to align, but we *can* influence alignment with surfactant molecules.

A surfactant molecule is an "amphiphilic" molecule that is used to stabilize an emulsion. An amphiphilic molecule has regions that are hydrophobic (dislikes water, likes oil) and regions that are hydrophilic (likes water). Surfactants are also commonly found in everyday products, like hand soap, dish soap, and shampoo. Surfactants make good cleaning products because of their amphiphilic nature and the fact that things we want to wash off (dirt) are hydrophobic. What happens is the hydrophobic ends of the soap surrounds the dirt so that the *hydrophilic* ends are exposed to the water. Then when you rinse off your hands the water carries away the surfactant covered dirt.

For my system, "oil" refers to the liquid crystal and "water" refers to the water-based surfactant background solution. Due to the dual preferences of the surfactant, it is energetically favorable to have them at the interface of oil and water. For us, this is the surface of the liquid crystal droplet. Where the hydrophilic groups can be in the water background, while the hydrophobic groups can be in the LC droplet.

When you add surfactant or an emulsion, you can change the boundary conditions which will change the internal configuration of the liquid crystal. The surfactant molecule is also responsible for keeping the droplets stable so that if two get close to each other they do not merge into one larger droplet. The fact that you can do something at the surface and get a change through the whole bulk of the droplet,

and not just right inside the surface, is why LCs are interesting and useful in general. I'll discuss the specifics of each surfactant molecule when I get to that particular experiment.

1.5.2 Surface Anchoring

The previous section of surfactants talked a lot about how we can change the boundary conditions using a surfactant. This can also be talked about as "surface anchoring" of the liquid crystal molecules. For a radial droplet (high surfactant concentration) we can say that the surface anchoring of the liquid crystal is strongly perpendicular. For a bipolar droplet, the surface anchoring of the liquid crystal is strongly parallel. These surface anchoring conditions are related to the concentration of surfactant at the surface of the droplet. In this work we always control the surface anchoring by controlling the concentration of surfactants.

Another example of surface anchoring is used in liquid crystal displays (LCDs). In a pixel of an LCD, the two surfaces are treated so that they have a strongly parallel surface anchoring. This causes the liquid crystal to be parallel to each surface the same way that the surfactants cause the liquid crystal to be parallel (or perpendicular) based on the concentration.

This idea of surface anchoring will come up in the theory section of Chapter 4 (project 1). We will see that a strong anchoring strength is not always sufficient to cause a transition by itself.

1.5.3 Emulsions

We still have an important question to ask. *How* do make these droplets of liquid crystal? In general, when you add two liquids together that do not mix, you form an emulsion. Emulsions are common in every day life. Some examples of emulsions are: milk, paint, blood, butter, salad dressing, and whipped cream. In my work the two liquids are a water based surfactant solution and 5CB (our liquid crystal). If

you add these two together, you have not made a very good emulsion because the two components are still fully intact. Next time you go grocery shopping, find the salad dressing section and look at the Italian ones. They're an emulsion and also completely separated. When you want to use the salad dressing you first have to shake the bottle to mix it up, and we have to do the same thing with our 5CB and water based surfactant system. Since we use such a small volume at once, we can flick the tube and cause the one large 5CB drop to break up into many tiny 5CB droplets. We do not need any complicated mixing equipment that you might find in an industrial paint factory.

1.6 Optics

We have built up some knowledge now about what liquid crystals are, the geometry of the system we study, and what the liquid crystal looks like inside a few different droplet configurations. I mentioned before that each liquid crystal molecule is only 1.5 nm long. This is too small to see with your bare eye or even with a typical microscope. So, how can we tell the configuration of any droplet in the sample? The answer is that we have to use a special type of microscopy called "polarizing optical microscopy" (POM). A schematic of the optical set-up with the light path is shown in figure 1.10.

Polarizing optical microscopy works by having a pair of polarizing filters. One polarizer (called the Polarizer) is placed after the microscope's lamp so that polarized light illuminates the sample. The second polarizer (called the Analyzer), oriented perpendicular to the Polarizer, is between the objective and camera (figure 1.9 a, top two). If there was no sample on the mircoscope, then the Analyzer will block all the light coming from the Polarizer (figure 1.9 b, red square). The camera would see nothing at all— just a black image. The only way for light to get through the

Analyzer and to the camera is if there is something between the polarizers that rotates the polarization (figure 1.9 c, blue triangle).

Fortunately for us, 5CB does exactly that. This property is called birefringence (another good name), because there are two (bi) indecies of refraction for the molecule. One is for light travelling along the length of the molecule and the second is for light traveling perpendicular to the molecule. So, when, let us say vertically polarized light, comes in through the polarizer and hits an angled 5CB molecule, this difference in indecies of refraction manifest themselves in differences in the speed of light for the parallel component and perpendicular components (with respect to the molecule orientation) of the light. This difference in speeds causes the polarization to rotate (called a phase shift).

What this means is that each 5CB molecule acts as a tiny polarizer in the direction of its director. A liquid crystal droplet would then be many of these tiny polarizers acting together. Since the director is in different directions in different parts of the droplet, we will get different amounts of light passing all the way to the camera.

So, the take-away is that if the 5CB is aligned either vertically or horizontally (the direction of the polarizer and analyzer) then the camera will not detect any light and will appear dark. If the 5CB is not perfectly horizontal or vertical, some light will get through. The maximum light is allowed through if the 5CB is perfectly 45 degrees, and gets less as the angle approaches 0 to 90.

All of this polarization stuff might sound very fancy, but just like emulsions polarizers are common in everyday life. Windshields on cars and sunglasses are polarized to prevent glares. Since most glares come from light bouncing off something on the ground, resulting in horizontally polarized light, windshields and sunglasses are vertical polarizers to block out all the glares. Another use of polarizers is in 3D glasses. Fun fact, they used to make 3D glasses with one eye being vertically polarized and other other eye being horizontally polarized. Then people would watch movies and

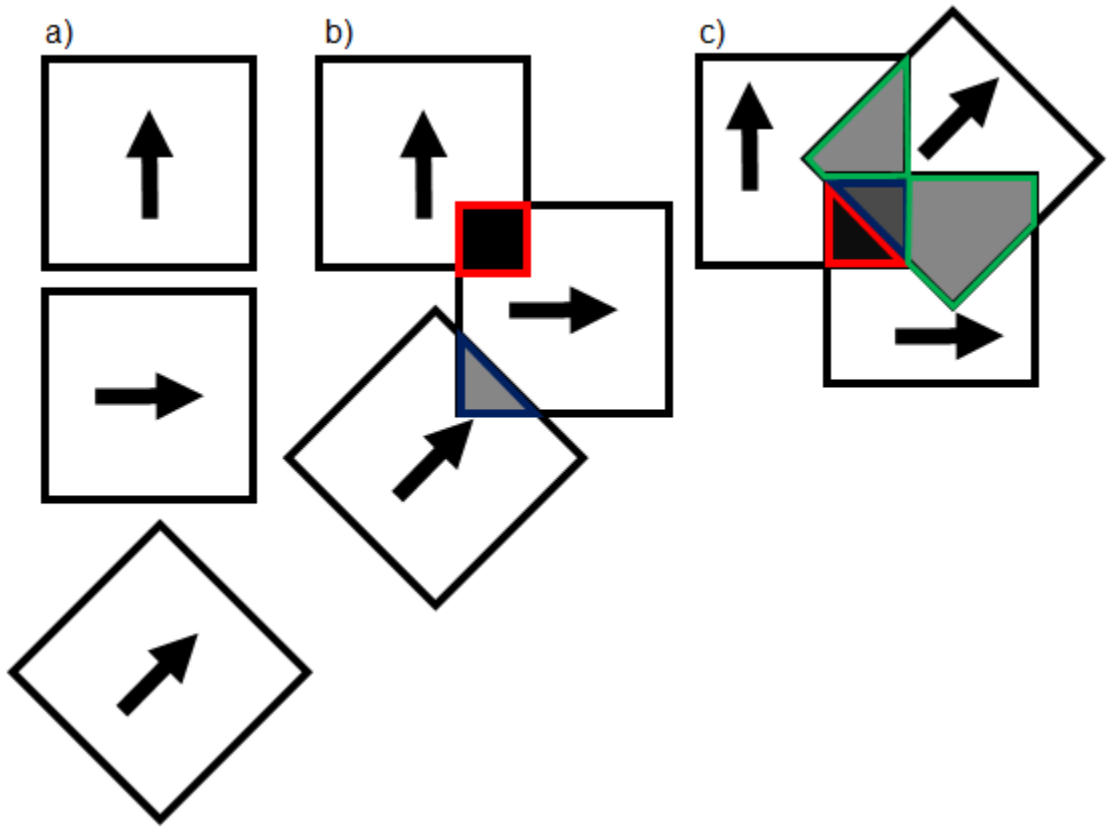

Figure 1.9. Cartoon of polarizing filters in various levels of ordering. The direction of each polarizer is shown with a black arrow. (a) When a polarizer is by itself, all light gets through no matter the orientation of the polarizer. (b) When you overlay two polarizers that are perpendicular to each other, all light passing through the cross section (red square) is blocked and appears black. If the polarizers are overlaid but *not* perpendicular (blue triangle), then only some light is blocked and appears grey. (c) If you put the polarizer that is at an angle between the two that are perpendicular (blue triangle), all of the light is no longer blocked and we see dark grey. The region that the intermediate rotated polarizer does not cover (red triangle) is still black. The green areas are where some light passes through and we see grey.

rest their head on their hand, rotating their head, and some of the light would get crossed (figure 1.9 c) and give people headaches! Now they use *circularly* polarized light, clockwise and counter clockwise, which does not depend on the orientation of your head.

1.6.1 Machine Learning for analysis

Over the course of the past few years Ben, Linda (another undergraduate physics major in the lab), and I have gotten really good at characterizing liquid crystal droplets based on their optical patterns. I am going to try my best to impart you, the reader, with the necessary tools to become proficient. The skill of characterizing droplets is something that will take literally hundreds of droplets to become proficient. Human brains are surprisingly good at image processing. I can teach you how to identify different droplet configurations in an afternoon. To teach a computer is much harder. The subject of machine learning applied to classifying liquid crystal droplets is something that is a current area of research in the field. For now, we will just use our build in image processors.

Radial droplets are very easy to classify. The internal configuration is perfectly spherically symmetric so no matter what way the droplet is rotated it looks the same. The small variations in radial droplets involve a little twist, usually localized at the core. Examples of radial droplets are shown in Appendix A, figure A.1 a.

Bipolar droplets are somewhat easy to classify because they are symmetric around the axis passing through their pole. They can also be "flipped" over the diameter bisecting the poles and look the same. To say that another way, the droplet can rotate 180 degrees and look the same when the poles have changed position. If we consider bipolar droplets with both poles in the plane of the page as the "standard", we can compare some common differences. For example, start with a bipolar droplet with poles making an angle θ with the x-y axis, and then rotate it a small angle ϕ out

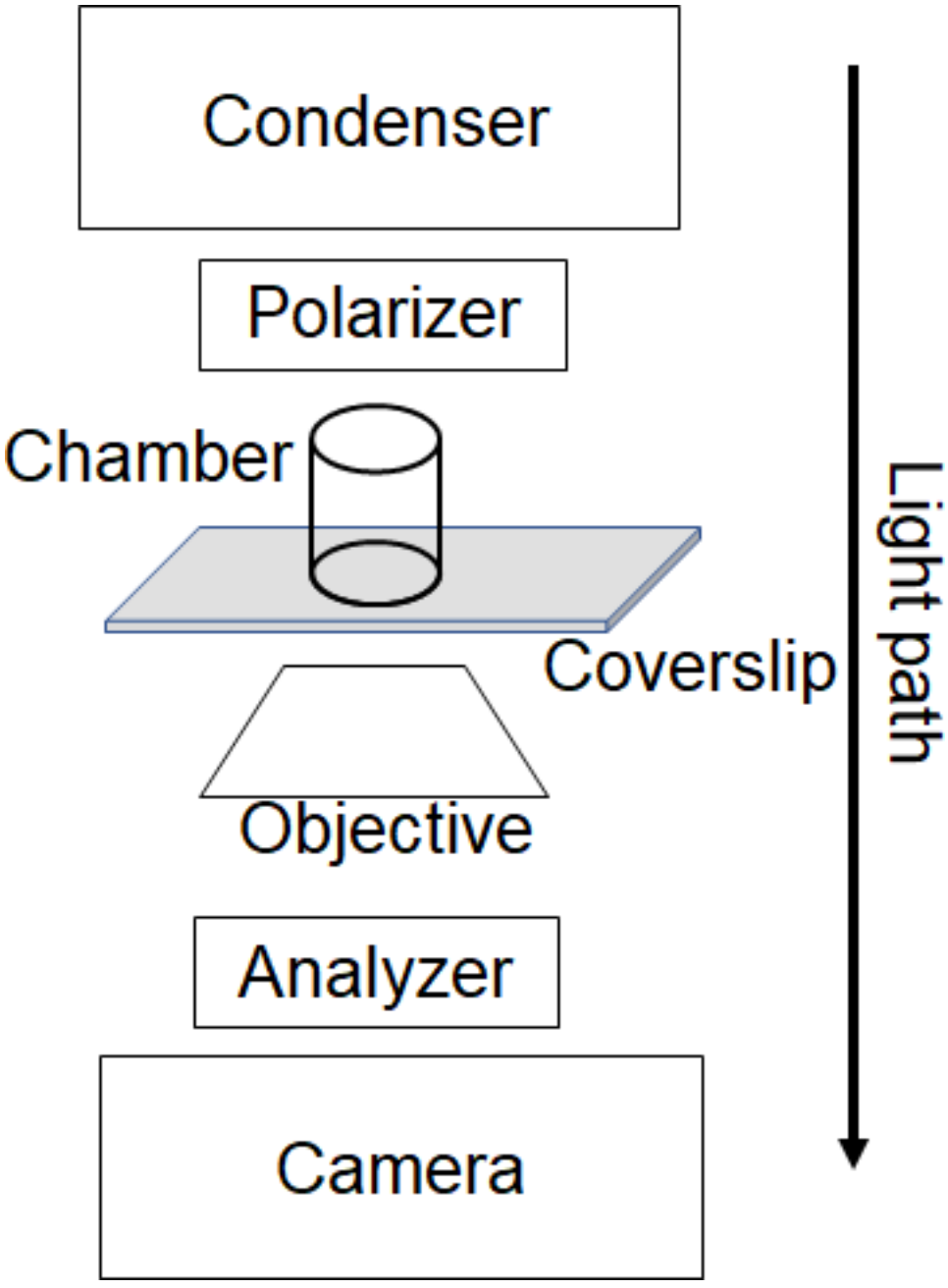

Figure 1.10. Cartoon schematic showing the optical path from the condenser to the camera. Note that the two polarizers (polarizer and analyzer) sandwich the sample.

of plane ("up" or "down"). Now one pole is slightly above the plane of the page and one is slightly below the plane of the page, but the bulk of the liquid is still essentially the same. So, it turns out that many bipolar droplets do look similar to one another. Examples of bipolar droplets are shown in Appendix A, figure A.1 b.

Monopolar droplets are often hard to classify and definitely take the most practice. This is because they have the least amount of symmetry. They are rotationally symmetric about an axis that passes through the pole and center of the droplet, but they do not have the "flip" symmetry that bipolar droplets do. A monopolar droplet with the pole at the "north" end of the drop and a monopolar droplet with a pole at the "south" end of the droplet look different. As you might guess though, the optical patterns (what it looks like using POM) are also rotated. In fact, often times we would classify monopolar droplets by noticing that "This droplet looks like this pattern but rotated". Further, since there are many subtypes of monopolar droplets that we are grouping into monopolar, there could be two droplets that have their poles in the same angular position but not look exactly the same (which they would for bipolar, for example). Examples of monopolar droplets are shown in Appendix A, figure A.1 c.

While Ben, Linda, or I would analyze data and record their configurations we had two additional categories. We had "unknown" droplets that when looking at individually we were unable to confidently sort into either radial, bipolar, or monopolar. Once every couple weeks the three of us would meet and go through the "unknown" droplets together to see if anyone else could figure out the configuration. If none of us could figure it out, we would call it "other" and omit it from the data series. We would also classify droplets as "other" if there was something wrong with them. Examples of "other" and "unknown" droplets are shown in Appendix A, figure A.1 d and e, respectively.

We used the images from the 2005 Prishchepa paper [40] as our basis for monopolar droplets. Each of us had a page of all these configurations hanging above our desks (Appendix B).

1.6.1.1 Rare Occurrences that are confusing

Often times bipolar droplets are drawn schematically so that both their poles are in the plane of the paper. Under the microscope, droplets have no obligation to be so convenient. For example, if a bipolar droplet were to "stand up" such that when you look at it from above you're looking down onto a pole, the bipolar droplet will look exactly like a radial one! So, how do we know that any radial droplet is truly radial and not an "upright" bipolar droplet? Luckily, due to Brownian fluctuations, the droplets are not stationary and rotate around on a time scale that is fast enough so that we can see them rotate in just seconds. I have at least one video of a droplet that looks radial in one frame and then in a frame or two (less than 1 second) looks bipolar. This is something that ONLY a bipolar droplet can do, so that is how it gets classified. If the droplet appears radial over the course of a few seconds, then it definitely IS radial.

Why does that mean it is bipolar and not monopolar? Good point, it doesn't! But, since bipolar droplets look relatively similar to one another when they are slightly rotated out of plane, it is easy to tell that they are bipolar. If it was an "upright" monopolar droplet, we would still see it rotate around due to Brownian fluctuations. If, while rotating, the droplet no longer appeared radial and did not look bipolar, then it would have to be monopolar.

Statistically, from a random distribution, bipolar droplets will most commonly have their poles NOT aligned with a polarizing axis and not in the imaging plane. Bipolar droplets that have their poles aligned with one of the polarizing axes looks pretty different from the common bipolar droplets that have their poles off of the

polarizing axis. Fortunately, even though they look different, they are easy to justify as being bipolar by imagining what the internal configuration looks like. Because the bipolar droplet is not symmetric with respect to rotations of 90 degrees, you can actually tell based on the light pattern which polarizer (either horizontal or vertical) the droplet is aligned with.

Monopolar droplets are very hard to classify. You might be thinking, "well, if its not radial and not bipolar, which are easy to tell, then does not it have to be monopolar?". The short answer is "no". The long answer is "no, because some droplets aren't monopolar either. A droplet might not fit into one of the three categories". If a droplet can not be confidently classified as one of the three, we call it "other" and do not include it in our data set. This is to play it on the safe side and only report information that we can justify and explain.

I have included some sample data (Appendix A), the cheat sheet we used based on the Prishchepa 2005 paper [40] (Appendix B), and a little "quiz" (Appendix C). For a little bit of practice, you can study Appendices A and B to solve Appendix C. This might be the first dissertation that assigns homework! Sorry.

1.7 A Typical Week

A typical week in the lab, when I'm focusing on experiments, would be:

- Monday: Prepare solutions, chambers, syringes, etc.
- Tuesday-Thursday: Take lots of data.
- Friday: Analyze data.

This gives you a nice weekly routine as well as minimizing burn out of taking lots of data in a row or analyzing lots of data. Taking data all day for three days in a row can be taxing though. For a less intense week you can replace Wednesday's

experiments with reading papers, professional development, additional data analysis, or organizational maintenance.

1.7.1 Lab Math

The first thing I do on Monday is make a stock concentration of SDS. A stock concentration is just a highly concentration solution that you can use to make small volume dilutions from. Because we have to make the stock each week, it is best to make relatively small amounts and in relatively low concentrations. For example, a more common buffer, say NaCl, may be 500 mL of 5 M solution and usable for months. I was making 5 mL of 30 mM SDS every Monday. The reason why we have to make SDS each week is that it "goes bad" by over time producing impurities. The SDS hydrolyzes into dodecanol over a work week [38] which can change the surface tension. Making the SDS on Monday and taking data on Friday is ok, but Thursday is a little safer.

Being able to calculate how much mass of a substance to add to solvent to make a particular concentration is also very important, as this is how I make the stock solution each Monday. I choose to make 5 mL of 30 mM SDS to be sure I have enough for the week. So, the question is "how much SDS powder do I have to mass out and add to 5 mL of 10 mM PBS buffer so that I make a 30 mM solution?". It depends on the molar weight of SDS, which is 288.38 g/mol. Keeping the dimensions of what we know and what we're looking for in mind, I set up equation 1.1 to solve for the mass needed.

$$mass = \frac{30mmol}{1L}\frac{1mol}{1000mmol}\frac{1L}{1000mL}\frac{288.38g}{mol}(5mL) = 0.043257g \qquad (1.1)$$

So, if I were to perfectly mass out 0.043257 g of SDS and add it all to 5 mL of 10 mM PBS, I'd have a 30 mM SDS solution. First of all, our most accurate scale in lab goes to four digits, so really the best we can mass is 0.0433 g of SDS. Second, that's

basically impossible to do, so instead I make sure that I have *at least* this amount. Why? Because I've already added the 5 mL of 10 mM PBS to a Falcon tube. If I add any less than 0.0433 g of SDS, I'll have a concentration less than 30 mM. If I add more than 0.0433 g of SDS, I'll have a higher concentration than 30 mM, but I can just add more PBS to get back down to 30 mM.

$$C_f = \frac{massadded}{5mL}\frac{1mol}{288.38g}\frac{1000mL}{1L}\frac{1000mmol}{mol} \tag{1.2}$$

This will give you your actual concentration of SDS. Now we can use

$$C_1V_1 = C_2V_2$$

to dilute down to 30 mM. $C_1 = C_f$ from equation 1.2, $V_1 = 5mL$ because that's how much we have, $C_2 = 30mM$ because that's what we want, and we solve for V_2. Note that you'll get some number larger than 5 mL. You need to add the difference to your current sample. If you calculated $V_2 = 5.0974mL$, then add 97.4 μL of 10 mM PBS to your SDS solution.

We use the equation

$$C_1V_1 = C_2V_2$$

all the time. This equation is something that I think all of the non-physics majors in lab are familiar with, but is new to most physics students. The way I think about this equation is that the product of concentration and volume is just a number of molecules, so this equation says that the total number of molecules are the same before and after. You can replace the subscripts with i and f instead of 1 and 2, if that makes more sense to you. We almost always know two of the variables and can choose what we want one of the two other ones to be, and then solve for the fourth as our only unknown.

For example, let us say I have 5 mL of 30 mM SDS solution that I just made. I want to dilute this down to 2 mM to use in an experiment. I would also need about 750 μL for my experiment, but I would make 1 mL so that I can pipette it more easily. The values that I *know* are the initial concentration, 30 mM, and the final concentration, 2 mM. I also *chose* my final volume, 1 mL. Now I have three known values, one unknown (the initial volume), and can solve. I calculated an initial volume of 66.66 μL repeating which is an awkward amount. What if, for the sake of pipetting, I instead make 1.2 mL my final volume? Now I calculate that the initial volume is 80 μL. Much better. So, I take 80 μL of my 30 mM SDS and add it to 1200-80=1120 μL of whatever buffer solution the high concentration was in. Because the 30 mM SDS is dissolved into 10 mM PBS, I use 10 mM PBS when I dilute the SDS to 2 mM.

CHAPTER 2

INTRODUCTION

Imagine the world with a new class of materials; materials that can sense stimuli and react to them autonomously. Imagine personal protective equipment (PPE) that can sense the presence of a harmful chemical gas or pathogen and alert you to the danger. This is what I am trying to make real. This work is the first step of many toward that future.

2.1 Objectives

Specifically, I have investigated the configurational transition of a liquid crystal (LC) droplet between two distinct internal configurations: radial and bipolar (figure 1.4). I aim to understand what conditions the radial or bipolar configuration can be found in and in what ways we can controllably switch between them. This work is split into four projects that share experimental techniques, but differ in the specific questions asked and the chemical triggers tested.

The first project, which I will just call Project 1, involves using sodium dodecyl sulfate (SDS) (figure 2.1 a) as the surfactant driving configurational change. We started with this system because SDS is a common surfactant used in the literature and will act as the control for the later projects and a "proof of concept" for the experimental technique. With the most consistent configurational phase space, using SDS as the driving agent for configurational transitions demonstrates that this could be applied to other systems.

The second project, Project 2, uses SDS in conjunction with a novel monomeric surfactant (figure 2.1 b) synthesized by the Thayumanavan lab. Since SDS is also a monomeric surfactant, the competition between these two at the droplet's surface could have an effect on the equilibrium droplet configurations or the transition dynamics. Here we can try to drive the transition using SDS *or* the novel monomeric surfactant.

The third project, Project 3, is the undergraduate thesis work of Benjamin Strain, whom I mentored and directed. Ben worked with four different trimeric surfactant molecules that differed from one another in a minor way: the length of only one of the hydrophobic tails (figure 2.1 c). Ben's work was to characterize the configurational phase space of these surfactants as a function of droplet diameter and surfactant concentration. The next step is to use his results and attempt to transition between two configurations.

The fourth project, Project 4, is primarily the work of undergraduate Linda Oster, whom I also mentored and supervised. Linda also works with a trimermic molecule, but this one is different from Ben's in that all the hydrophobic tails are identical and one of the hydrophobic tails has a functional group that was designed to specifically bind to the protein carbonic anhydrase (CA) (figure 2.1 d). This project is unique in that it is the only one where the configurational transition is not driven by surfactant concentration, but instead driven by protein concentration.

Each of these four projects will be discussed in more detail in their own chapters. By investigating and understanding how different surfactants influence the transition between LC droplet configurations, and how different methods of triggering happen, I take a first step toward making responsive materials.

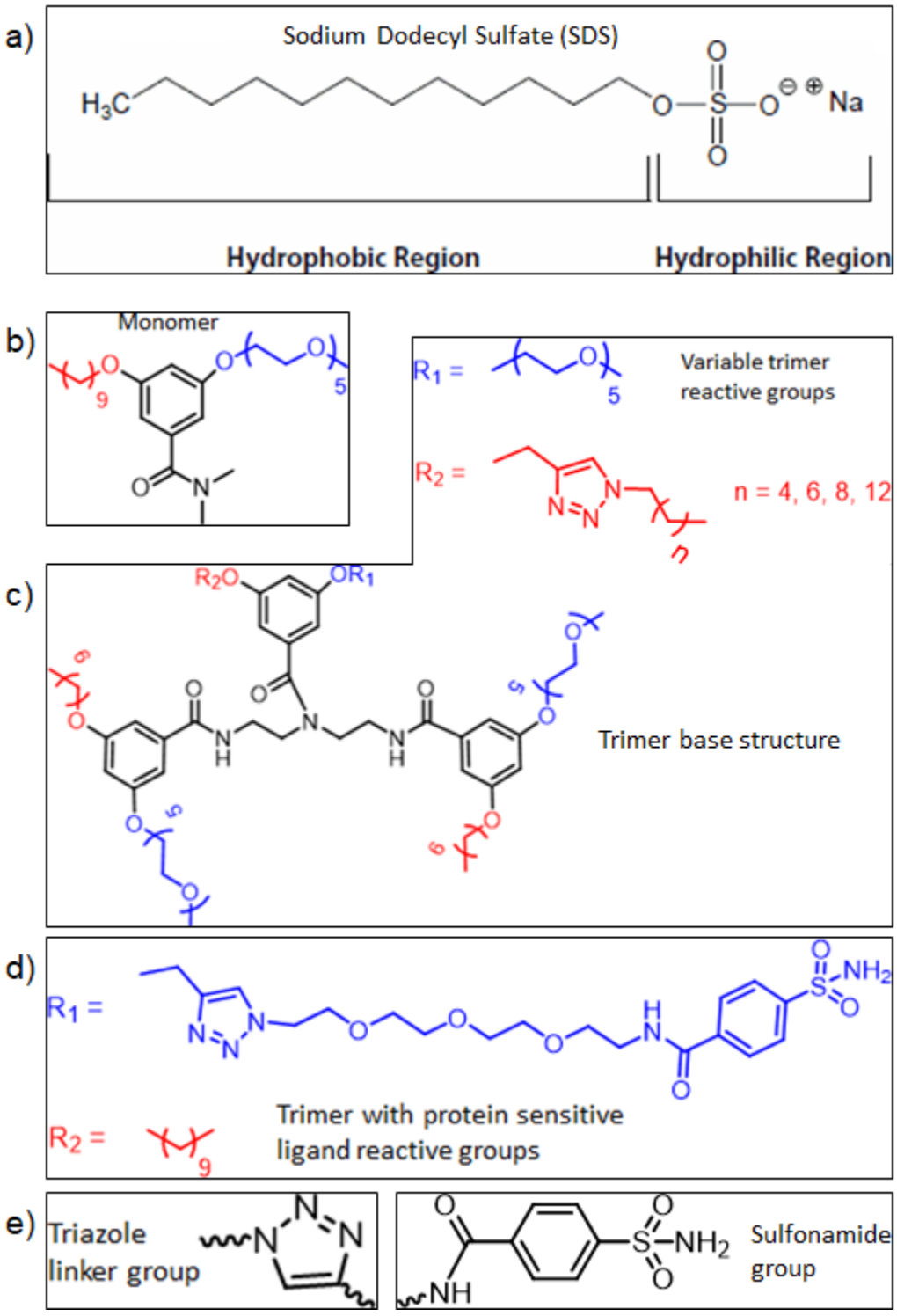

Figure 2.1. Chemical strucutres of all surfactants used in this dissertation. (a) sodium dodecyl sulfate (SDS), (b) monomer, (c) variable tail length trimer with reactive groups, (d) reactive groups for the trimer with protein sensitive ligand (TPSL), (e, left) triazole linker group used in the reactive groups of the variable tail trimer and TPSL, (e, right) sulfonamide functional group that binds specifically to carbonic anhydrase (CA). SDS carries a negative charge on the head group.

2.2 Inspired by nature

Humanity has long been inspired by nature. A story as old as that of Icarus and Daedalus shows we have been envious of a bird's ability to fly for thousands of years. It was not until just over 100 years ago that we were able to finally recreate flying for ourselves. Human envy is not limited to flight. Over millions of years organisms have evolved mechanisms critical to their survival. These mechanisms are what I seek to emulate. For example, the retraction of leaves from a touch-me-not plant, or the gelification of water around an alarmed hagfish, protect them from predators. Inspired by these phenomena, I aim to create the first steps of a system that behaves in a similar way. The range of applications for reactive materials are beyond my imagination.

2.3 Literature Review

In the past couple decades there has been a substantial movement to investigate responsive or "smart" materials [16, 35, 37, 48, 53, 55]. Responsive materials are a broad class of materials that change their structure, behavior, or properties in response to a stimulus.

Examples of stimuli are electric and magnetic fields [33, 44], mechanical stresses [45], pH modulation [6, 29], light (typically UV) irradiation [4, 18, 24, 49, 54], protein binding [17, 39], and temperature change [27, 41]. These responsive materials are the foundation for advanced sensor technology [26, 50] and for controlled spatiotemporal release of cargo, such as medicine [30, 35].

A common sensor technology that primarily utilizes LCs are liquid crystal displays, commonly known as LCDs. Liquid crystals are a class of molecules that exhibit orientational (crystal) order and fluidic (liquid) properties, making them a rich area of research because of the exciting technological opportunities they present [23].

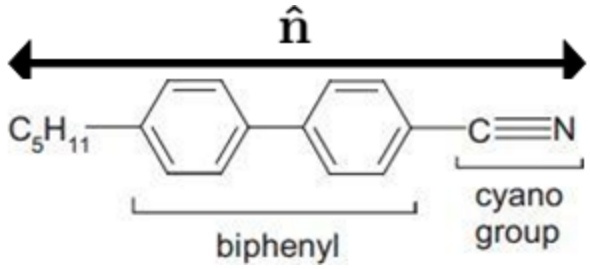

Figure 2.2. Chemical structure of the liquid crystal 4-Cyano-4'-pentylbiphenyl (5CB). The director, $\hat{\mathbf{n}}$, is shown above the molecule. Structure obtained from: http://www.sjsd.net/ gjohnson/FOV1-00053FB3/Chapter%2014.pdf

For example, an LCD is a device that gives an optical response to the sensing of electric fields. The rod-like LC molecules used have a high aspect ratio and prefer to all align parallel to each other. The LCs also exhibit different optical properties along their short and long axes, known as birefringence [23]. Specifically, the polarization of light tends to align with the "director" of the LC, a dimensionless unit vector quantity, $\hat{\mathbf{n}}$, that describes the orientation of the LC [23]. The director is typically parallel to the long axis of the molecule. By using polarizing filters, optical information can signal the presence of an electric field.

In figure 2.2, the director is shown above and parallel to the liquid crystal's orientation. There is no distinction between $\hat{\mathbf{n}}$ and $-\hat{\mathbf{n}}$ [23] due to the geometric symmetry of the molecule. At room temperature, this particular liquid crystal is in the nematic phase. The bulk alignment has a one-dimensional crystal ordering, and the mobility of the individual molecules is fluid like. In this nematic ordering, the distribution of the center of masses is random [23].

Here, I am interested in obtaining LC droplets, where the LC acts as an oil phase in an oil-in-water (O/W) emulsion (figure 2.3, left [32]). My experiments will use the LC 4'-Pentyl-4-biphenylcarbonitrile (5CB), a rod-like molecule whose structure is shown in figure 2.2. The rod-like molecular geometry gives these LC the unique ability

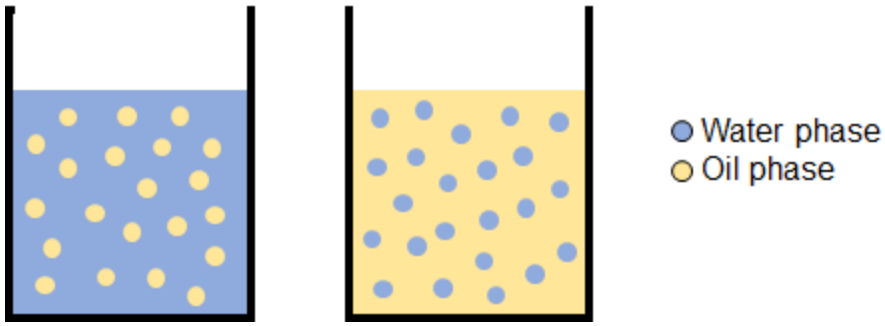

Figure 2.3. Cartoon of an emulsion. On the left is an oil (yellow) in water (blue) emulsion (O/W). On the right is a water in oil (W/O) emulsion. The Liquid crystal we use is hydrophobic and acts as an oil phase. All of the emulsions described in this dissertation are O/W emulsions.

to form a variety of configurations. For a complete list, see figure 2 of Lopez-Leon 2011 [32].

One can get information on the organization of the LCs by observing LC systems using polarized light microscopy, exploiting the LC's birefringent nature [34].

A simulation of the light pattern seen for a bipolar and radial droplet is shown in figure 2.5. A transition between the bipolar and radial configurations can be triggered by electric fields, magnetic fields, or other interactions [25]. Exploring new ways to manipulate LCs, particularly in geometries other than square lattices, can lead to promising new applications.

The two main configurations relevant to my work are the radial and bipolar configurations. In the radial configuration, there is a single point defect at the volumetric center of the droplet, and the director field of the LC points radially outward everywhere. The LCs at the interface of the droplet are perpendicular to the interface (figure 2.4 left).

In the bipolar configuration, there exist two point defects on the surface of the droplet a diameter apart. Immediately surrounding these defects, the LC director is away from the defect. Here, however, the LC at the interface is parallel and forms

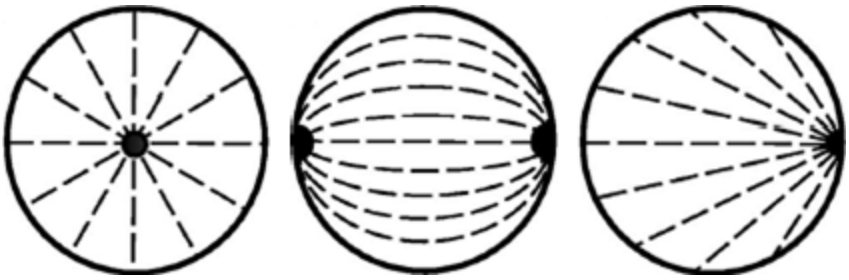

Figure 2.4. Cartoon of a liquid crystal (LC) droplet in the radial configuration (left), bipolar configuration (center), and monopolar configuration (right). The dotted lines in the drop follow the director of the LC. Cartoons reproduced from partial figures in Prishchepa 2005 [40] with permission.

lines of longitude between the two poles. Through the bulk of the bipolar phase, the LC aligns to be parallel to the surface layer (figure 2.4 center).

When we undergo the transition between the radial and bipolar configuration we pass through an intermediate monopolar configuration. This configuration is different from the previous two because the boundary conditions are not uniform. The angle between the LC and the interface is 0 degrees at the location of the pole, but is 90 degrees on the opposite side of the droplet with intermediate angular values in between. We observe this configuration in our characterization experiments as well. A cartoon schematic of these three phases is shown in figure 2.4.

Computer simulations can be used to predict what the optical pattern of the droplet will appear as given a certain internal organization. The simulated images of the director cartoons in figure 2.4 are shown in figure 2.5. Note that these simulations are only for the specific orientation of the droplets shown in figure 2.4. While the radial droplet is totally spherically symmetric, the bipolar and monopolar droplets are not. A bipolar or monopolar droplet can have various optical patterns based on the orientation of the pole(s) relative to the polarizer orientations and viewing angle. A listing of observed optical patterns is attached as Appendix C. Ben, Linda, and I used this list as a reference when categorizing our own data.

Figure 2.5. Simulation of what a droplet in the radial (left), bipolar (center), and monopolar (right) configuration would look like using polarizing microscopy [40]. Note that this is only the case if the bipolar or monopolar droplet is oriented as in figure 2.4 center or right, respectively. The radial configuration, unlike the bipolar and monopolar configurations, is rotationally symmetric and always appears the same. Simulations reproduced from partial figures in Prishchepa 2005 [40] with permission.

The droplet's internal configuration can be controlled by modulating the interface between the organic liquid crystal 5CB and the aqueous surfactant medium [32] with surfactant molecules. The surface conditions impose boundary conditions on the anchoring of the LC molecules at the droplet's surface. This is an interesting physical system because of the geometry of the interface and the molecules at the surface, which can alter the organization of the LC throughout the interior [11, 32, 39, 42, 51]. The bulk internal LC has elastic deformation due to these boundary conditions. Any elastic deformation can be split into four elastic modes: splay, twist, bend, and "biaxial splay" [46]. Any arbitrary deformation is a combination of these four modes. The elastic energy per unit volume, F_d, for a nematic liquid crystal is described by equation 2.1 [46].

$$F_d = \frac{1}{2}K_{11}(\nabla\cdot\hat{\mathbf{n}})^2+\frac{1}{2}K_{22}(\hat{\mathbf{n}}\cdot\nabla\times\hat{\mathbf{n}})^2+\frac{1}{2}K_{33}(\hat{\mathbf{n}}\times(\nabla\times\hat{\mathbf{n}}))^2-K_{24}\nabla\cdot(\hat{\mathbf{n}}(\nabla\cdot\hat{\mathbf{n}})+\hat{\mathbf{n}}\times(\nabla\times\hat{\mathbf{n}})) \tag{2.1}$$

The constants K_{11}, K_{22}, K_{33}, and K_{24} are the elastic constants associated with splay, twist, bend, and "biaxial splay" respectively. Splay is related to the divergence of the LC. Twist is related to the out-of-plane curl of the LC. Bend is related to the

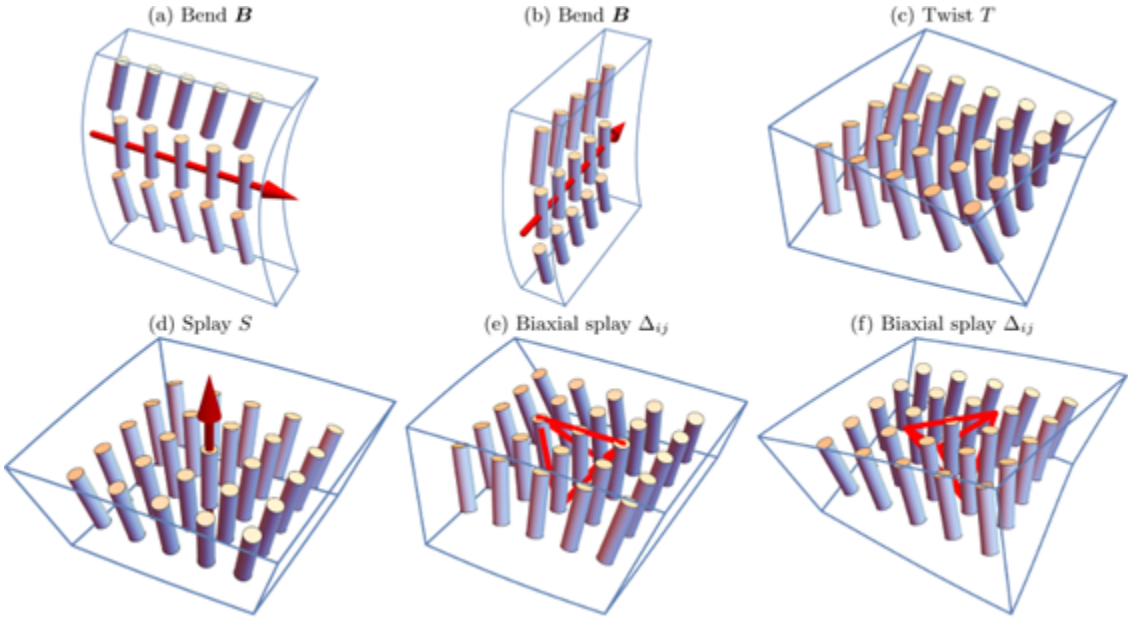

Figure 2.6. Cartoons of the elastic modes in nematic liquid crystals. (a) and (b) show both directions of bend with the bend vector shown, (c) twist, (d) splay with splay vector shown, and (e) and (f) biaxial splay. The red tetrahedra in (e) and (f) represent the third-rank tensor $\Delta_{ij}n_k$. Figure reproduced from Selinger 2019 [46] with permission.

in-plane curl of the LC. Biaxial splay is a saddle-splay mode where the splay is in different directions along different axis. The deformations of splay, twist, bend, and biaxial splay are shown in figure 2.6 [46].

It has been shown that one way to alter the phase of a LC droplet is to alter the interfacial tension [32, 42, 51]. In my system, the interfacial tension is controlled using surfactant molecules. Surfactants are amphiphilic molecules characterized by possessing one or more hydrophobic and hydrophilic regions. Modifications to the hydrophobic and hydrophilic regions, the number of those regions, or the geometry of the amphiphile can alter the interfacial properties of the amphiphile [24]. My collaborators in the Thayumanavan lab (UMass Amherst, Chemistry Department) synthesize novel amphiphiles that are responsive to a stimulus such as: pH, light, or protein binding [27]. I chose to focus on amphiphiles responsive to protein binding. It has been shown that amphiphiles sensitive to protein binding change their chemical

properties, and thus their interfacial properties [17, 39]. This change in interfacial tension can result in a phase change of the LC droplet [25, 32, 42, 51]. By characterizing the response of LC droplets to these novel amphiphiles, I can obtain LC droplets with various internal configurations, understand them, then refine the response to the designed trigger. To help understand the dynamics of the transition between phases, I compared my experiments to simulations from the de Pablo group at University of Chicago.

2.4 Remotivation

As stated in the introduction chapter, my dissertation will consist of four projects. All projects revolve around the configurational transition of a liquid crystal droplet between the radial and bipolar configurations. These transitions will be controlled using the concentration of a surfactant in projects 1, 2, and 3, and with a protein in project 4. Each project will involve more complex surfactant molecules than the last.

2.4.1 Impact

These results below are exciting for a few reasons. One, you can change the configuration of a LC droplet by changing the SDS concentration. This is exciting because then the question can be reframed to, "How can I trigger a change in SDS concentration?", which adds a second level of triggering and customization. For example, the first trigger would have the effect of changing the SDS concentration, which would change the configuration of a LC droplet.

Second, I observed that the SDS concentration that the bipolar to radial phase transition happens is less than the SDS concentration for the radial to bipolar phase transition. The hysteresis in a cycle of configurational transitions is interesting in what it reveals about the dynamics of the surfactant molecules.

Third, I found that the SDS controlled transition has a critical SDS concentration that varies in the presence of novel surfactants. Different novel surfactants have different effects. I observed that SDS combined with a novel trimeric surfactant have a bipolar to radial transition at a lower SDS concentration. In a system with SDS and novel monomeric surfactant, the bipolar to radial transition happened at the same SDS concentration. This showed that the presence of trimers facilitates the transition from bipolar to radial.

For the radial to bipolar transition, however, all novel surfactants assisted the transition and the radial to bipolar transformation started at a higher SDS concentration. If the critical SDS concentration needed to transition from bipolar to radial or radial to bipolar depends on the presence and concentration of a second surfactant species, it suggests that further studies could be done to optimize the transition concentrations by adjusting the novel surfactant structure.

All of these results are still many steps removed from recreating a material that has a hagfish-like response. The work done in this dissertation is just the first step toward the biomimicry of a hagfish. It will be another 50 years before I predict something like this to be manufacturable. The progress made in this dissertation is in the form of understanding the role and importance of surfactants on the internal configuration of a liquid crystal droplet. By being able to finely control the optical response of a liquid crystal droplet to a specific response we are one step closer to a designable automatic sensing system.

CHAPTER 3

EXPERIMENTAL DETAILS

3.1 Using Surfactants to Stabilize Droplets

The novel surfactants used throughout this dissertation were synthesized in the Thayumanavan lab by graduate students Mansiha Chahar and Uma Sridhar. These two were always very prompt to requests for additional surfactant. Beyond the actual synthesis, they also measured the CAC of each surfactant they made.

Since our plan is to use surfactants to influence the boundary conditions of liquid crystal (LC) droplets, we need to talk about their behavior when added to aqueous solutions. When surfactant molecules are dispersed into an aqueous solution, the hydrophobic regions have a large energy cost associated with their exposure. As one might intuit, these amphiphilic molecules self assemble into aggregates that shield their hydrophobic regions by facing the hydrophilic regions toward the water. The concentration of surfactant molecules needed to spontaneously form these aggregates is called the critical aggregate concentration (CAC). As more and more surfactant molecules are added, raising the concentration above the CAC, nearly all of the additional surfactant molecules added form aggregates. There are always some surfactant molecules existing as individuals in the bulk solution. The concentration of free surfactant molecules is always less than or equal to the CAC. Below the CAC, there are only free surfactant molecules and no aggregates, so the concentration of free surfactant molecules is exactly the concentration of the surfactant in the system. The entropy available to individual molecules is favorable compared to shielding the hydrophobic regions. For some surfactants, such as sodium dodecyl sulfate (SDS), these

aggregates form micelles and we instead call the critical concentration the critical micelle concentration (CMC). If the aggregate structure is unknown, CAC is used.

Novel surfactants were synthesized and their CACs determined by a collaborator in the Thayumanvan lab. The CAC for the surfactant molecules is measured by preparing several dilutions and mixing them with a hydrophobic dye. The dye used is 1,1'-Dioctadecyl-3,3,3',3'-Tetramethylindocarbocyanine Perchlorate (DiI). Above the CAC the dye can become sequestered inside the hydrophobic core of an aggregate of surfactant molecules. At higher surfactant concentrations, there were more aggregates and thus more dye enclosed. Below the CAC the dye was not encapsulated by the surfactant. By filtering out the free dye molecules and measuring the intensity of the solution as a function of concentration, one can deduce the critical concentration that the intensity starts increasing because of the presence of encapsulated dye. This concentration is the CAC. A representative intensity plot is shown in figure 3.1. By calculating 10 raised to the power of the x-intercept, the concentration in molar is determined. In figure 3.1 the x-intercept of the best-fit line is approximately -4.8. Calculating $10^{-4.8}$ we get $16 * 10^{-6}$ M, or 16 μM.

The CAC for the novel trimer molecules (trimer, variable trimer, and trimer with protein sensitive ligand (TPSL)) is approximately 10 μM in water. The CAC of the monomer molecule is 75 μM in water. Experiments are run at approximately 70 % of the CAC for all novel surfactants, at our collaborator's suggestion. The CMC for SDS is around 10 mM at room temperature. Our choice of SDS concentrations were empirically chosen based on where we measure the transitions between radial and bipolar phases.

At even the lowest concentrations listed in table 3.1 we have a stable LC emulsion. Note that when use 0 mM SDS there is another surfactant present that stabilizes the emulsion. If we had no surfactant in the system we would not have a stable LC emulsion because droplets would coalesce.

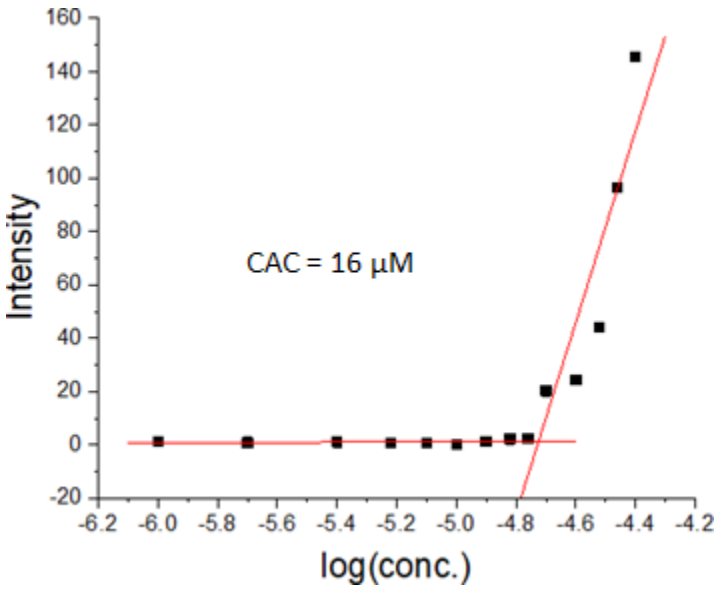

Figure 3.1. A representative plot that yields the critical aggregate concentration of a molecule. This plot is not for any of the molecules described in this dissertation.

Surfactant	CAC	Concentration Used
SDS	10 mM	0-2 mM
Monomer	75 μM	50 μM
Variable Trimer C6	13 μM	1, 5, 10, 50, 100 μM
Variable Trimer C8	15 μM	1, 5, 10, 50, 100 μM
Variable Trimer C10	11 μM	1, 5, 10, 50, 100 μM
Variable Trimer C14	14 μM	1, 5, 10, 50, 100 μM
TPSL	10-15 μM	0-20 μM

Table 3.1. Table listing the CAC or CMC (SDS only) of each surfactant used in the work.

3.1.1 Data Acquisition

Data were collected using a Nikon Eclipse Ti microscope, Nikon 60x water immersion objective, and Andor Zyla sCMOS camera. Data were collected with an exposure time of 100 ms, and a time interval between frames of 200 ms, unless stated otherwise. The duration of the movies varied. The scale for all data was 1000 pixels = 110 μm. We used polarizing microscopy to image our liquid crystal (LC) droplets to get information about the internal director alignment. Details of how the data were recorded can be found in Appendix E.

3.1.1.1 Polarizing Microscopy

Polarizing microscopy uses two linearly polarizing filters, called the polarizer and analyzer, that are oriented perpendicular to each other. The light path starts at the condenser lamp, goes through the polarizer, the sample, the analyzer, and ends at the camera. A cartoon schematic of the light path is shown in figure 1.10.

Outside of the droplets there is an aqueous surfactant solution and no free LC. The polarized light that passed through the polarizer was not rotated as it passed through the glass and surfactant solution, so all of the light was blocked by the analyzer, thus the background is black.

The liquid crystals inside the droplets, which are birefringent, caused the polarization of light to rotate. The polarization rotated to be parallel with the director, effectively making each individual LC molecule a polarizer. If the polarization of the light was rotated at all in the sample, then some projection of the polarization is able to pass through the analyzer and could be detected on the camera. That is, if the liquid crystal was at an angle that was not parallel to either the polarizer or analyzer, the camera will detect some light. The intensity was related to the projection of the polarization that was parallel to the analyzer, and thus related to the projection of the LC that was parallel to the analyzer. The maximum intensity occurred when

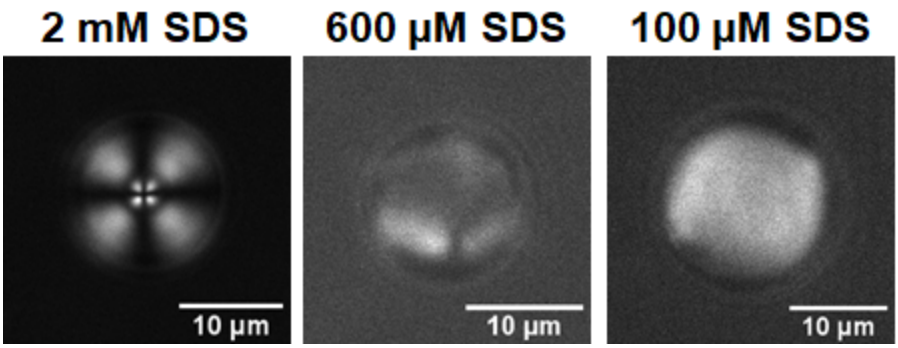

Figure 3.2. Liquid crystal droplets in the radial configuration (left), monopolar configuration (center) and bipolar configuration (right) as seen using polarizing microscopy. The monopolar droplet has its defect at the 6 o'clock position on the droplet. The bipolar droplet is oriented at an angle with respect to the cross polarizers. The SDS concentration is 2 mM for this radial droplet, 600 μM for the monopolar droplet, and 100 μM for the bipolar droplet.

the LCs were rotated 45° with respect to the analyzer, with decreasing intensity for steeper or shallower angles. If the LC director is aligned with either the polarizer or analyzer, the polarization of the light was not altered and the light was again blocked completely. Because all unaltered light was blocked, but there was a signal from the presence of LC, the signal-to-noise ratio was very high. Figure 1.9 shows how the intensity of light through various polarizer overlays changes.

For example, consider the radial droplet in the cartoon of Figure 2.4. Along the vertical and horizontal cords of the circle, the LC is aligned with either the polarizer or analyzer and we expect to have a dark region. In each quadrant the LC is oriented at varying angles, so we expect brightness here that peaks at 45°. Additionally, we expect the area around the droplet to be perfectly black. This is what is predicted by simulations (figure 2.5). In experiments (figure 3.2) the lookup table is adjusted so that the intensity of the droplet is not saturated and so the background also appears grey instead of black.

3.1.1.2 Optical Tweezers

In order to observe the same droplet for an hour or more, with changing conditions and flow in the chamber, I used optical tweezers to hold the droplet in place. Optical tweezers are an experimental tool used to hold an object with a different refractive index than the medium it is surrounded by [15]. We only need to use the optical tweezers in the experiments where we flow into the chamber and not in the experiments where we characterize droplet configurations at a static surfactant concentration. The wavelength used for the optical tweezers was 1064 nm, the near infrared (IR). Near IR is used because of its high transmittance through many materials. By focusing this near IR laser beam in the plane of the sample, we can center it on a particular droplet in the LC emulsion. Positioning the focal point of the laser over a LC drop holds the drop in place, or "traps" it. The width of the beam at the focal point, called the beam waist, is approximately half the wavelength of the beam. In the plane of the sample, the trap beam has an intensity profile of 2-dimensional Gaussian. The trapped particle or droplet experiences a restoring force due to radiation pressure that causes it to move toward the peak [15].

We call the imaging plane the x-y plane, with the z-direction pointing towards the ceiling. The optical trap passes perpendicular through the imaging plane and exits in the +z-direction. The trapped droplet sits slightly "downsteam" of the focal point, meaning its z position is slightly higher than the z position of the focal point. A cartoon schematic of the optical trap set-up is in figure 3.3 (top), with a real picture of the set-up shown below.

3.2 Overivew of Experimental Methods

There are two experimental methods that I used to investigate the questions outlined in Chapter 2, referred to as method 1 (equilibrium) and method 2 (dynamic). These methods complement each other and using both I could investigate our sys-

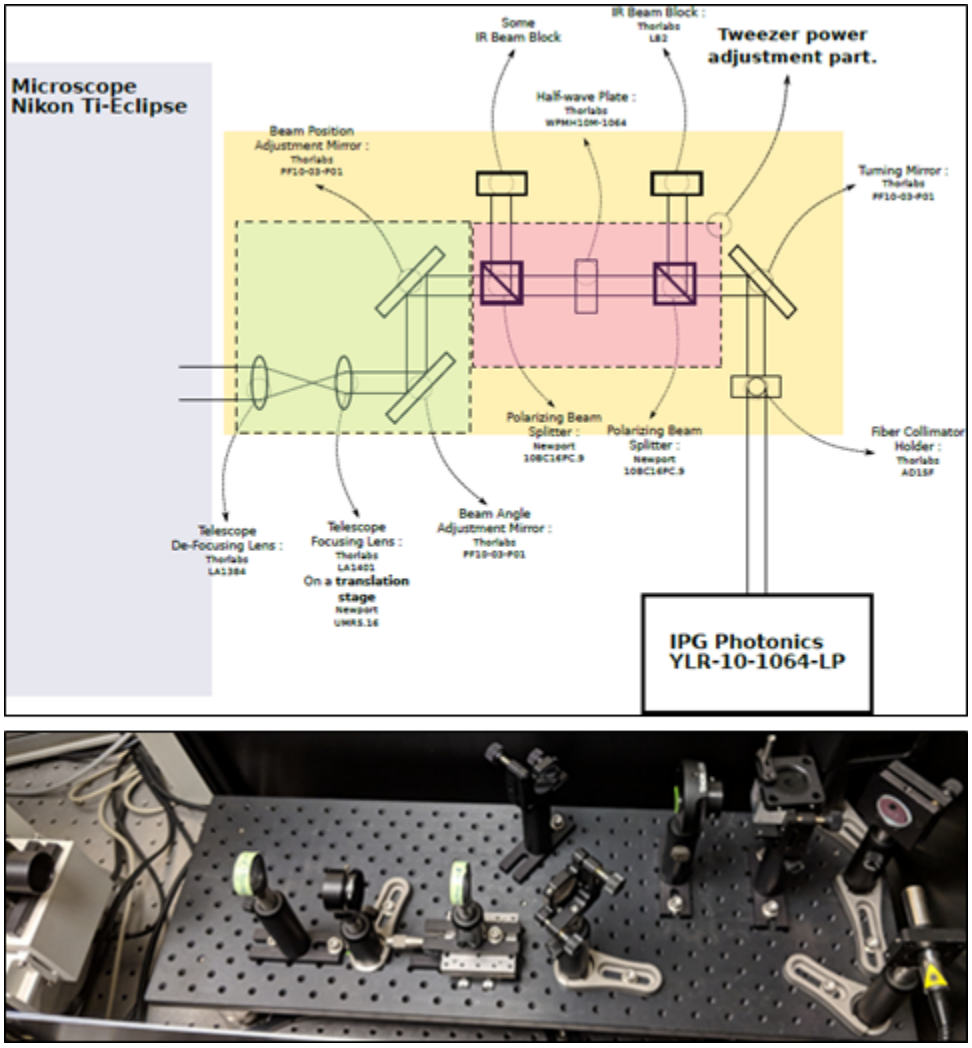

Figure 3.3. Cartoon schematic of the optical trap set up (top). In lab image of the optical trap set up (bottom).

tem deeply. Details of how to make the PBS buffer, prepare LC emulsion samples, chamber construction, and data acquisition details can be found in Appendix E.

3.2.1 Method 1 - Equilibrium Characterization

Method 1 is used to characterize the equilibrium LC configuration in each droplet. The goal of these experiments was to determine the dependence of the internal configuration on surfactant concentration and droplet diameter. The images of each droplet, taken using polarizing microscopy, were classified as radial, bipolar, or monopolar and their diameter quantified. If a droplet could not be confidently classified as either radial, bipolar, or monopolar we classified it as "other" and omitted it from the data set. Each data point represents a specific droplet. These experiments were good for obtaining a large number of droplets per chamber at specific concentrations. Data were taken as videos, individual still frames are used to classify droplets, and thus these experiments can be thought of as equilibrium experiments. The drawback of these experiments was that they do not explore the intermediate concentrations between the chosen ones and they do not reveal dynamics of changes in configuration. This was addressed with a dynamically changing SDS concentration in the second experimental method.

3.2.1.1 Sample Preparation

All surfactant solutions are diluted to the desired concentration using 10 mM phosphate-buffered saline (PBS) buffer solution. A polydisperse LC droplet sample is produced by adding 2 μL of 5CB LC to 98 μL of surfactant solution, and agitated by flicking. Before agitation, the LC can be seen as a single drop in the solution as in figure 3.4.

Once the characterization chamber has been made, the LC emulsion is flowed into the chamber and immediately sealed with epoxy. The chamber is imaged without any incubation period.

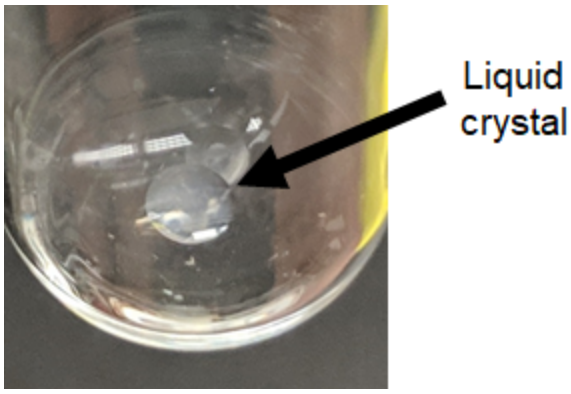

Figure 3.4. Image of the liquid crystal (LC) in a sodium dodecyl sulfate surfactant solution before mechanical agitation. The LC is in a single large drop, which appears cloudy, in the center of the image.

3.2.1.2 Microscopy

Data videos collected from the equilibrium characterization experiments were analyzed by hand. Each video is typically three minutes long (900 frames). For each frame of the video, all droplets in focus were measured. For each droplet, the diameter was measured, and the droplet classified as radial, bipolar, or monopolar based on the optical pattern seen through crossed polarizers (cf. figure 3.2). The droplet was observed over several frames to get multiple views for an accurate classification. We aim to get at least 50 droplets per concentration for statistical integrity.

All data pertaining to a surfactant are on a single chart. We plot surfactant concentration on the y-axis and droplet diameter in micrometers on the x-axis. Data points are small red diamonds for radial droplets, green triangles for monopolar droplets, or large blue diamonds for bipolar droplets. The phase space plot for SDS is shown as an example in figure 3.5.

3.2.2 Method 2 - Transition Dynamics

Method 2 is used to observe the dynamics of the transition. Both the radial to bipolar and bipolar to radial transitions are studied using method 2. The goal of these experiments is to measure the concentration the transition begins and ends while ob-

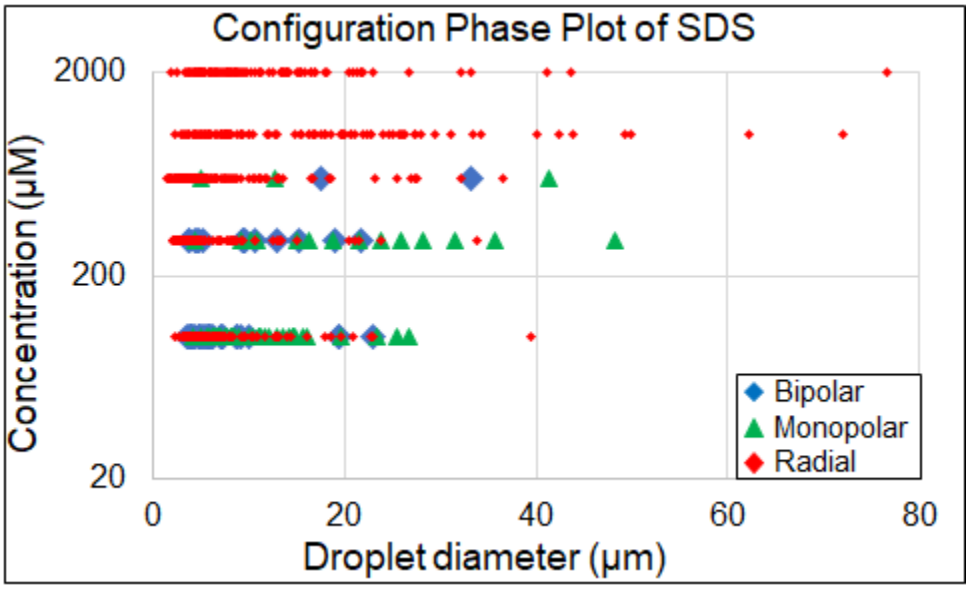

Figure 3.5. Configuration of 5CB liquid crystal droplets as a function of SDS concentration and droplet diameter. Bipolar droplets are represented with a large blue diamond, monopolar droplets are represented with a green triangle, and radial droplets are represented with a small red diamond.

serving the intermediate LC configurations. These experiments are done dynamically and analyzed based on a subset of frames that encompass the transition. The surfactant (e.g. SDS) concentration is changing continuously through the experiment, by flowing in a higher concentration of surfactant, or buffer with no surfactant, into the experimental chamber using a syringe pump. To continuously look at the same droplet, I use optical tweezers to hold it in place. The drawback of these experiments is that only one drop can be measured at a time.

3.2.2.1 Sample Preparation

The transition experiments use two surfactant solutions. One to make the LC emulsion, called the initial solution, and one added later to change the SDS concentration, called the secondary solution. Only one surfactant concentration is changed at a time. If there is a two surfactant system, one of the surfactants is held at a constant concentration. All surfactant solutions are made in 10 mM PBS. The final

SDS concentration, after the syringe is done, for a bipolar to radial transition is 2 mM. The final SDS concentration, after the syringe is done, for a radial to bipolar transition is 400 μM.

A polydisperse LC droplet emulsion is produced by adding 1 μL of 5CB LC to 250 μL of initial solution. This lower ratio of LC to initial solution gives a lower population of LC droplets in the flow chamber. I prefer to minimize the number of droplets per chamber, to avoid the possibility of a second droplet colliding with the trapped droplet of interest during the flow. For the bipolar to radial transitions, 100 μL is taken from the emulsion and added to the cylindrical chamber. Depending on where the 100 μL is drawn from in the sample tube, a variable amount of LC enters the chamber. For the radial to bipolar transitions, 50 μL is drawn instead of 100 μL.

The method used to construct the experimental chamber is described in Appendix D.

3.2.2.2 Experimental Method

We used a WPI SP200I syringe pump and 1 mL BD plastic syringe with Luer-Lok tip connected to a 30G x 1/2 BD PrecisionGlide needle to flow into the chamber, using PTFE #30 AWG thin wall tubing from Cole-Parmer Instrument Company. Details on how to set up a syringe pump are in Appendix D.

The droplet is optically trapped before the secondary solution is flowed into the transition chamber to hold it steady during flow.

3.2.2.3 Bipolar to Radial Transition

Using the syringe pump, 100 μL of initial solution (recall Table **??**) is flowed into the chamber at a rate of 100 μL/min. This flow serves to test the tubing connection as well as add some initial solution to the chamber. Of this 100 μL, 24.1 μL is still in the inlet tube, and only 100-24.1=75.9 μL make it into the chamber. Then, 100 μL of LC emulsion is then pipetted into the chamber by hand. We swap the syringe

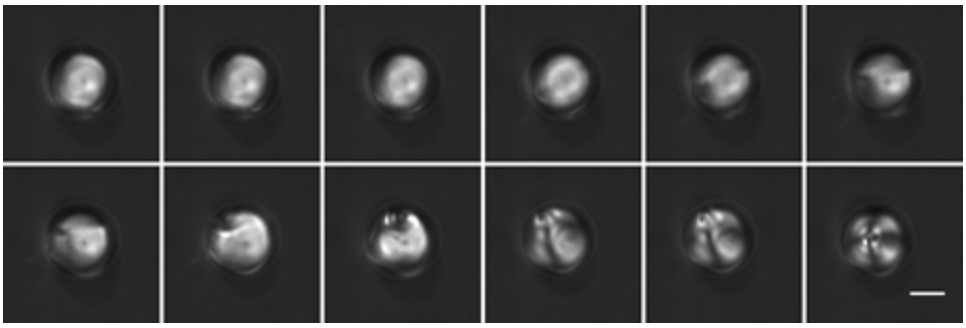

Figure 3.6. Montage time series of a bipolar to radial transition. Each frame is 25 frames and therefore a 5 second interval. This data shows the formation of a ring defect on the drop's surface that contracts to a point on the droplet's surface that becomes a point and moves to the droplet's volumetric center. Scale bar is 10 μm.

full of initial solution with the syringe filled with secondary solution. Then, 124.1 μL of secondary solution is flowed into the chamber at a rate of 3 μL/min. The first 24.1 μL of flow is still initial solution, and now there is 200 μL of initial solution in the chamber. The last 100 μL that enters the chamber is the secondary solution that has SDS. The concentration of SDS in the chamber increases monotonically to a final concentration of 2 mM. There is some global motion in the chamber due to the incoming flow, causing droplets to move around in the chamber. The droplet of interest is held in place using optical tweezers so that it does not flow away. A time series of a sample SDS driven bipolar to radial transition is shown in figure 3.6.

3.2.2.4 Radial to Bipolar Transition

Using the syringe pump, 50 μL of initial solution was flowed into the chamber at a rate of 50 μL/min, which tests the tubing connection. Of this 50 μL, 24.1 μL was still in the inlet tube, and only 50-24.1=25.9 μL made it into the chamber. Then, 50 μL of LC emulsion was pipetted into the chamber by hand. Using a smaller initial volume for these transitions allowed me to achieve a greater SDS concentration change. I swapped syringes to the one filled with secondary solution. Then, 424.1 μL of secondary solution was flowed into the chamber at a rate of 3 μL/min. The first

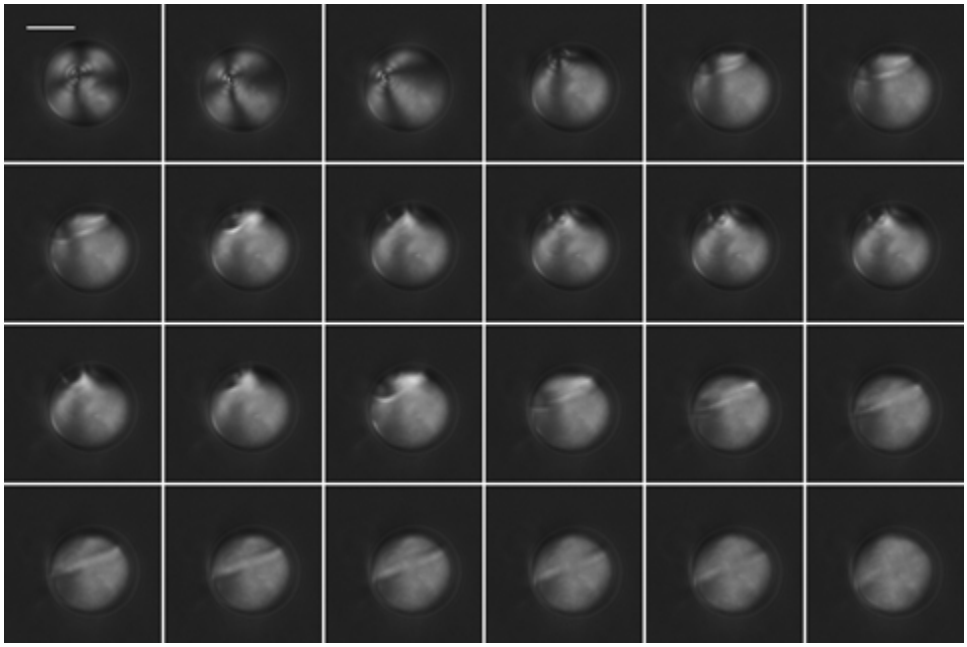

Figure 3.7. Montage time series of a radial to bipolar transition. Each frame is 100 frames and therefore a 20 second interval. Qualitatively, this transition is the reverse of that shown in Figure 3.6. Here the volumetric point defect moves toward the droplet's surface, becomes a ring defect on the surface, and expands to the drop's full diameter before disappearing. Scale bar is 10 micron.

24.1 μL of flow was still initial solution, to make a total of 100 μL of initial solution in the chamber. The last 400 μL that entered the chamber was the secondary solution that has no SDS. The concentration of SDS in the chamber decreased monotonically to a final concentration of 400 μM. As with the bipolar to radial transitions, there was some global flow in the chamber due to the incoming flow and the droplet was held using optical tweezers. A time series of a sample SDS driven radial to bipolar transition is shown in figure 3.7.

3.2.2.5 Data Analysis

The concentration of SDS in the chamber can be calculated with the following equation.

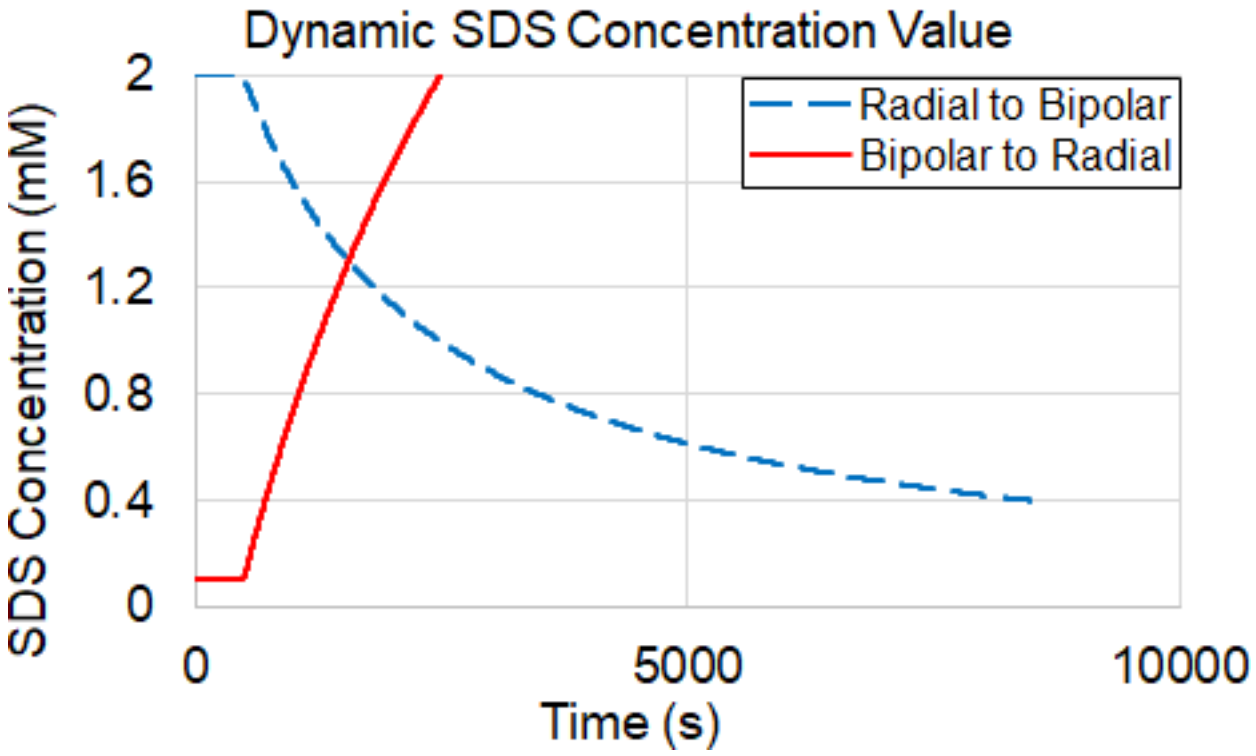

Figure 3.8. Plot of the SDS concentration as a function of time inside the chamber during the bipolar to radial transition (red, solid) and radial to bipolar transition (blue, dashed).

$$C(t) = \frac{(C_i V_i + C_f(rt - 24.1))}{(V_i + (rt - 24.1))} \tag{3.1}$$

The initial concentration of SDS in the chamber is called C_i. The concentration of SDS being flowed in from the syringe pump is called C_f. The flow rate, r, is 3 μL/min, and t is time since flowing began. Therefore, the quantity rt is the volume that has been flowed in from the pump. The volume, in μL, in the cylinder before the secondary solution reaches the end of the inlet tubing is V_i. The (-24.1 μL) is the internal volume, in μL, of the inlet tube and is subtracted to avoid double counting it in rt as well as V_i. Using the equation above, we can calculate the SDS concentration when a droplet begins and finishes a transition from the bipolar state to the radial state. A plot of the SDS concentration as a function of time can be found in figure 3.8.

3.2.3 Adaptability and Implementation

The methods described above have the benefit that they are easily modified by changing the concentrations, surfactants, or LC volumes used. For example, in project 4 I used the same techniques in method 2 but vary the concentration of the protein carbonic anhydrase (CA) instead of SDS.

Using these methods I propose to investigate the LC droplet configuration transitions between the radial and bipolar phases. In the next chapters I will detail the specific concentrations, surfactants, results, discussion, and conclusion.

3.3 Approach

To complete each objective, I will first characterize the configuration of many droplets, in equilibrium, as a function of surfactant concentration and droplet diameter using method 1 described above. After characterizing the configuration of the droplets at several concentrations for each surfactant in the project, I will perform the dynamic transition experiments using method 2.

For project 1 I will measure the SDS concentration when a droplet begins and finishes a transition from the bipolar to radial configuration or vice versa.

In project 2 I will use both SDS and novel monomer surfactant. I will test the same configurational transition as a function of monomer concentration. I will also investigate keeping the monomer concentration constant and using SDS as the driving agent again.

In project 3 I being investigating trimeric surfactant molecules. Here we use a set of four related trimers that differ in the carbon tail length of one of their three hydrophobic ends. This is the thesis work of Ben Strain. No transitions are done in this project, but based on the characterization results it looks like the C8 trimer would be most effective as a transition driving agent.

Project 4 differs from the first three in that we try to use a protein instead of a surfactant to drive the transition between the bipolar and radial configurations. Unfortunately, our preliminary data suggest that the protein is not capable of changing a droplet's configuration.

CHAPTER 4

PROJECT 1: SDS

This chapter is largely reproduced from my paper [47]. Some figures were adjusted to fit within the margins of this document. Minor edits were made to fit in with the structure of the dissertation.

Although the steady-state orientation of LCs in the presence of surfactants has been studied in some detail, no direct experimental evidence existed that revealed the dynamics of the transition between bipolar to radial or from radial to bipolar configurations. Our collaborators have previously performed simulations to predict the dynamics in the orientational change from bipolar to radial [22, 2], but there were no measurements to test their predictions. The lack of empirical data arose from the experimental challenges of performing dynamic experiments where the surfactant concentration is changed while individual droplets stay in view.

We have developed an experimental method to overcome the challenge of directly measuring the LC configuration while changing the surfactant concentration in the background. We performed these experiments using droplets of 5CB in an aqueous SDS solution, and we used an optical tweezer to hold a single LC droplet while we slowly modified the SDS concentration. We changed the configuration from bipolar to radial, radial to bipolar, and performed cycles where the configuration was returned to the original state, all while monitoring the same droplet with known SDS concentrations. We compared the experimental results to the previous simulation predictions for the transition from bipolar to radial and created a new simulation to test the change in configuration from radial to bipolar.

4.1 Motivation

The novel technique demonstrated here provides an important step to understanding the behaviors of LC molecules during structural transitions. The simulations relate the optical results to molecular organization. The combination of experimental and theoretical predictions are particularly useful for testing future triggerable assemblies of LC emulsions, which could serve as a hierarchical building block for responsive materials on the macroscale.

4.2 Experimental Details

4.2.1 Equilibrium Configuration Experiments

LC emulsions were prepared by mixing 5CB liquid crystal into aqueous SDS surfactant solutions of varying concentrations. The concentration of the SDS was varied depending on the experiment from 100 μM to 2 mM in phosphate buffered saline (100 mM PBS, pH 7.6: 1.97 mM monobasic KH_2PO_4, 15.30 mM dibasic Na_2HPO_4, 148.86 mM NaCl). Using a 10 μL glass Hamilton syringe, 2 μL of 5CB LC was added to a culture tube with 98 μL of surfactant solution. The Hamilton syringe was washed with chloroform before and after each LC volume was taken and dried using filtered compressed air. The culture tube was sealed with parafilm and then agitated by flicking the culture tube to produce a polydisperse emulsion. We found that the degree of agitation had little effect on the polydispersity of the emulsion sample in our hands. To minimize the effect of any dodecanol impurity introduced by the SDS, we made a fresh SDS soluion each week [38, 12]. The oldest our SDS could have been was 4 days, from Monday to Friday.

To classify the configuration of the LC within droplets, LC samples were inserted either into a flow chamber made from a cleaned slide and cover slip (Fisherbrand, Fisher Scientific) separated by two pieces of permanent double stick tape (3M) or added to a 10 mm x 10 mm pyrex cloning cylinder (Fisher) attached to a clean cover

slip with epoxy. Cover glasses and slides were cleaned by washing with ethanol, deionized water, and ethanol again, and then air dried.

Images or movies of LC emulsion droplets were recorded at 5-10 frames per second using an inverted Nikon Ti-U microscope with polarization optics in the condenser and below the objective. Images were made using a 60x NA 1.2 water immersion objective to an Andor Zyla sCMOS camera where the magnified pixel size was 110 nm/pixel. The polarizer in the condenser was removed for regular transmitted light imaging.

Data were recorded using Nikon Elements and saved as .nd2 files with metadata attached. To record many droplets in different focal planes, image data were taken as movies over 3 min intervals while the stage was moved through the chamber. Each droplet recorded was quantified only once in the image analysis.

Images were analyzed using ImageJ/FIJI. Droplet diameter was quantified using a cross-section through the center of the droplet. Details on the quantification techniques are in appendix E. Each droplet was classified as radial, bipolar, monopolar, or other. Radial and bipolar are familiar configurations. We grouped all variations of monopolar configurations (monopolar, destroying boojum, sunset, and preradial) as monopolar, using the nomenclature from Prishchepa [40]. Droplets that could not be classified as radial, bipolar, or monopolar were classified as "other" and omitted from the data presented here. Percentages and N values reported are only for the classified droplets.

4.2.2 Dynamic Configuration Experiments

For experiments with dynamic control over the surfactant concentration, one or two-stacked cloning cylinders were epoxied to the cover glass (figure 4.1a). The inner diameter of the cylinder is 8 mm, and one cylinder can hold up to 500 μL of solution. To control the concentration of surfactant in the chamber, we attached a tube (Cole-

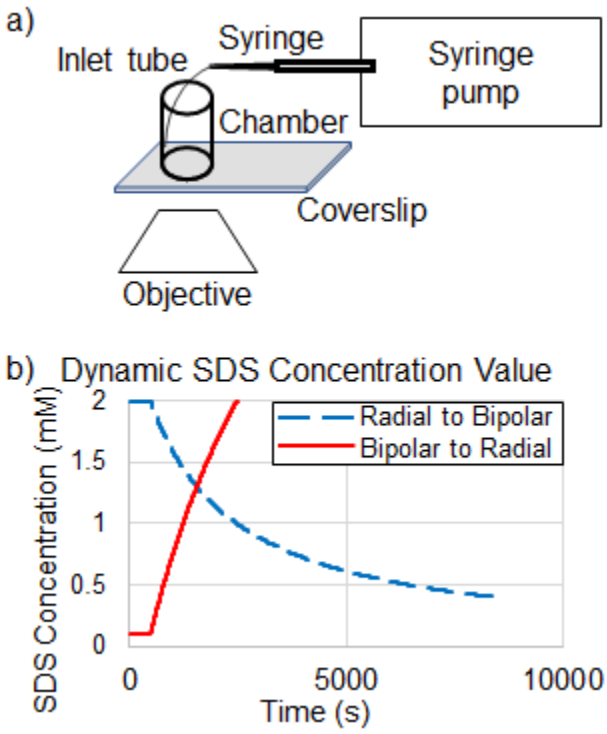

Figure 4.1. Dynamic configurational transition method. (a) Experimental apparatus to perform optical trapping uses a cylindrical chamber epoxied to a coverslip on an inverted microscope. SDS concentrations are altered using the inlet tube attached to a syringe on a syringe pump. (b) We estimated the change in SDS concentration over time for going from high to low SDS (radial to bipolar, blue dashed line) or from low to high (bipolar to radial, red solid line) using eq 4.1

Parmer) to the inside of the chamber wall with epoxy (figure 4.1a). The tube was connected to a syringe on a syringe pump (World Precision Instruments) so that the concentration change was controlled precisely (figure 4.1a). The length of tubing used was 330 mm with an internal volume of 24.1 μL.

In order to observe the exact same droplet while changing the surfactant solution, we held the droplet using an optical tweezer. The home-built optical tweezer was created using a fiber laser (λ = 1064 nm, maximum of 1 W, IPG Photonics) beam expanded to overfill the back aperture of the objective (60x, NA 1.2 water immersion, Nikon). At the focal point, the laser light held objects with an index of refraction higher than water. The index of refraction for the LC is approximately 1.5, making it

easy to capture. The laser power controlled the strength of the potential well, and we performed experiments at 50% power. Time-series data were collected as described above for 1-4 h.

The trapping power of the tweezers limited the speed at which we could change the solution concentration. If the inlet flow speed was too high, the flow in the chamber would dislodge the droplet from the optical tweezer. We found that 3 μL/min was the fastest we could flow without losing the droplet at 50% laser power. We chose this laser power to reduce the likelihood that another droplet would get pulled into the potential well of the trap and dislodge the first droplet during recording. Higher powers resulted in more droplets colliding with the trapped droplet. We also purposely trapped droplets on the opposite side of the chamber from the inlet tube to reduce collisions due to flow.

When performing experiments changing the surfactant concentration from low to high, we started the initial concentration of SDS at 100 μM so that droplets were stable and bipolar. Given the concentrations of the starting and flowed in solutions and the rate of buffer addition to the experimental chamber, we estimated the concentration of SDS using this equation:

$$C(t) = \frac{C_i V_i + C_f(rt - 24.1)}{V_i + (rt - 24.1)} \tag{4.1}$$

where $C(t)$ was the concentration as a function of time, t, C_i was the initial concentration of SDS, V_i was the initial volume of solution, C_f was the concentration of SDS flowed in, and r was the flow rate. The 24.1 denoted the dead volume, in μL, inside the tube delivering the new concentration of SDS from the syringe pump (figure 4.1a). The SDS concentration as a function of time is plotted in figure 4.1b.

Due to the volume limitations of the chamber (max 500 μL), we calculated the SDS concentration needed to reach 2 mM final SDS. Our final volume was 300 μL, our initial volume was 200 μL, so we added 5.8 mM SDS to the chamber. The SDS

concentration needed to trigger the configurational transition was less than the critical micelle concentration (CMC) of SDS, which is approximately 10 mM.

When performing experiments changing the SDS from high to low concentration, we started with an SDS concentration of 2 mM so that droplets were radial. In order to speed up the transition rate, we diluted the chamber using pure buffer (10 mM PBS, 0 mM SDS), and the final concentration was 400 μM SDS. The SDS concentration as a function of time, determined from eq 4.1, is plotted in figure 4.1b.

4.3 Theory

This section is reproduced from my paper [47]. Theory work was done by Ali Mozaffari, Noe Canas, and Rui Zhang who work in Juan de Pablo's research group.

Free Energy

The reorganization of LCs in droplets is described with a continuum model for the free energy of the material in terms of the tensorial order parameter of the LC, $\mathbf{Q}$, defined as

$$\mathbf{Q} = S(\hat{n}\hat{n} - \frac{1}{3}\mathbf{I}), \tag{4.2}$$

where S is the scalar order parameter, $\hat{n}$ is the director field, and $\mathbf{I}$ is the identity matrix [7]. The free energy functional (F) is the sum of two volumetric terms (Ω) and a surface energy contribution ($\partial\Omega$) given by:

$$F = F_{\mathrm{LdG}} + F_{\mathrm{Elas}} + F_{\mathrm{Surf}}, \tag{4.3}$$

where F_{LdG} is the Landau-de Gennes bulk free energy, F_{Elas} is the elastic free energy, and F_{Surf} is the surface free energy.

The Landau-de Gennes free energy [10] describes the isotropic-nematic transition

$$F_{\mathrm{LdG}} = \int_{\Omega} f_{\mathrm{LdG}} \mathrm{d}V. \tag{4.4}$$

This transition is described through a power series expansion of $\mathrm{Tr}(\mathbf{Q})$

$$f_{\mathrm{LdG}} = \frac{A}{2}\left(1 - \frac{U}{3}\right)\mathrm{Tr}\left(\mathbf{Q}^2\right) - \frac{AU}{3}\mathrm{Tr}\left(\mathbf{Q}^3\right) + \frac{AU}{4}\left[\mathrm{Tr}\left(\mathbf{Q}^2\right)\right]^2, \tag{4.5}$$

where parameter A denotes the energy density scale and U is a dimensionless, temperature dependent constant. The transition from isotropic to nematic occurs at $U = 2.7$.

Elastic distortions are modeled through the Frank-Oseen free energy[14]

$$F_{\mathrm{Elas}} = \int_{\Omega} f_{\mathrm{Elas}} \mathrm{d}V, \tag{4.6}$$

where f_{Elas} is the elastic free energy density for an achiral nematic given by

$$f_{\mathrm{Elas}} = \frac{1}{2}k_1\left(\nabla\cdot\hat{n}\right)^2 + \frac{1}{2}k_2\left[\left(\nabla\times\hat{n}\right)\cdot\hat{n}\right]^2 + \frac{1}{2}k_3\left[\hat{n}\times\left(\nabla\times\hat{n}\right)\right]^2. \tag{4.7}$$

Here k_1, k_2, and k_3 are the splay, twist, and blend elastic constants, respectively. This free energy can be expressed in terms of $\mathbf{Q}$ as follows[36]

$$F_{\mathrm{Elas}} = \frac{1}{2}\int\left\{L_1\frac{\partial Q_{ij}}{\partial r_k}\frac{\partial Q_{ij}}{\partial r_k} + L_2\frac{\partial Q_{jk}}{\partial r_k}\frac{\partial Q_{jl}}{\partial r_l} + L_3 Q_{jk}\frac{\partial Q_{lm}}{\partial r_j}\frac{\partial Q_{lm}}{\partial r_k}\right\}\mathrm{d}V, \tag{4.8}$$

where $\mathbf{r}$ is the position vector. The elastic constants k_i are related to the moduli L_i through the following expressions:

$$L_1 = \frac{1}{2S^2}\left[k_2 + \frac{1}{3}\left(k_3 - k_1\right)\right], \tag{4.9}$$

$$L_2 = \frac{1}{S^2}\left[k_1 - k_2\right], \tag{4.10}$$

$$L_3 = \frac{1}{2S^3}\left[k_3 - k_1\right]. \tag{4.11}$$

The anchoring of LC molecules at the droplet surface is accounted for by the following surface free energy expression

$$F_{\text{Surf}} = \int_{\partial\Omega} f_{\text{Surf}} \, \mathrm{d}S, \tag{4.12}$$

where f_{Surf} is the surface free energy density. For homeotropic (perpendicular) anchoring, the surface energy density is written in the common Rapini-Papoular form [43]

$$f_{\text{Surf}} = \frac{W_{\text{H}}}{2} \text{Tr}\left[(\mathbf{Q} - \mathbf{Q}_{\perp})^2\right], \tag{4.13}$$

where W_{H} is the strength of the homeotropic anchoring, $\mathbf{Q}_{\perp} = S\left[\hat{\nu}\hat{\nu} - \frac{1}{3}\delta_{ij}\right]$, and $\hat{\nu}$ is the unit vector normal to the surface.

For planar (parallel) anchoring, we use the Fournier-Galatola form [13]

$$f_{\text{Surf}} = \frac{W_{\text{P}}}{2} \text{Tr}\left[\left(\overline{\mathbf{Q}} - \overline{\mathbf{Q}}_{\perp}\right)^2\right], \tag{4.14}$$

where W_{P} is the strength of the surface anchoring related to the planar orientation, $\overline{\mathbf{Q}} = \mathbf{Q} + \frac{S}{3}\mathbf{I}$ its projection to the surface $\overline{\mathbf{Q}}_{\perp} = \Upsilon \cdot \overline{\mathbf{Q}} \cdot \Upsilon$, and $\Upsilon = \mathbf{I} - \hat{\nu}\hat{\nu}$.

Temporal Evolution

The evolution of $\mathbf{Q}$ is determined using a Ginzburg-Landau equation

$$\partial_t \mathbf{Q} = \frac{1}{\gamma}\mathbf{H} \tag{4.15}$$

where γ is the rotational viscosity and $\mathbf{H}$ is the molecular field that relaxes the system towards the minimum of free energy, defined as [31]

$$\mathbf{H} = -\frac{\delta F}{\delta \mathbf{Q}} + \frac{1}{3}\text{Tr}\left[\frac{\delta F}{\delta \mathbf{Q}}\right]\mathbf{I}. \tag{4.16}$$

The simulation domain was discretized into 10^6 elements, each with a discrete length equal to the nematic coherence length of 10 nm. The following set of values were used to describe our experimental system: $A \approx 10^5$ J/m^3, $k_1 = k_2 \approx 7.0$ pN, $k_3 \approx 9.5$ pN, $\gamma \approx 0.1$ Pa·s, for a room temperature $U \approx 3.5$ which resulted in an equilibrium value of $S \approx 0.62$; the nematic coherence length was set to $\lambda_N = 10$ nm [2, 5, 9, 3]. We simulated a droplet with diameter of $100\lambda_N$ and $200\lambda_N$ and observed similar behavior. Since the behavior does not appear to depend on mesh size, for the sake of computational cost, simulations and results shown here are using the $100\lambda_N$ model.

The transition from a bipolar to a radial configuration was simulated by initializing the bipolar configuration with two boojums at the poles. The anchoring was then changed to homeotropic by imposing a moderate anchoring strength of $W_H = 0.25$ mJ/m^2. The evolution of the morphology was followed as the droplet transitioned from bipolar to radial.

The transition from radial to bipolar started from a radial configuration with a hedgehog defect of +1 topological charge at the center. The anchoring strength was reduced to a weak homeotropic ($W_H = 0.0025$ mJ/m^2), which drived the point defect to the surface. This configuration evolved into a uniform, defect-free state (homogeneous nematic). Finally, we applied a relatively strong planar anchoring of strength $W_P = 1.0$ mJ/m^2 to further push the droplet into a bipolar configuration.

4.4 Results and Discussion

4.4.1 Equilibrium Configuration of LC Droplets Depends on the Droplet Diameter and the SDS Concentration

In order to observe the configurational transition of spherical LC droplets triggered by a changing surfactant concentration, we needed to know the concentrations of surfactant that resulted in a specific orientation of the LC. We created emulsions

by agitating 5CB with solutions of known SDS concentration and directly imaged with cross-polarizers to determine the equilibrium morphology. We classified these as radial, bipolar, or monopolar. Droplets that were difficult to classify were eliminated from the measurement.

Using agitation to create droplets caused the size distribution to become polydisperse, and the LC configuration depended both on the size of the droplet and SDS concentration [19]. The largest measured droplet was around 80 μm in diameter; most droplets were below 20 μm in diameter (89.6% of droplets). We characterized the droplet configuration and diameter at various SDS concentrations: 100 μM (N=201), 300 μM (N=161), 600 μM (N=135), 1 mM (N=104), 2 mM (N=96) (Figure 4.2). We used this range of concentrations because we were able to create stable droplets at the lowest concentration, and we were below the critical micelle concentration (CMC) for SDS: 10 mM. SDS is known to change the surface tension over time, so we were careful to make new SDS weekly for all our samples [38, 12]. Additionally, we imaged samples within 8 h of emulsification.

We found that bipolar and monopolar droplets are most common at the lowest two concentrations (figure 4.2b, c). At an SDS concentration of 600 μM, almost all droplets were radial; only two droplets were bipolar and three were monopolar (figure 4.2d). Somewhat surprisingly, given prior reports [20], we found a significant fraction (84.6% of droplets) were radial even at the lowest concentration of SDS. On the basis of these equilibrium results, we performed dynamic experiments by changing the SDS concentration between 100 μM and 2 mM SDS.

4.4.2 Configurational Transition from Bipolar to Radial

Our goal was to directly visualize the LC configurational transition from bipolar to radial for a droplet by increasing the SDS concentration. We used an optical tweezer to hold one LC droplet while a syringe pump slowly changed the SDS surfactant

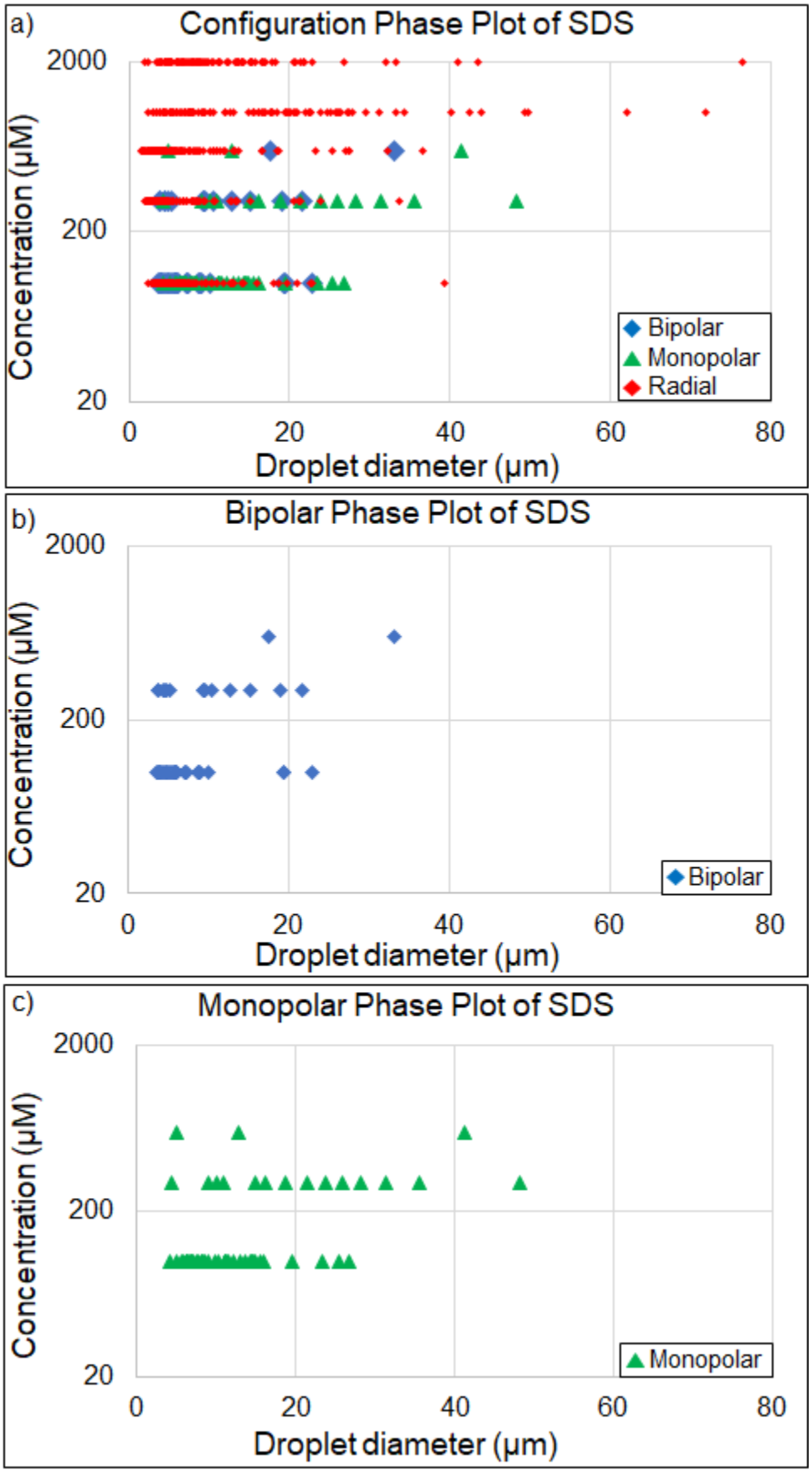
a)
Configuration Phase Plot of SDS
Concentration (μM)
2000
200
20
0
20
40
60
80
Droplet diameter (μm)
Bipolar
Monopolar
Radial
b)
Bipolar Phase Plot of SDS
Concentration (μM)
2000
200
20
0
20
40
60
80
Droplet diameter (μm)
Bipolar
c)
Monopolar Phase Plot of SDS
Concentration (μM)
2000
200
20
0
20
40
60
80
Droplet diameter (μm)
Monopolar

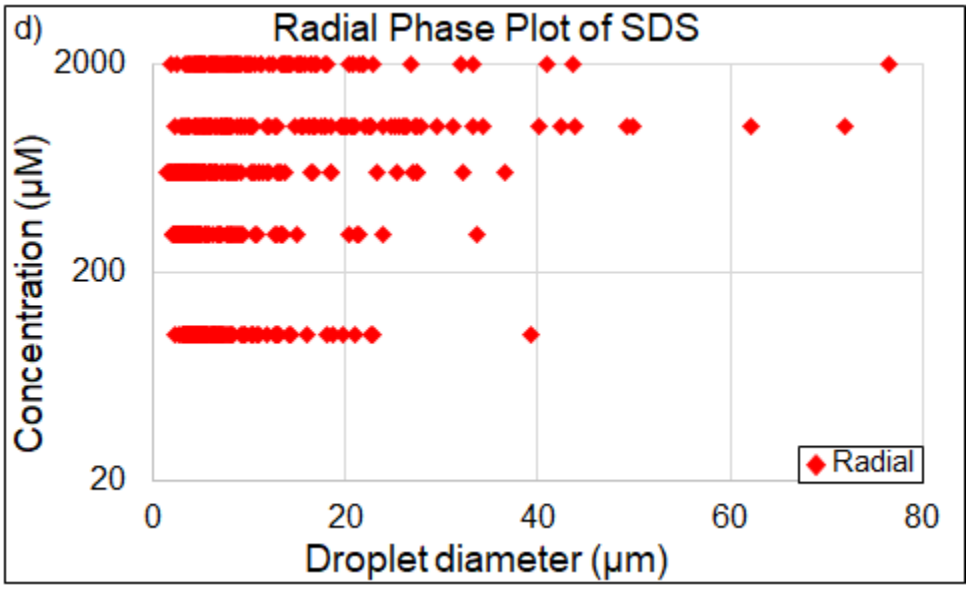

Figure 4.2. Concentration-diameter phase diagram of the 5CB liquid crystal droplets as a function of droplet diameter and SDS concentration. (a) All configurations including bipolar (blue diamonds), monopolar (green triangles), and radial (red diamonds) represented together. (b) Same data as part a with only bipolar droplets shown. (c) Same data as part a with only monopolar droplets shown. (d) Same data as part a with only radial droplets shown.

concentration from 100 μM to 2 mM (figure 4.3a-c). Prior to adding extra SDS, the droplet was clearly in the bipolar configuration, as viewed through cross-polarizers (Figure 4.3a). The droplet was in the bipolar configuration for about 10 min before the transition began (Figure 4.3b).

During the transition between the bipolar and radial structures we observed the formation of a ring defect across the equator of the droplet, which signified the start of the transition and that the droplet was now in the axial configuration (figure 4.3b, 630.4 s). As time progressed and SDS concentration continued to increase, the ring defect contracted along the surface of the droplet until the ring collapsed to a point at the surface (figure 4.3b, 630.4—645.8 s). The point defect lived on the surface for a brief lifetime (figure 4.3b, 645.8—652.1 s) before moving into the center of the droplet creating a volumetric hedgehog defect (figure 4.3b, 655.2 s). After the defect came to

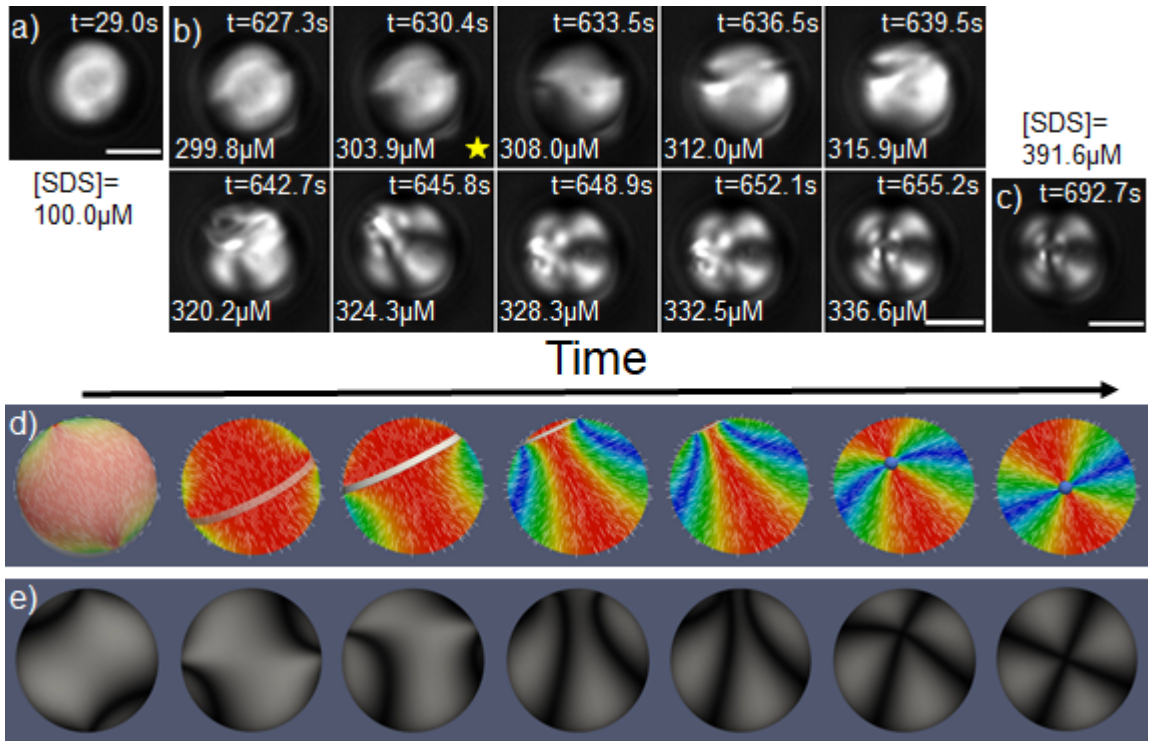

Figure 4.3. Example time-series and simulation of bipolar to radial transition. (a) Initial image of bipolar droplet held with optical tweezers and imaged with cross-polarizers at an initial SDS concentration of 100 μM at time of 29 s. (b) Time-series of bipolar to radial transition of same droplet in (a) progressing over time (627.3 s—655.2 s) and SDS concentration (299.8 μM—336.6μM). (c) Final image of radial droplet at time 692.7 s and SDS concentration of 391.6 μM. All scale bars denote 10 μm. (d) Simulated time-series of bipolar to radial transition using rainbow scale to denote LC director. The highlighted region denotes molecules that are parallel to the surface. (e) Same simulation rendered as if viewed via cross-polarizers.

rest at the center of the droplet, it was in the radial configuration, and the transition was complete. We monitored each droplet for some time after the configurational transition was complete and detected no further changes in the configuration (figure 4.3c).

Previously, we used time evolution of the free energy for LCs to simulate molecules confined in spherical droplets and predicted the structure inside the droplet during the transition from bipolar to radial [2]. We have recreated the simulation for the bipolar to radial transition in figure 4.3d,e. In the simulations, the bipolar droplet

transitioned to the axial configuration and then transformed into the radial configuration, in agreement with our experimental results (figure 4.3a-c, d). The movement of the ring defect along the droplet's surface, its collapse into a point, and finally its descent into the center of the droplet were also predicted by these simulations (figure 4.3d, e). We found that there was a narrow window of anchoring strength (W_H) where one could obtain the behavior observed in experiments. At higher anchoring strengths, either the ring defect shrunk to the point defect at the center of the droplet directly, or a stable loop defect formed around the equator.

We also compared the time scales of the transitions between the experiment and model. In the experiment, the dynamics could be broken into three regimes: (1) collapse of the ring defect into a point on the surface, (2) pausing of the surface defect, and (3) movement of the point defect from the surface to the center. For each of these regimes, the duration was compared between the simulation and the experiment. Simulations predicted that the collapse of the ring (Regime 1) should take longer than the motion of the defect to the center (Regime 3), which we also observed experimentally. One difference between the experiment and the simulation was that the pausing of the defect at the surface (Regime 2) was absent in the simulations. This difference could be due to the slower change in anchoring when real molecules were engaging at the surface, possibly causing a gradient in the anchoring strength over time. It could also be due to the fact that hydrodynamic effects are not included in these calculations. Future work could directly probe altered anchoring strengths or schemes.

In order to directly compare the simulation to the experiment, we represented the molecular organizations as simulated images as if viewed through cross-polarizers (figure 4.3e). Interestingly, the simulated droplet images did not show the same white highlight of the ring defect that we observed in the real droplets (figure 4.3b). One possible explanation is that the index of refraction of the surfactant is not accounted

for in the simulation. Since surfactant concentration is higher at the defect, changing the local index of refraction, we were able to optically visualize the ring in experiments [52].

4.4.3 Configurational Transition from Radial to Bipolar

Using the same method, we directly visualized the configurational transition from radial to bipolar for a droplet by decreasing the SDS concentration from 2 mM to 400 μM (figure 4.4a-c). We could not dilute down to 100 μM SDS due to volume constraints of the chamber, but we found that the droplets were able to change configuration in our experiments. Prior to flowing in buffer, the droplet was clearly radial, as viewed through cross-polarizers (figure 4.4a). The droplet remained in that radial state for about 50 min before the transition began.

Qualitatively, the radial to bipolar transition appeared to be the exact reverse of the bipolar to radial transition. The defect moved to the edge of the droplet (Regime 1), stayed at the surface for a brief time (Regime 2: pause), and then transitioned into a ring defect on the surface that expanded to the equator (Regime 3), eventually relaxing to an orientation parallel to the surface (Figure 4.4b). These same dynamics were observed for all droplets.

Some, but not all droplets, showed an oscillation in the transition. In the example shown, the point defect moved to the surface (Regime 1), became a ring (Regime 3), and temporarily collapsed back to a point on the surface (Regime 2) (figure 4.4b, 584.1 – 688.2s). The monopolar configuration, with the defect on the edge (Regime 2), remained paused for some time (figure 4.4b, 688.2 – 757.4 s). When the ring defect collapsed back to a point, it never re-entered the droplet's bulk. Finally, this point defect was observed to expand into a ring again and commit to the transition to bipolar (Regime 3) (figure 4.4b, 792.2 – 1034.8 s). The ring defect was visible at the equator for some time (figure 4.4b, 930.8 – 965.5 s), signaling the axial configuration.

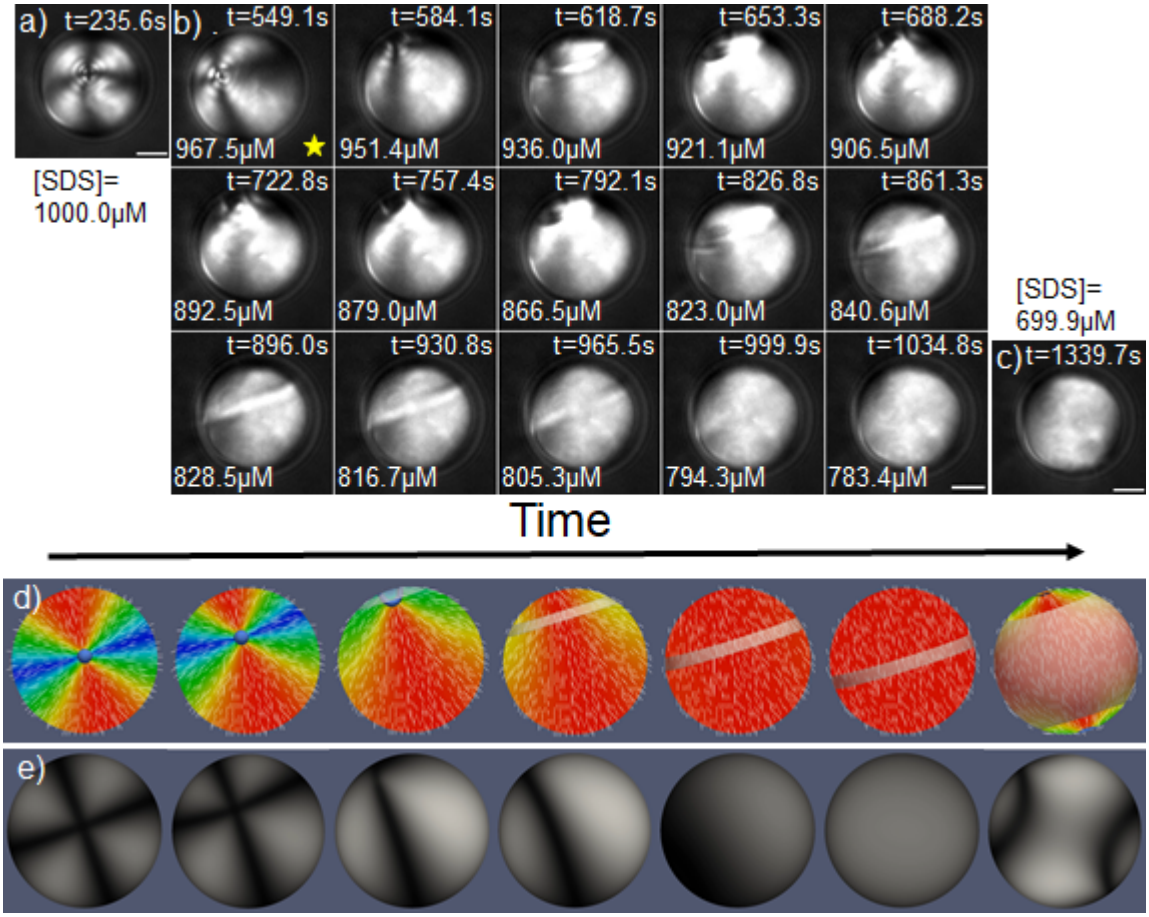

Figure 4.4. Example time-series and simulation of radial to bipolar structural transition. (a) initial image of radial droplet held with optical tweezers and imaged with cross-polarizers at an initial SDS concentration of 1 mM at time of 235.6 s. (b) Time-series of radial to bipolar transition of same droplet in (a) progressing over time (549.1 s—1034.8 s) and SDS concentration (967.5 μM—783.4μM). (c) Final image of bipolar droplet at time 1339.7 s and SDS concentration of 699.9 μM. All scale bars are 10 μm. (d) Simulated time-series of radial to bipolar transition using rainbow scale to denote LC director. The highlighted band denotes molecules that are parallel to the surface. (e) Same simulation rendered as if viewed via cross-polarizers.

Eventually, the defect ring faded away (figure 4.4b, 999.9 s) as the droplet took on the bipolar configuration (figure 4.4b, 1034.8 s). As before, we continued to monitor the droplet for some time to determine that the transition was complete and the droplet was stable in the bipolar configuration (figure 4.4c).

Although we have previously predicted the transition from bipolar to radial [2], no prior predictions existed for the radial to bipolar transition. Using the same time evolution approach, we were able to find a parameter space to simulate the same basic dynamics we observed in experiments (figure 4.4d). The highlighted band around the droplet that widens at the end of the simulation is the region on the surface of the droplet where there is perfect planar anchoring of the LC. A perfectly bipolar droplet should be totally highlighted (figure 4.4d).

We could not find a single value of the anchoring strength that could perfectly reproduce the experimental results. In order to recapitulate the experiments, we first weakened the perpendicular anchoring strength (W_H) to drive the point defect to the surface (Regime 1). With the same weak anchoring, this system evolved to a uniform nematic without defects within the spherical droplet (figure 4.4 d, second to last frame). This structure is reminiscent of a homogeneous tactoid where the two defects are positioned at infinity. In order to transition to the bipolar structure, the planar anchoring was increased in a stepwise manner to a relatively high level ($W_P = 1.0$ mJ/m). It is interesting that the entire transition from radial to bipolar could not be performed with a single anchoring strength. Yet, the motion of the defect from the center to edge, and the creation of the ring defect were all accomplished with almost no anchoring of any kind ($W_H = 0.0025$ mJ/m). One might have expected that a strong parallel anchoring would drive the entire transition, but we found the simulated dynamics did not proceed in the same pathway observed experimentally when W_P was high from the start of the simulation.

4.4.4 Hysteresis in the Configurational Transition

We repeated these experiments to observe multiple droplets transitioning in one direction, either bipolar to radial (N = 6) or radial to bipolar (N = 7), to determine if the dynamics were consistent. Each of these transition measurements were performed in a different chamber on a unique droplet. We quantified the droplet diameter and estimated the concentration values of the configurational transition for each droplet (figure 4.2a, eq 4.1). We compared the concentration at which the configurational transition started and the droplet diameter for all droplets (figure 4.4.4a). We found that the radial to bipolar transition occurred at a higher SDS concentration for all droplets, on average, regardless of the droplet size (diameters between 5 and 40 μm).

Given that the droplet size was inconsequential, we averaged the concentrations over all droplets for transitions of the same type. We determined the SDS concentration when the transition was initiated and completed. The final condition for the bipolar to radial transition was identified as when the hedgehog defect stopped moving toward the center of the droplet. The final condition for the radial to bipolar transition was when the ring defect disappeared, signaling the end of the intermediate axial configuration. The average concentrations were plotted on a phase diagram where the vertical axis denotes the configuration of the droplet (figure 4.4.4b). Interestingly, the complete transition for the bipolar to radial occurred over a lower SDS concentration range ($\sim$400—500 μM) than the complete radial to bipolar transition ($\sim$750—900 μM).

The unidirectional configurational transition results implied that there was hysteresis in the transition. In order to double check that the hysteresis was not an artifact of averaging over several unique droplets, with different diameters, that only transition in one direction, we performed experiments where we cycled the SDS concentration for a single droplet. We observed that for both the bipolar to radial to bipolar transition (figure 4.4.4c) and the radial to bipolar to radial transition (figure

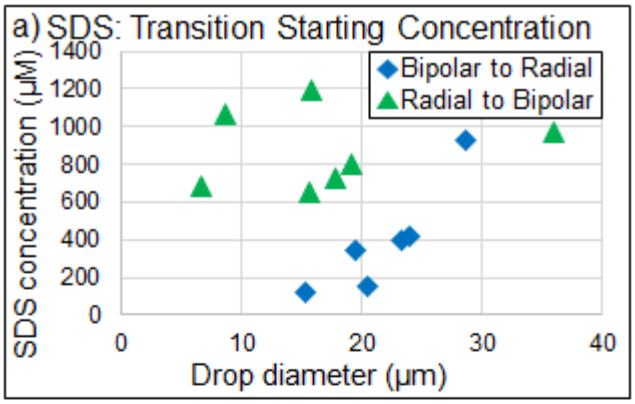
a) SDS: Transition Starting Concentration
SDS concentration (μM)
1400
1200
1000
800
600
400
200
0
0
10
20
30
40
Drop diameter (μm)
Bipolar to Radial
Radial to Bipolar

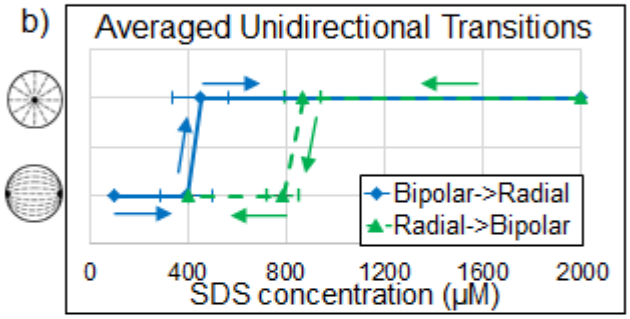
b)
Averaged Unidirectional Transitions
Bipolar->Radial
Radial->Bipolar
0
400
800
1200
1600
2000
SDS concentration (μM)

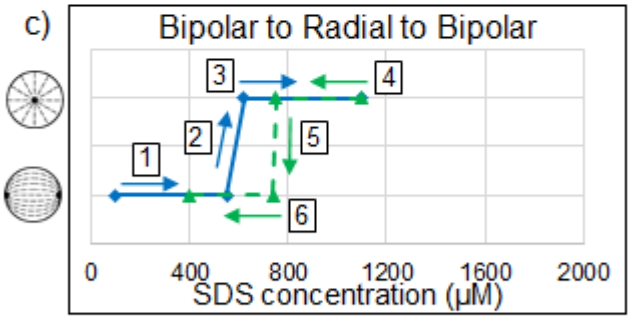
c)
Bipolar to Radial to Bipolar
1
2
3
4
5
6
0
400
800
1200
1600
2000
SDS concentration (μM)

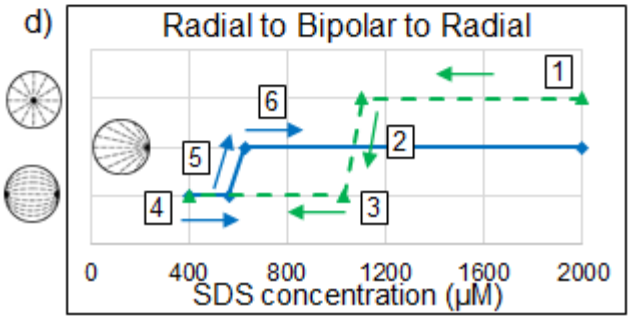
d)
Radial to Bipolar to Radial
1
2
3
4
5
6
0
400
800
1200
1600
2000
SDS concentration (μM)

Figure 4.5. Surfactant concentration for structural transitions. (a) SDS concentration that each droplet transitioned from bipolar to radial (blue diamonds, N = 6) or from radial to bipolar (green triangles, N = 7). (b) Average SDS concentrations for droplets that transition. LC configuration denoted on the y-axis. Mean values of transition concentrations are given for bipolar to radial (blue diamonds) or radial to bipolar (green triangles). Error bars denote the standard error of the mean of the distribution. Transitions denoted for bipolar to radial (blue solid line) and radial to bipolar (green dashed line). Arrows denote the direction of the transition. (c) Cyclic driving of configurational transition from bipolar to radial to bipolar for the same droplet. The cycle stages follow from 1 to 6. (d) Cyclic driving of configurational transition from radial to bipolar to radial for the same droplet. The cycle stages follow from 1 to 6. This droplet never returned to the radial configuration, but stayed in a monopolar state. Blue denotes bipolar to radial; green denotes radial to bipolar.

4.4.4d), the same hysteresis was observed, adding validity to our averaged results (figure 4.4.4b). Data taken for these full cycle experiments had a time interval of 300 ms between frames.

Surprisingly, for the radial to biopolar to radial cycle, we observed that the radial configuration was never re-established fully, even after increasing the SDS concentration all the way back up to 2 mM. The droplet stayed in the preradial configuration, with a single point defect on the droplet's surface. To indicate this difference, the hysteresis diagram does not complete a full loop (figure 4.4.4 d). Despite the incomplete transition back to radial, the same hysteresis pattern is observed where the transition from bipolar to radial occurs at a lower concentration than the transition from radial to bipolar (figure 4.4.4 d).

The hysteresis of the structural transition curves implied that there was a range of intermediate SDS concentrations where the droplet could fluctuate between the bipolar or radial configurations ($\sim$400—600 μM). Examining the equilibrium configuration of the droplets in this SDS concentration range, we found that droplets displayed bipolar, monopolar, and radial configurations in this same range (figure 4.2 a-d). Further evidence of the "indecisiveness" of droplet configuration in this inter-

mediate concentration range was the pausing in the dynamics and the reversals we observed (figures 4.3 and 4.4).

4.5 Conclusions

We performed new experiments to empirically observe the structural transition for 5CB LC confined to a spherical geometry. We observed a single droplet, held by an optical tweezer, and triggered the morphological change through alterations in SDS surfactant concentration, which controlled the interface anchoring of the LCs in the droplets. For each transition, we also simulated the expected molecular organization of the LCs in the droplet. Qualitatively, the simulations captured the dynamics we observed experimentally with minor differences in the time of the dynamics and the ability to observe the ring defect on the droplet. The experiments showed hesitation and oscillation in the dynamics, likely due to the slow change of surfactant molecules required to perform the experiment. We anticipate that future studies using this technique will enable direct visualization of LC droplets changing configuration with a variety of surfactants. Novel designer surfactants could display different transition pathways. Future work could also include fluorescently labeled surfactants to report on their location before, after, and during the configurational transition. Further, light or other additives could be used to trigger the configurational change by driving changes in the local surfactant concentration.

CHAPTER 5

PROJECT 2: SDS AND MONOMER

This project involves a novel surfactant that was synthesized in the Thayumanavan lab. It is a monomeric surfactant in that it has only one hydrophobic domain (red) and one hydrophilic domain (blue) (figure 5.1). Throughout this chapter and the rest of the dissertation, I will refer to this molecule as "Monomer". This is the only monomeric surfactant we use and with a capital "m" it helps distinguish between other times where I might want to use the word monomer to refer to a sub-unit of a polymer.

5.1 Motivation

There are two main goals of this project. The first is to compare SDS, which we studied in project 1, to a system of pure Monomer. This is an interesting comparison to investigate because both SDS and Monomer are monomeric. The main differences between these two surfactants is that SDS has a hydrophilic "head" group instead of

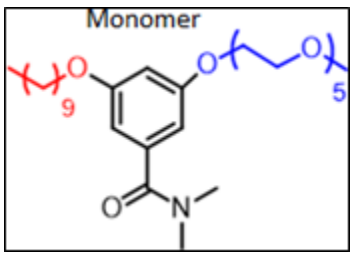

Figure 5.1. Chemical structure of the Monomer surfactant. Reproduced from figure 2.1 b.

a hydrophilic tail like the Monomer. The second difference is that hydrophilic head group of SDS carries a negative charge (figure 2.1 a).

The second goal of this project is to investigate how a two surfactant system behaves. We can think of using Monomer as a dopant to an SDS system and study how this will affect the configuration phase space of the droplets and the transition dynamics that we saw in project 1. Using dopants in any system can be a powerful tool because they can cause significant behavioral changes with a small amount of material.

5.2 Experimental Details

The sample preparation and emulsification process used in this project are the same as those previously described in sections 3.2.1, 3.2.2, and 4.2.

As before, samples are made of 2 μL 5CB liquid crystal (LC) and 98 μL of surfactant solution. Using the cylindrical chamber, 50 or 100 μL of surfactant solution is added to the chamber before 50 μL of LC emulsion is added to make characterization measurements.

For the transition experiments, there are 4 types to define. Two are SDS driven and **two are Monomer driven.** For the SDS driven transitions, the bipolar to radial transition starts with an SDS concentration of 0 mM and ends at 2 mM while maintaining 50 μM Monomer. Note that this is slightly different from the SDS only system in the previous chapter where we started at 100 μM SDS. The reason why we can start all the way down at 0 μM here is because the 50 μM of Monomer present is sufficient to stabilize the LC droplets against coalescence. For the SDS driven radial to bipolar transition, the SDS concentration starts at 2 mM and decreases down to 400 μM, while maintaining 50 μM Monomer.

PENDING LAB WORK IN JULY For the Monomer driven transitions there is no SDS in the system. For the bipolar to radial transition, we start with an initial

concentration of 75 μM and end at 750 μM. For the radial to bipolar transition we start at 750 μM, but are only able to dilute down to 150 μM due to volume constraints in the chamber.

5.3 Results and Discussion

5.3.1 Equilibrium Configuration Experiments

5.3.1.1 Monomer Only

Just as we made a concentration vs diameter configuration plot of the pure SDS system (figure 4.2) in the previous chapter, we can do the same using a pure Monomer system. Because the CAC of the Monomer is 75 μM, we decided to take data at 5 concentrations: 2 below the CAC, 1 at the CAC, and 2 above the CAC, spanning an order of magnitude in either direction. The Monomer concentrations we measured were 7.5 μM, 37.5 μM, 75 μM, 37.5 μM, and 750 μM. We present the data in the same style as figure 4.2.

What we see is that concentrations below or at the CAC, 7.5 μM (98.7% bipolar), 37.5 μM (97.5% bipolar)), and 75 μM (100% bipolar)), are dominated by the bipolar configuration. At the two concentrations above the CAC, 375 μM (55.5% radial) and 750 μM (50% radial), we see a mix of configurations, but at least half are radial. If we compare figures 4.2 a and 5.2 a, we notice that for both surfactants radial droplets are more common at high surfactant concentrations.

For the same reasoning as in project 1 with only SDS, we hypothesize that if you start with a low concentration of Monomer in a system and increase the Monomer concentration, it may be possible to cause a transition from the bipolar to radial configurations.

One thing to keep in mind is that for the Monomer data the radial concentrations were above the CAC, meaning that there must be aggregates of surfactant in the system. It is possible that the presence of aggregates somehow influences the droplet

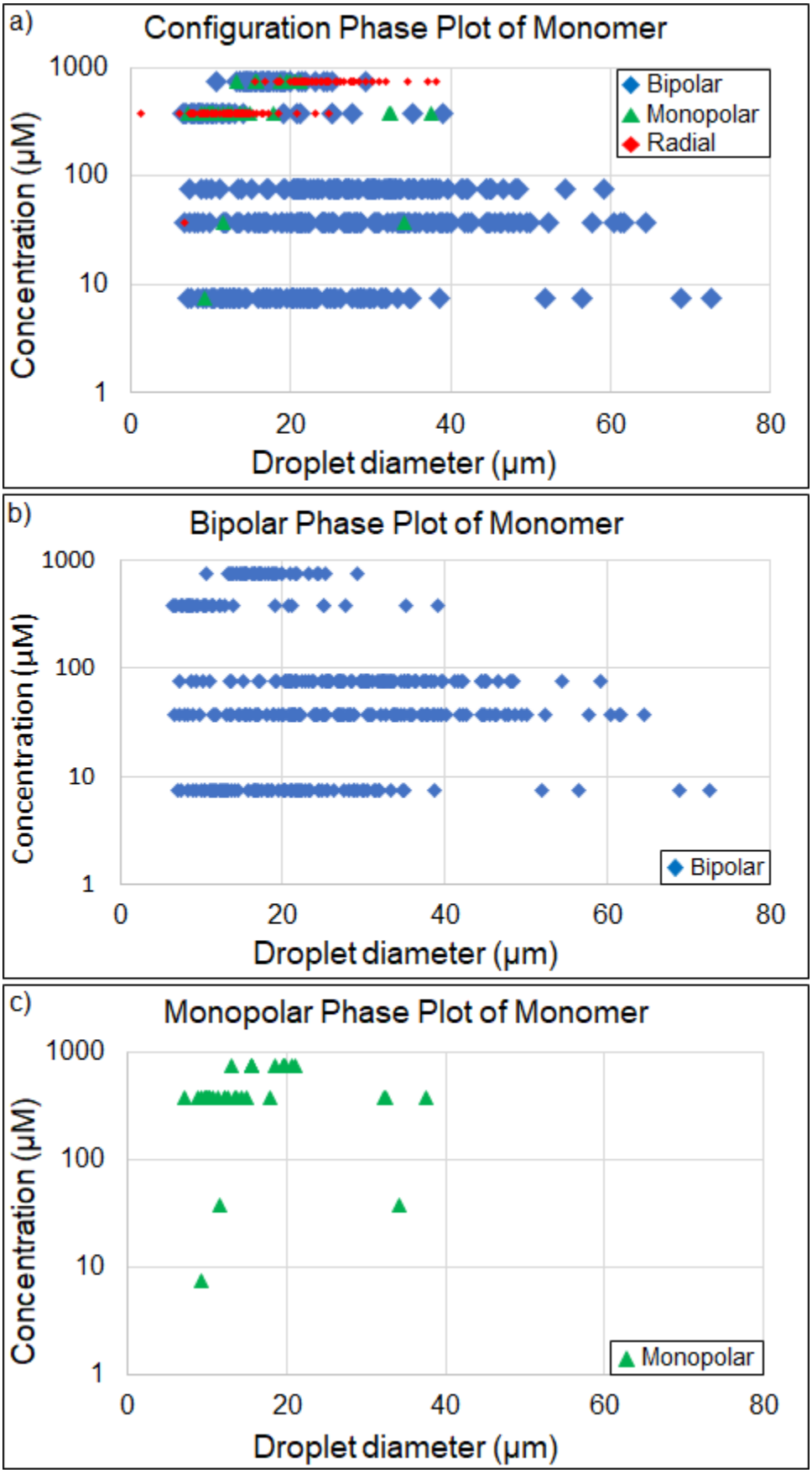
a)
Configuration Phase Plot of Monomer
Concentration (μM)
1000
100
10
1
0
20
40
60
80
Droplet diameter (μm)
Bipolar
Monopolar
Radial
b)
Bipolar Phase Plot of Monomer
Concentration (μM)
1000
100
10
1
0
20
40
60
80
Droplet diameter (μm)
Bipolar
c)
Monopolar Phase Plot of Monomer
Concentration (μM)
1000
100
10
1
0
20
40
60
80
Droplet diameter (μm)
Monopolar

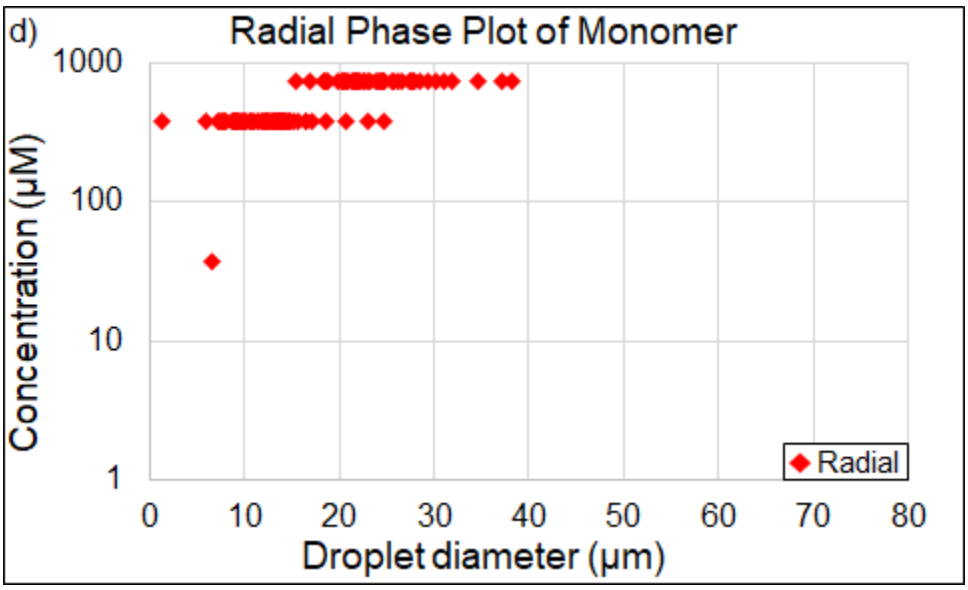

Figure 5.2. Concentration-diameter phase diagram of the 5CB liquid crystal droplets as a function of droplet diameter and Monomer concentration. (a) All configurations including bipolar (blue diamonds), monopolar (green triangles), and radial (red diamonds) represented together. (b) Same data as part a with only bipolar droplets shown. (c) Same data as part a with only monopolar droplets shown. (d) Same data as part a with only radial droplets shown.

configuration, because even at the CAC of 75 μM we did not observe the radial configuration. We chose SDS concentrations below the CMC and were able to still get radial droplets. Even in the highly concentrated SDS solution used to increase the SDS concentration in the experimental chamber we did not go above the CMC.

One potential hurdle is that to get to a final concentration of 750 μM, we need a flowed in concentration of about 3 times that, and our stock concentration is only 1000 μM. If we used all the available volume in the chamber, we can get closer, but it'll still be difficult. It also means that we can not do many experiments if we are taking straight from the stock. The transition might be at a lower concentration, because it looks like it is somewhere between 75 μM and 375 μM, which gives us much more flexibility.

So, it might be easier to just use the Monomer as a dopant in a Monomer-SDS mixed system.

5.3.1.2 Monomer and SDS

We wanted to keep the concentration of Monomer lower than the SDS concentration (otherwise SDS would be the dopant), and we also decided to keep it lower than the CAC so that no aggregates of Monomer existed in solution. We chose to use 50 μM as our fixed Monomer concentration. We used the same 5 SDS concentrations from project 1: 100 μM, 300 μM, 600 μM, 1 mM, and 2 mM.

The results of figure 5.3 a-d brings good new and bad news. Bad news first. The bad news is that qualitatively plots 4.2 a (the SDS only plot) and 5.3 a are fairly similar. What I mean is that the bipolar and monopolar configurations seem to be less frequent in general, but still more common at the lowest SDS concentrations of 100 μM (47.1% bipolar and 32.4% monopolar). We also observe primarily radial droplets at the three highest concentrations of 600 μM (91.5% radial), 1 mM (100% radial), and 2 mM (96% radial). At the intermediate concentration of 600 μM SDS, we see a mix of all three configurations (16.7% bipolar, 16.7% monopolar, 66.7% radial) We also see radial droplets at every SDS concentration, similar to 4.2 d. That means that the presence of the Monomer dopant, at a concentration of 50 μM, does not have a large affect on the equilibrium configurations.

The good news is that we can still ask the question, "How does the presence of Monomer affect the *transition* between configurations?" Because when we look the configurations at a concentration of less than 75 μM Monomer and 0 μM SDS (figure 5.2 a) we see primarily bipolar droplets but at concentrations of 50 μM Monomer and 2 mM SDS (figure 5.3 a) we see many radial droplets. So, we still expect a transition if we keep the Monomer concentration fixed at 50 μM and increase the SDS concentration from 0 to 2 mM.

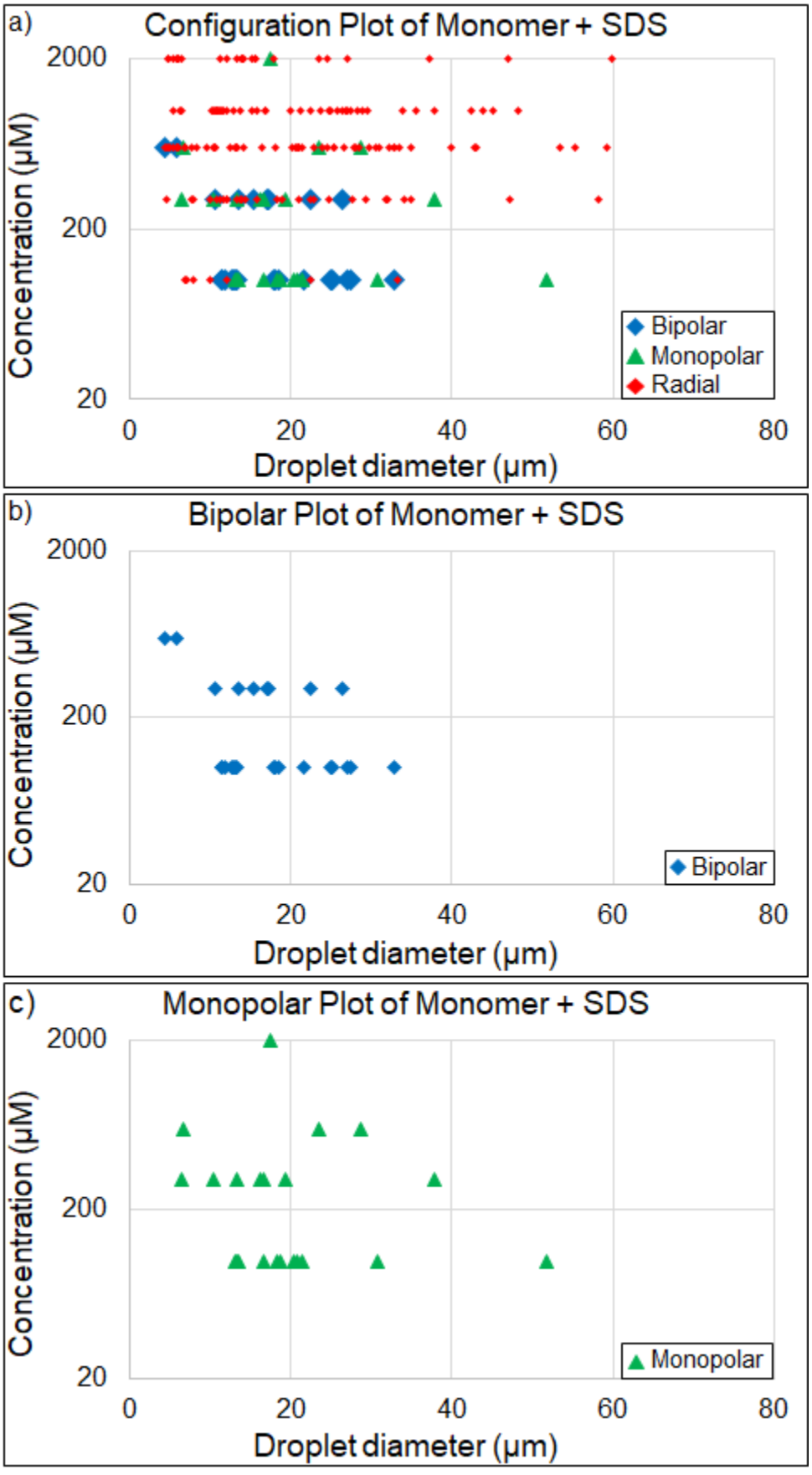
a)
Configuration Plot of Monomer + SDS
Concentration (μM)
2000
200
20
0
20
40
60
80
Droplet diameter (μm)
Bipolar
Monopolar
Radial
b)
Bipolar Plot of Monomer + SDS
Concentration (μM)
2000
200
20
0
20
40
60
80
Droplet diameter (μm)
Bipolar
c)
Monopolar Plot of Monomer + SDS
Concentration (μM)
2000
200
20
0
20
40
60
80
Droplet diameter (μm)
Monopolar

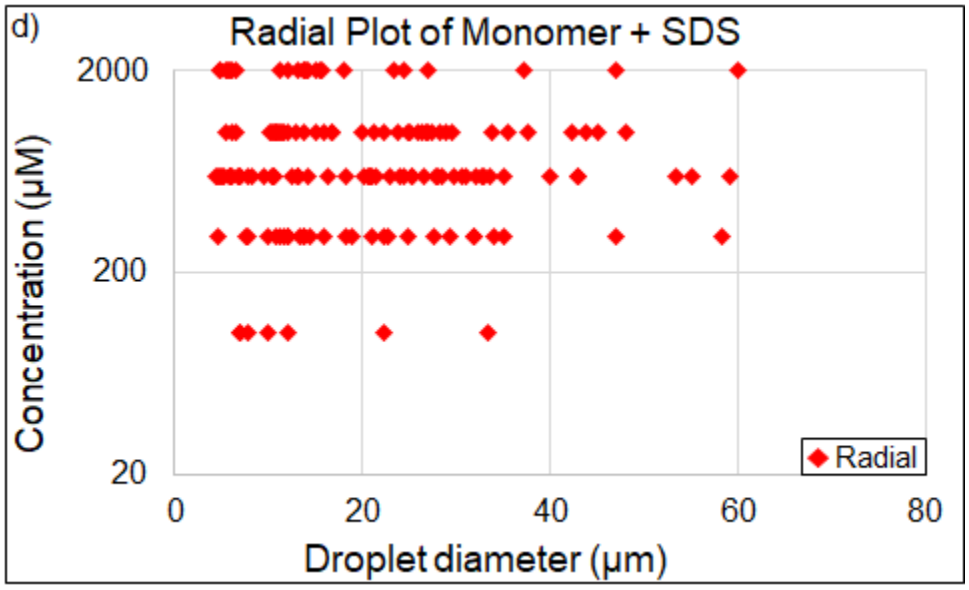

Figure 5.3. Concentration-diameter phase diagram of the 5CB liquid crystal droplets as a function of droplet diameter and SDS concentration, with a constant 50 μL Monomer present. (a) All configurations including bipolar (blue diamonds), monopolar (green triangles), and radial (red diamonds) represented together. (b) Same data as part a with only bipolar droplets shown. (c) Same data as part a with only monopolar droplets shown. (d) Same data as part a with only radial droplets shown.

5.3.2 Dynamic Configuration Experiments

Using the same techniques previously described, we performed the transition experiments using just Monomer, or SDS doped with Monomer.

Using the same techniques previously described, we performed the transition experiments using a different set of surfactants. The dynamics of the transitions and intermediate states are exactly the same as in the previous chapter, though we will see differences in *when* the concentrations happen.

5.3.2.1 Monomer Only

This work is ongoing in the lab and at the time of writing there are no significant results to share. Preliminary experiments suggest that the increasing the Monomer concentration from 75 μM to 750 μM does not cause a bipolar to radial transition.

5.3.2.2 Monomer and SDS

CHECK ME We did several repeats of each unidirectional transition. We show 11 transitions from bipolar to radial as red diamonds in figure 5.3.2.2 a. The 8 blue triangles in 5.3.2.2 a are for the radial to bipolar transitions. The size of the droplet is plotted on the x-axis and the SDS concentration that the transition starts is plotted on the y-axis. Recall that the "start" of the transition depends on which type of transition it is. A bipolar to radial transition starts when the droplet goes into the axial configuration and a ring defect forms on the surface. The radial to bipolar transition starts when the central hedgehog defect begins moving toward the droplet's surface.

If we average over droplet concentration, we can get a value with some uncertainty of when we expect a droplet to transition in either direction. The results shown in figure 5.3.2.2 b show that, on average, the bipolar to radial transition happens in the range of 900-1100 μM SDS and the radial to bipolar transition happens in the range of 900-800 μM SDS. Note that the error bars do slightly overlap.

To investigate further, we again did a full cycle transition where we start and end at the same configuration. The bipolar to radial to bipolar (BRB) transition (figure 5.3.2.2 c) and the radial to bipolar to radial (RBR) transition (figure 5.3.2.2 d) show something interesting.

First, in the BRB transition in figure 5.3.2.2 c, we notice that the colors are reversed. That means that it is actually the bipolar to radial leg of the transition that happens at a lower SDS concentration. Second, in the RBR transition in figure 5.3.2.2 d, we see a "crossing" of the lines (ill advised according to the Ghost Busters)! This seems to be mostly because the radial to bipolar transition takes a long time and the final SDS concentration when the droplet is in the bipolar state is lower than anticipated. With 2 additional repeats of this RBR cycle, we see the "crossing" again.

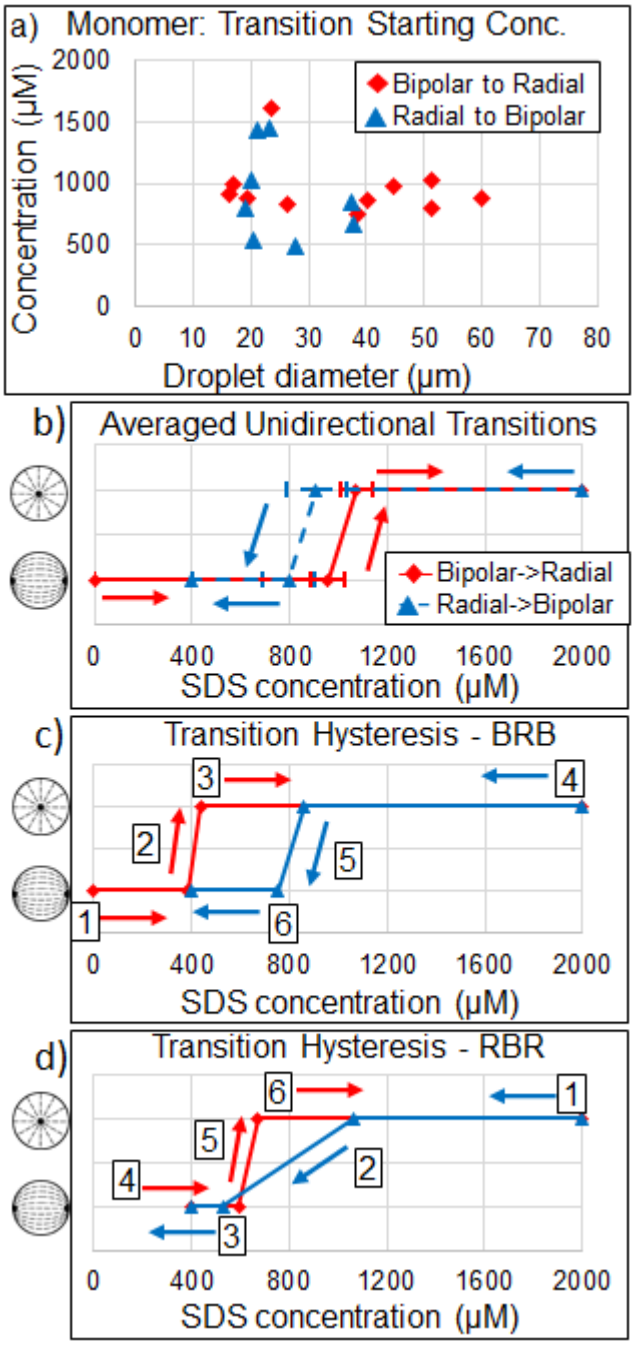
a) Monomer: Transition Starting Conc.
Concentration (μM)
2000
1500
1000
500
0
0 10 20 30 40 50 60 70 80
Droplet diameter (μm)
Bipolar to Radial
Radial to Bipolar
b)
Averaged Unidirectional Transitions
Bipolar->Radial
Radial->Bipolar
0 400 800 1200 1600 2000
SDS concentration (μM)
c)
Transition Hysteresis - BRB
1
2
3
4
5
6
0 400 800 1200 1600 2000
SDS concentration (μM)
d)
Transition Hysteresis - RBR
1
2
3
4
5
6
0 400 800 1200 1600 2000
SDS concentration (μM)

Figure 5.4. Surfactant concentration for structural transitions. (a) SDS concentration that each droplet transitioned from bipolar to radial (red diamonds, N = 11) or from radial to bipolar (blue triangles, N = 8). (b) Average SDS concentrations for droplets that transition. LC configuration denoted on the y-axis. Mean values of transition concentrations are given for bipolar to radial (red diamonds) or radial to bipolar (blue triangles). Error bars denote the standard error of the mean of the distribution. Transitions denoted for bipolar to radial (red solid line) and radial to bipolar (blue dashed line). Arrows denote the direction of the transition. (c) Cyclic driving of a configurational transition from bipolar to radial to bipolar for the same droplet. The cycle stages follow from 1 to 6. (d) Cyclic driving of configurational transition from radial to bipolar to radial for the same droplet. The cycle stages follow from 1 to 6. Red denotes bipolar to radial; blue denotes radial to bipolar.

5.4 Conclusions

But, recall that our main question was how do the transitions seen in figure 5.3.2.2 compare to those in figure 4.4.4. Comparing specifically part b of both plots, we can say that the the radial to bipolar transitions both happen in the range of 900-800 μM SDS. We see a difference, however, in the bipolar to radial transition. For the SDS only transition (SDS driven), the transition is around 400-500 μM SDS, but for the Monomer+SDS transition (SDS driven), the transition is around 900-1100 μM SDS. This means that the presence of the Monomer actually *hinders* the configurational transition from bipolar to radial!

Why could this be the case? Think about what happens at the surface when the SDS concentration is changing. The concentration of SDS in the system is related to the concentration of SDS at the surface. Recall that there is also Monomer present that also wants to live at the surface. If the SDS concentration is low, and Monomer is instead at the droplet surface, then the SDS has to displace the Monomer before the transition can happen. This might be difficult to do. The reverse, however, might be simple. This could be the case if there is a larger energetic barrier for removing a Monomer molecule from the interface as compared to SDS. As the SDS is becoming more dilute, it is easier to get out of the interface and the Monomer can replace it.

That is why the radial to bipolar could be the same with or without the Monomer present, but we see a higher SDS concentration for the bipolar to radial transition.

CHAPTER 6

PROJECT 3: VARIABLE LENGTH TRIMER

This project also involves a novel surfactant that was synthesized in the Thayumanavan lab. This one is different from SDS and the Monomer we previously examined because this one is trimeric. This novel trimeric surfactant has the same base structure as the Monomer (figure 5.1 b), but has three repeating units. There is an additional complexity in that one of the hydrophobic domains is not exactly like the Monomer's hydrophobic domain because it has a variable tail length (figure 6.1). In the Monomer surfactant, the hydrophobic tail is always exactly 10 carbons long. Here, the family of trimers with variable tail length have 6, 8, 10, or 14 carbons in one of the three hydrophobic domains. Note that because there is a triazole linker group (figure 6.1 top left) even the 10 carbon variant is not fully symmetric.

To refer to the family of trimeric surfactants with variable tail length, I will call them "Cx trimers" or "Cx" for short. To refer to a specific member of the family, I will call them by the number of carbons in their tail, so "C6", "C8", "C10", or "C14".

This project is also different in that we do not use SDS at all in these experiments. We have a single surfactant system and never mix two different tail lengths of surfactants together.

6.1 Motivation

Why the sudden shift to a trimeric surfactant? Well, chronologically, we actually did these experiments *before* the work described in project 2. At the time we were doing these experiments we were still pretty new to the field and thought these Cx

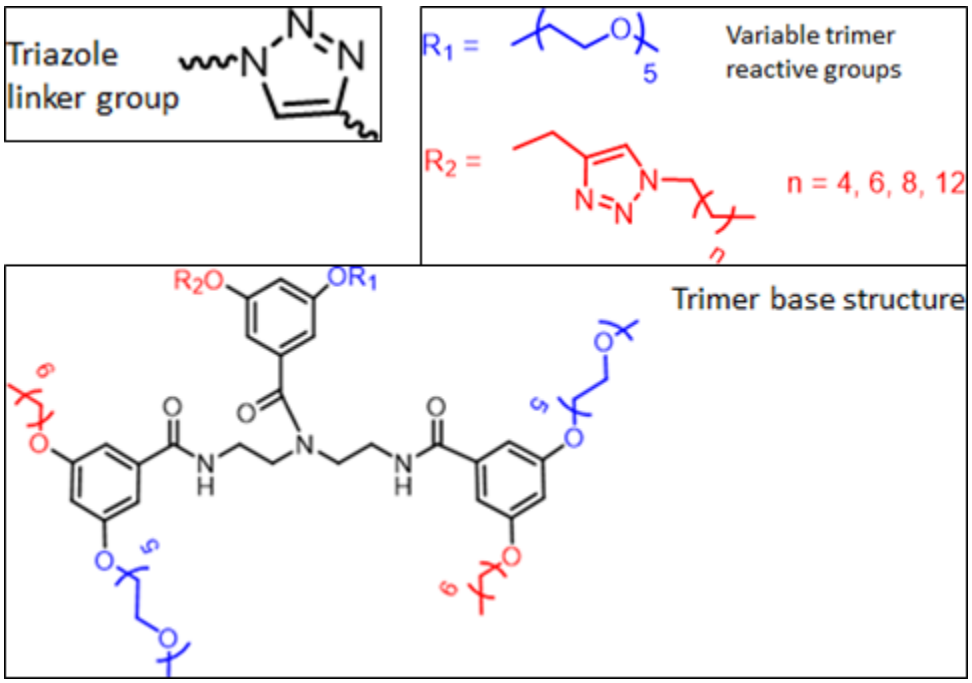

Figure 6.1. Chemical structure of the variable trimer surfactant with functional groups in the top right. Triazole linker group is shown in the top left. Reproduced from figure 2.1 c and e.

trimers were interesting because the possibility of a *very* small structural change (only 2 carbons and 4 hydrogen) might have a large affect on the droplet configuration.

6.2 Experimental Details

The results in this chapter are only using the equilibrium characterization method to make configurational phase plots like figure 4.2, 5.2, or 5.3. There are no dynamic transition experiments to share here. At the end, I will discuss what transitions might be most successful based on the results of the configurational phase plots.

Emulsions were made using 2 μL of 5CB and 98 μL of surfactant and prepared as previously described. The critical aggregate concentration (CAC) of each Cx trimer is around 10 μM (cf. table 3.1), so we did 5 sets of experiments at different concentrations centered around this value. We took data at 1 μM, 5 μM, 10 μM, 50 μM, and 100 μM.

6.3 Results and Discussion

We might as well pick an arbitrary order in which we will discuss the Cx trimers. I start with the shortest variation, C6, and go up in size ending with C14.

Before looking at the plots, we can make some predictions about what we expect to see. Our arguments are based on the relative length between the hydrophobic tails of the trimer, especially the variable one, and the 5CB molecule. As a rough estimate, using 1 atom $\approx$ 1 Angstrom, a 5CB liquid crystal is about 15 angstrom long (1.5 nm). The two non-variable tail lengths of the Cx trimers are 10 angstrom long (1 nm). The length of the variable hydrophobic tail is the length of the triazole linker group plus the tail length. The triazole linker group is about 3 Angstroms, and the length of a Cx tail is the value of x, so the total lengths are 9, 11, 13, and 15 angstroms for the C6, C8, C10, and C14 trimers, respectively.

This means that any of the hydrophobic tails of the trimer are less than or equal to the length of a LC molecule. We think that the hydrophobic tails of *any* surfactant molecule interdigitate between the LC molecules and are the main reason why the LC anchoring becomes homeotropic (perpendicular). Our hypothesis was that the longer the tail length of the trimer, the better it would be at causing the LC to go from planar (parallel) to homeotropic and make radial droplets. From our experiments with SDS and Monomer, we also expect to find more radial droplets at higher surfactant concentrations.

While the data are presented in the same style as a configuration phase space like figure 4.2 a-d, we have less data points in these experiments and in most cases looking at only part a of the figure is sufficient. Parts b-d with the individual configurations are included for consistency and clarity.

Lastly, I have to mention that most of this data was taken in 2018 before we noticed that monopolar droplets were a common configuration that we should classify. Ben Strain went through the data all over again and reclassified the nearly 1000

droplets you are about to see. This reclassification and analysis is the work of his undergraduate thesis.

6.3.1 C6 Trimer

When we look at the configurations of the droplets in the presence of C6 trimer surfactant solution (figure 6.2 a) we can make a couple broad observations immediately.

First, notice that there are primarily bipolar droplets at the lower concentrations of 1 μM (84.8 % bipolar), 5 μM (78.6 % bipolar), and 10 μM (82.9 % bipolar). We have mostly *monopolar* droplets, however, at the higher concentrations of 50 μM (91.3 % monopolar) and 100 μM (69.8 % monopolar). We do see some radial droplets, and they are more common at higher concentrations than lower concentrations, but even at 100 μM less than 10 % of the droplets are radial. A complete table of the percentage of each configuration at each concentration is shown in table 6.1.

So, what does this tell us about what the C6 trimer is doing at the droplet interface? It tells us that the C6 trimer is doing *something*, otherwise there would be no concentration dependence. Similar to the Monomer only experiments (figure 5.2 a) the only concentration that are mostly non-bipolar are the two concentrations above the CAC of the molecule. This makes us think again to the Monomer only system and ask if the presence of aggregates somehow influences the droplet configuration. I don't have a great answer, but my thought is that since the aggregates are in the free solution they should not have an affect on the droplet configuration. I do not think that an aggregate of surfactant molecules, be it Monomer or C6 trimer, would be in contact with the droplet's surface.

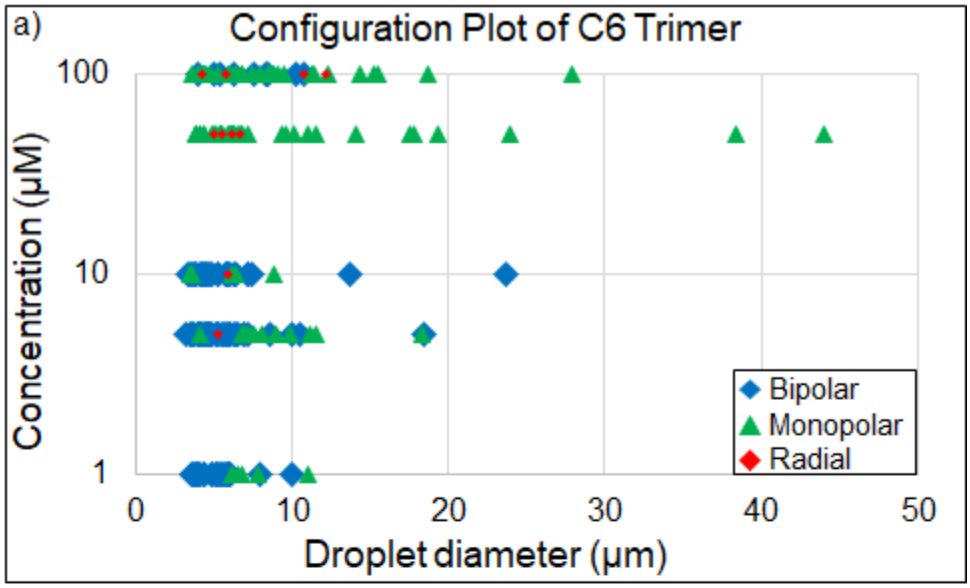
a)
Configuration Plot of C6 Trimer
100
10
1
Concentration (μM)
0
10
20
30
40
50
Droplet diameter (μm)
Bipolar
Monopolar
Radial

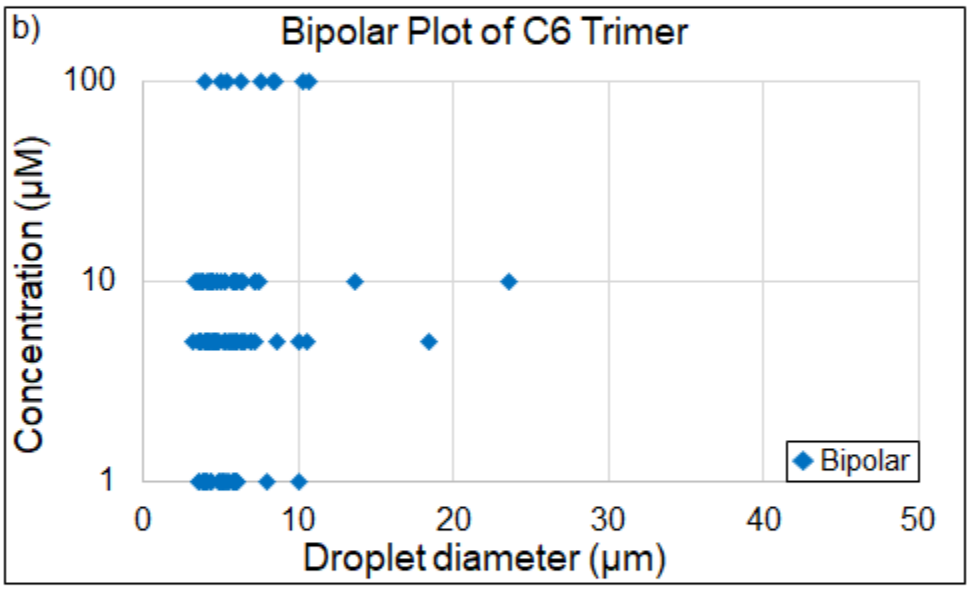
b)
Bipolar Plot of C6 Trimer
100
10
1
Concentration (μM)
0
10
20
30
40
50
Droplet diameter (μm)
Bipolar

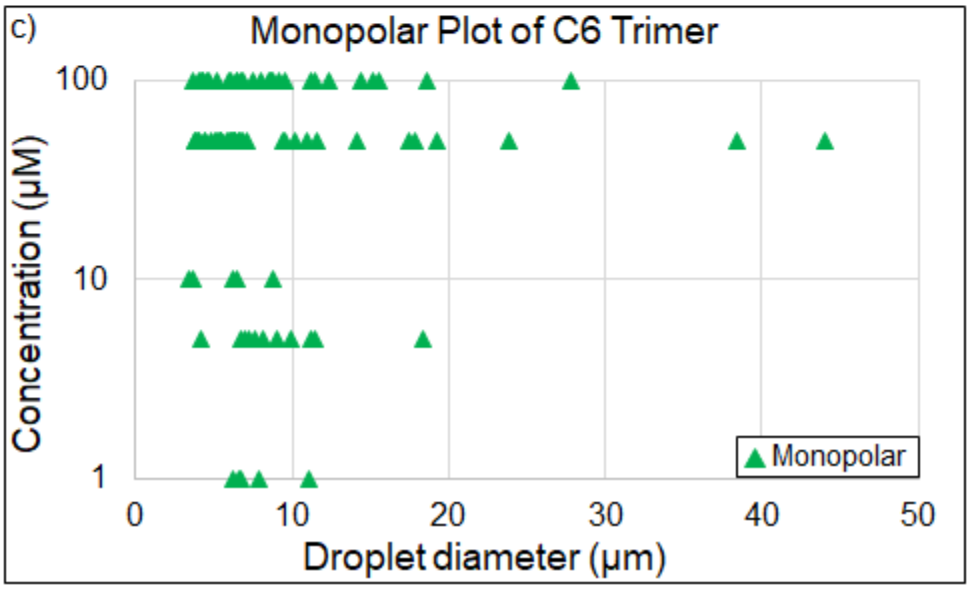
c)
Monopolar Plot of C6 Trimer
100
10
1
Concentration (μM)
0
10
20
30
40
50
Droplet diameter (μm)
Monopolar

C6 Trimer	1 μM	5 μM	10 μM	50 μM	100 μM
Bipolar	84.8	78.6	82.9	0	20.9
Monopolar	15.2	19.6	14.3	91.3	69.8
Radial	0	1.8	2.9	8.7	9.3

Table 6.1. Table of configuration percentages for the C6 trimer. Columns are concentrations and rows are configurations.

C8 Trimer	1 μM	5 μM	10 μM	50 μM	100 μM
Bipolar	97.9	83.6	30.3	0	0
Monopolar	2.1	10.9	51.2	55.3	52
Radial	0	5.4	18.2	44.7	48

Table 6.2. Table of configuration percentages for the C8 trimer. Columns are concentrations and rows are configurations.

6.3.2 C8 Trimer

What happens when we slightly increase the variable tail? This time in figure 6.3 a we see exactly 0 bipolar droplets at the two concentrations above the CAC. The difference is that we see a fairly even split between the monopolar and radial configurations at these concentrations with 55.3 % monopolar at 50 μM and 52 % monopolar at 100 μM.

What is interesting about figure 6.3 a is that it is only the two lowest concentrations of 1 μM and 5 μM that are mostly bipolar, 97.9 % and 83.6 %, respectively. This means that the middle concentration of 10 μM has a mixture of each configuration (30.3 % bipolar, 51.5 % monopolar, and 18.2 % radial). A complete table of the percentage of each configuration at each concentration is shown in table 6.2.

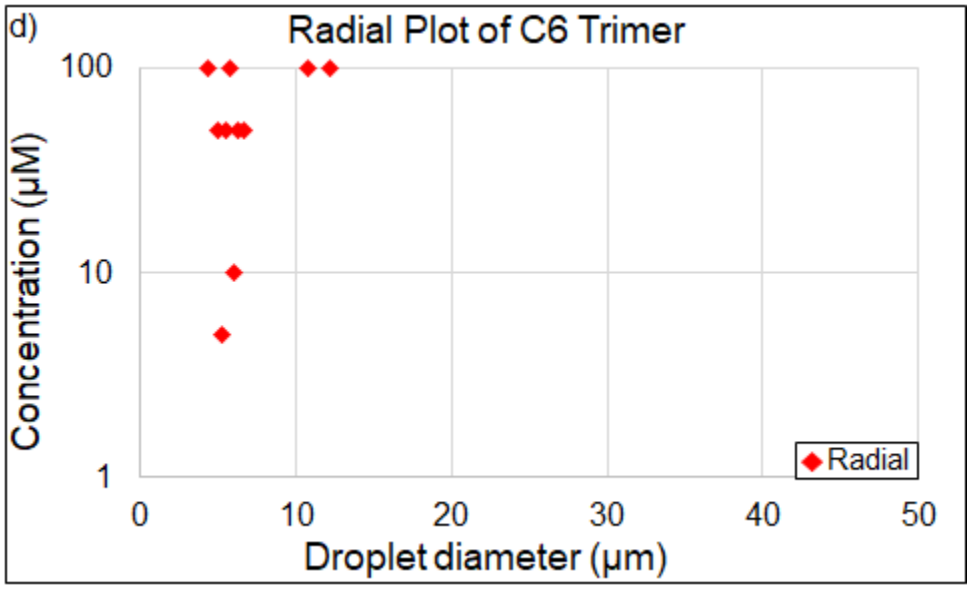

Figure 6.2. Concentration-diameter phase diagram of the 5CB liquid crystal droplets as a function of droplet diameter and C6 trimer concentration. (a) All configurations including bipolar (blue diamonds), monopolar (green triangles), and radial (red diamonds) represented together. (b) Same data as part a with only bipolar droplets shown. (c) Same data as part a with only monopolar droplets shown. (d) Same data as part a with only radial droplets shown.

6.3.3 C10 Trimer

The C10 configuration phase plot (figure 6.4 a) is rather different from the C6 and C8 configuration phase plots we just saw. Most saliently, there are only *five* radial droplets across *all* concentrations! This is about 2 % of the total number of drops shown in figure 6.4 a). Further, except for 100 μM, bipolar droplets are more common than monopolar droplets. The bipolar percentages at concentrations 1 μM, 5 μM 10 μM and 50 μM are 85.2 %, 65.1 %, 79.4 %, and 57.1 %, respectively. At 100 μM C10 trimer there are 25 % bipolar and 71.4 % monopolar droplets. A complete table of the percentage of each configuration at each concentration is shown in table 6.3.

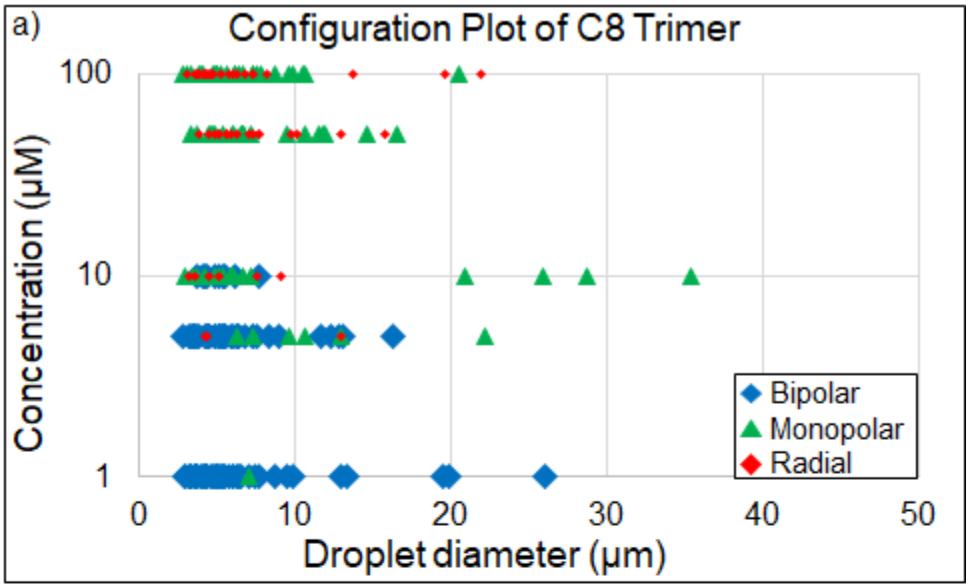
a)
Configuration Plot of C8 Trimer
100
10
1
Concentration (μM)
0
10
20
30
40
50
Droplet diameter (μm)
Bipolar
Monopolar
Radial

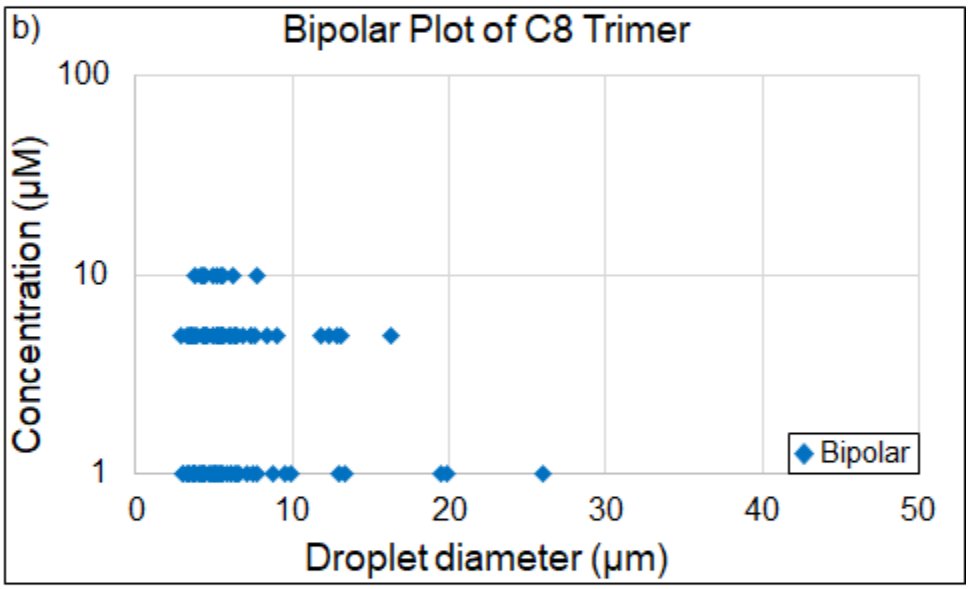
b)
Bipolar Plot of C8 Trimer
100
10
1
Concentration (μM)
0
10
20
30
40
50
Droplet diameter (μm)
Bipolar

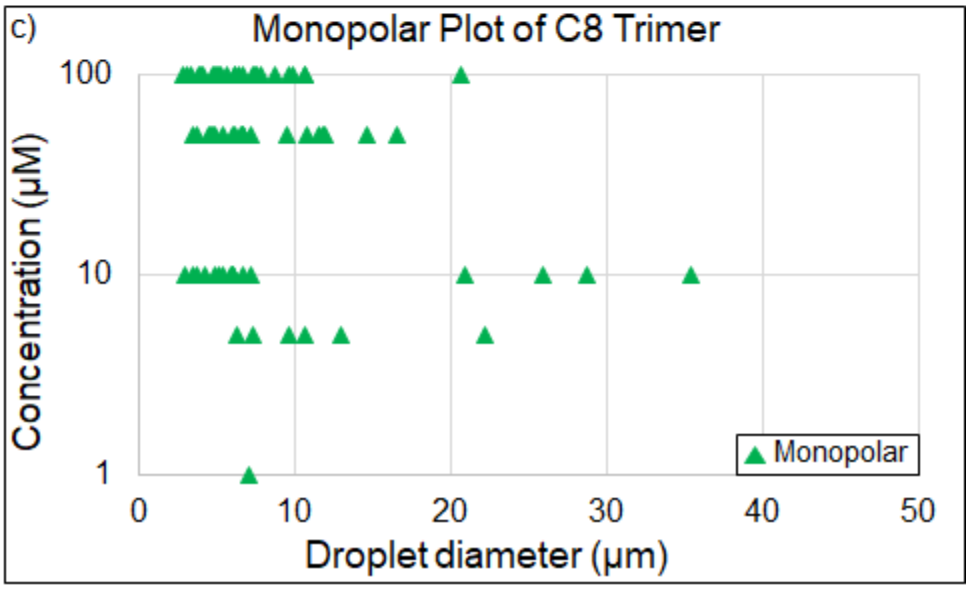
c)
Monopolar Plot of C8 Trimer
100
10
1
Concentration (μM)
0
10
20
30
40
50
Droplet diameter (μm)
Monopolar

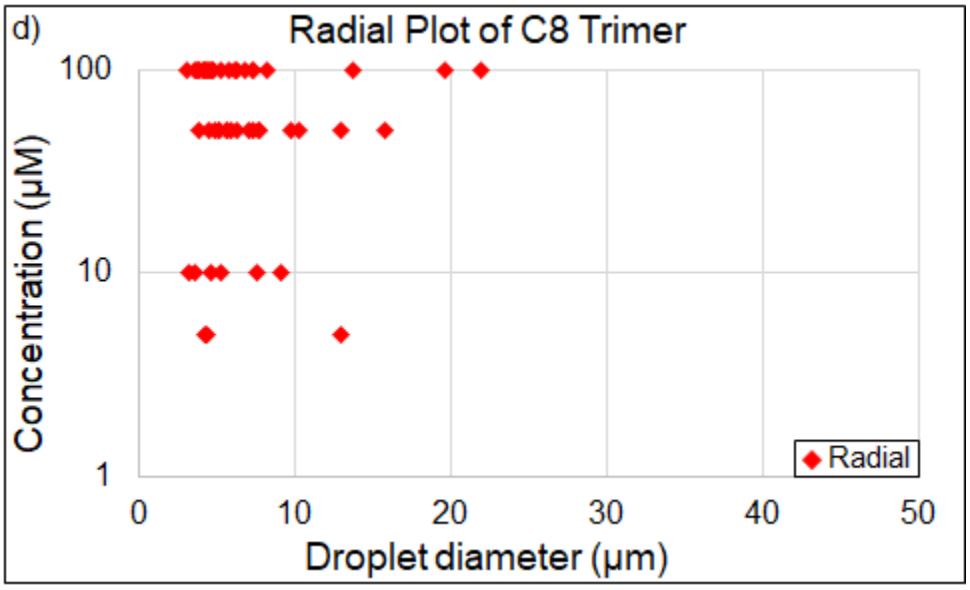

Figure 6.3. Concentration-diameter phase diagram of the 5CB liquid crystal droplets as a function of droplet diameter and C8 trimer concentration. (a) All configurations including bipolar (blue diamonds), monopolar (green triangles), and radial (red diamonds) represented together. (b) Same data as part a with only bipolar droplets shown. (c) Same data as part a with only monopolar droplets shown. (d) Same data as part a with only radial droplets shown.

6.3.4 C14 Trimer

The C14 trimer configuration phase plot (figure 6.5 a) is very similar to the configuration phase plot of the C10 trimer (figure 6.4 a) that we just talked about. This time there are about 10 % radial droplets total, which is more than C10, but is still very small. The radial droplets are also spread over all concentrations and not significantly more present at any particular concentration compared to another. Just as

C10 Trimer	1 μM	5 μM	10 μM	50 μM	100 μM
Bipolar	85.2	65.1	79.4	57.1	25
Monopolar	14.8	32.6	14.7	38.1	71.4
Radial	0	2.3	5.9	4.8	3.6

Table 6.3. Table of configuration percentages for the C10 trimer. Columns are concentrations and rows are configurations.

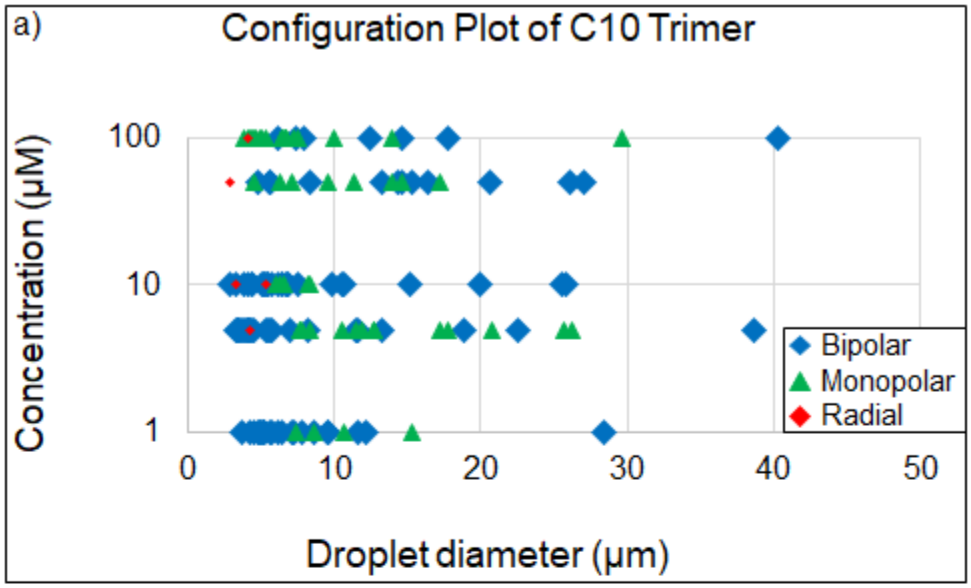
a)
Configuration Plot of C10 Trimer
Concentration (μM)
100
10
1
0
10
20
30
40
50
Droplet diameter (μm)
Bipolar
Monopolar
Radial

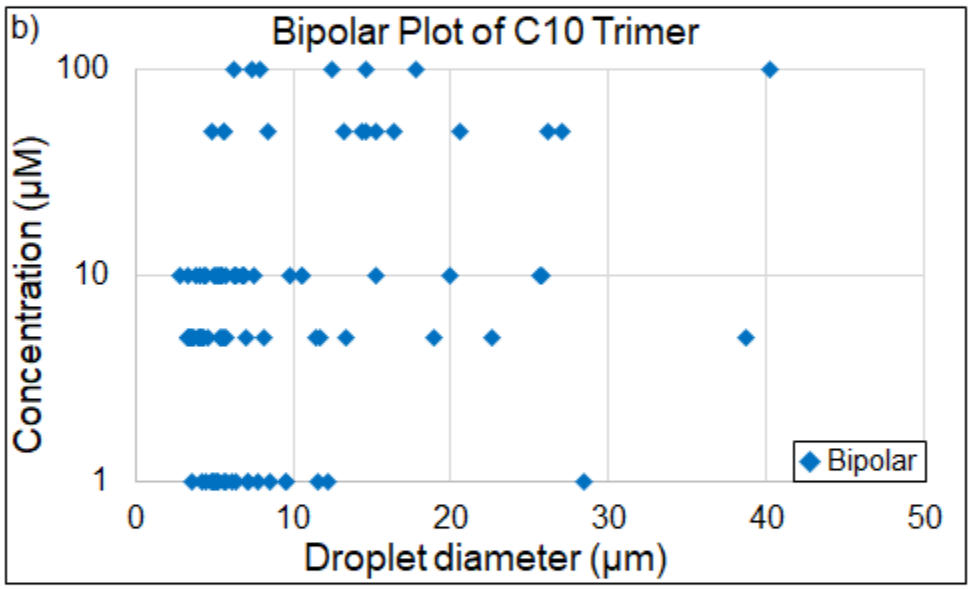
b)
Bipolar Plot of C10 Trimer
Concentration (μM)
100
10
1
0
10
20
30
40
50
Droplet diameter (μm)
Bipolar

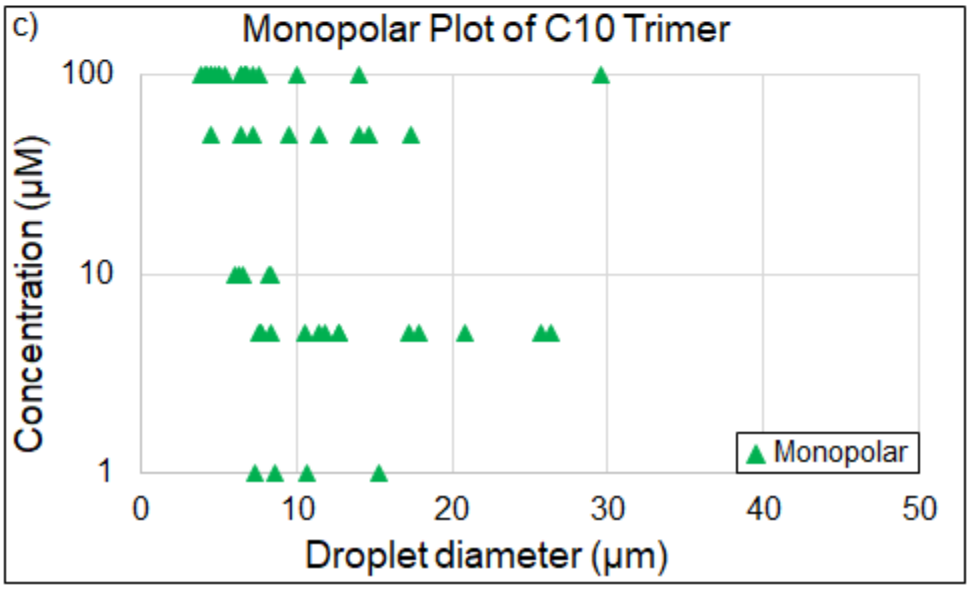
c)
Monopolar Plot of C10 Trimer
Concentration (μM)
100
10
1
0
10
20
30
40
50
Droplet diameter (μm)
Monopolar

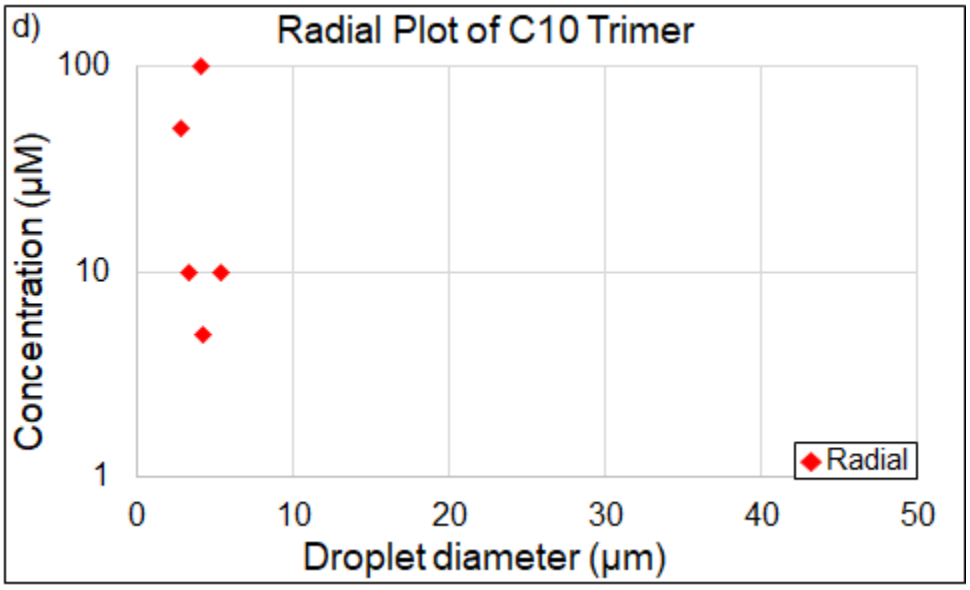

Figure 6.4. Concentration-diameter phase diagram of the 5CB liquid crystal droplets as a function of droplet diameter and C10 trimer concentration. (a) All configurations including bipolar (blue diamonds), monopolar (green triangles), and radial (red diamonds) represented together. (b) Same data as part a with only bipolar droplets shown. (c) Same data as part a with only monopolar droplets shown. (d) Same data as part a with only radial droplets shown.

with figure 6.4 a, we have a split between bipolar and monopolar at each concentration. The only difference between C10 and C14 is that in the C14 plot there are more monopolar droplets at the highest *two* concentrations as opposed to the single highest concentration in the C10 plot. From lowest to highest concentration, the percentages of bipolar droplets are 80.5 %, 66.7 %, 69.0 %, 22.2 %, and 18.2 %. In the same order, the percentages of radial droplets are 14.6 %, 19.0 %, 21.4 %, 66.7 %, and 66.7 %. A complete table of the percentage of each configuration at each concentration is shown in table 6.4.

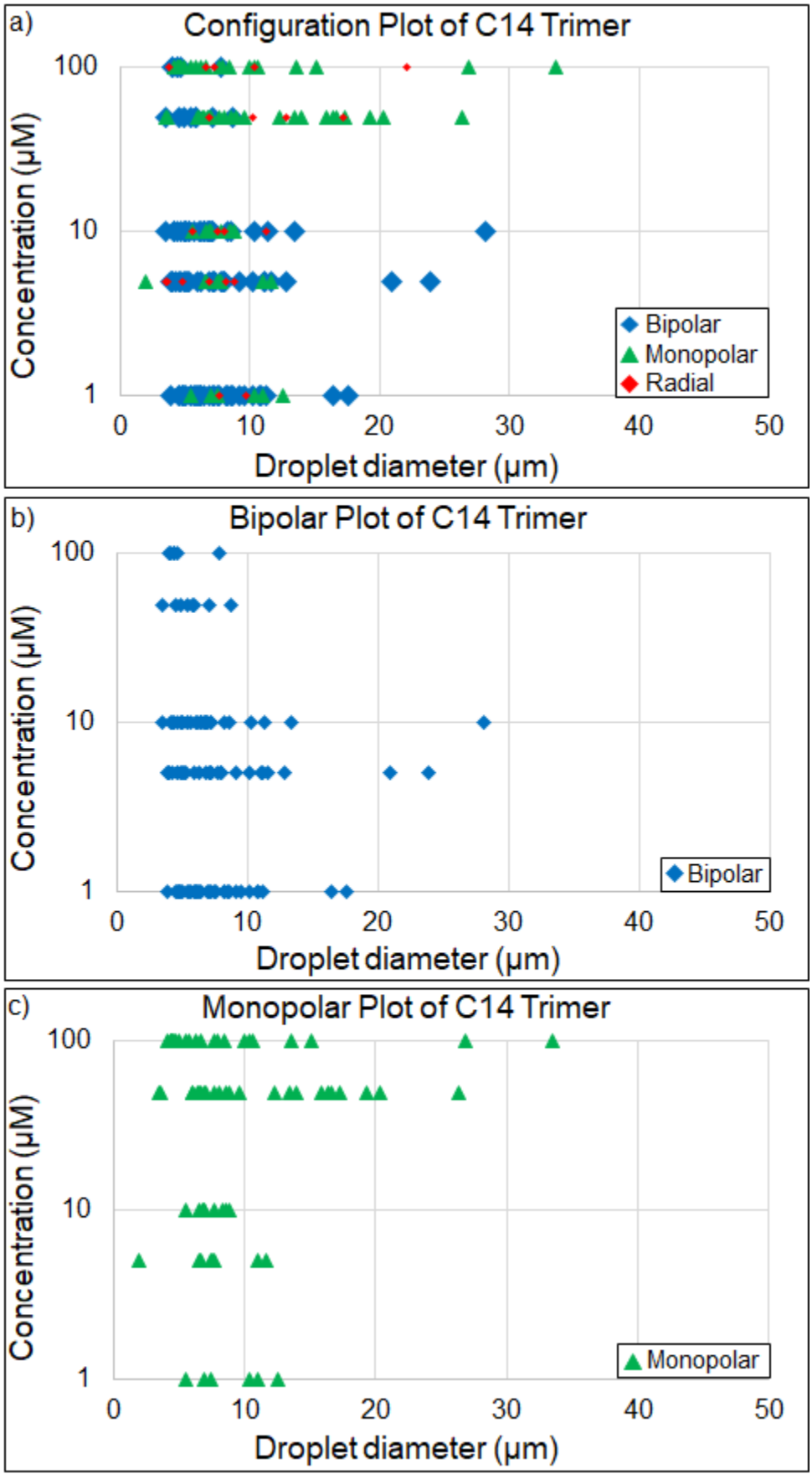
a)
Configuration Plot of C14 Trimer
Concentration (μM)
100
10
1
0
10
20
30
40
50
Droplet diameter (μm)
Bipolar
Monopolar
Radial
b)
Bipolar Plot of C14 Trimer
Concentration (μM)
100
10
1
0
10
20
30
40
50
Droplet diameter (μm)
Bipolar
c)
Monopolar Plot of C14 Trimer
Concentration (μM)
100
10
1
0
10
20
30
40
50
Droplet diameter (μm)
Monopolar

C14 Trimer	1 μM	5 μM	10 μM	50 μM	100 μM
Bipolar	80.5	66.7	69.0	22.2	18.2
Monopolar	14.6	19.0	21.4	66.7	66.7
Radial	4.9	12.3	9.5	11.1	15.2

Table 6.4. Table of configuration percentages for the C14 trimer. Columns are concentrations and rows are configurations.

6.3.5 By Internal Configuration

Another way to look at the data in this chapter is to consider one *configuration* at a time instead of one Cx trimer at a time. For example, by taking part b of figures 6.2, 6.3, 6.4, and 6.5 I made figure 6.6.

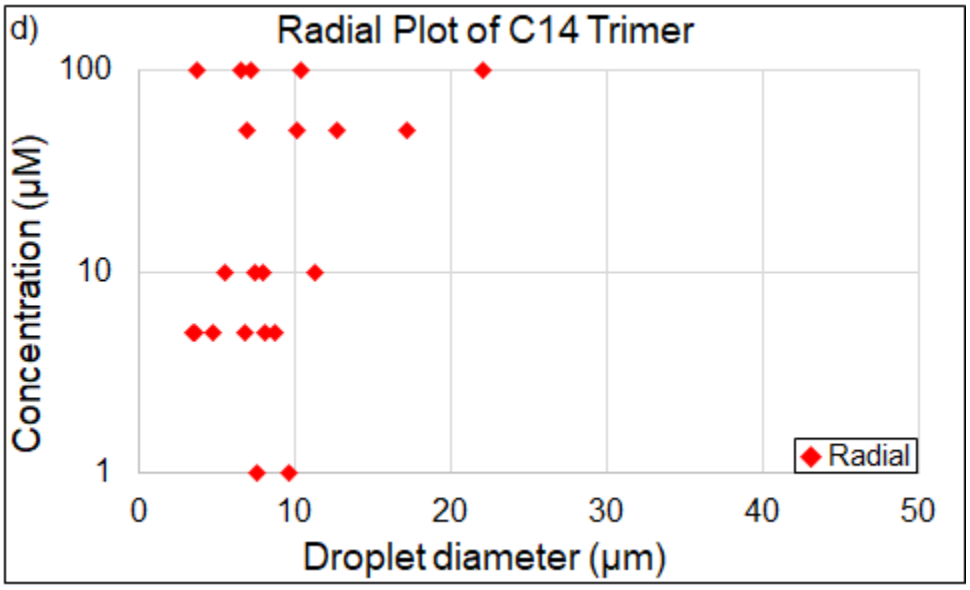

Figure 6.5. Concentration-diameter phase diagram of the 5CB liquid crystal droplets as a function of droplet diameter and C14 trimer concentration. (a) All configurations including bipolar (blue diamonds), monopolar (green triangles), and radial (red diamonds) represented together. (b) Same data as part a with only bipolar droplets shown. (c) Same data as part a with only monopolar droplets shown. (d) Same data as part a with only radial droplets shown.

6.3.5.1 Bipolar

When considering only the bipolar phase the first thing we noticed was that the C10 trimer (figure 6.6, c) was the only one that had bipolar droplets at 100 μM that were larger than $\approx$ 11 μm in diameter. Further, the C10 trimer in general had a larger diameter range where bipolar droplets were found.

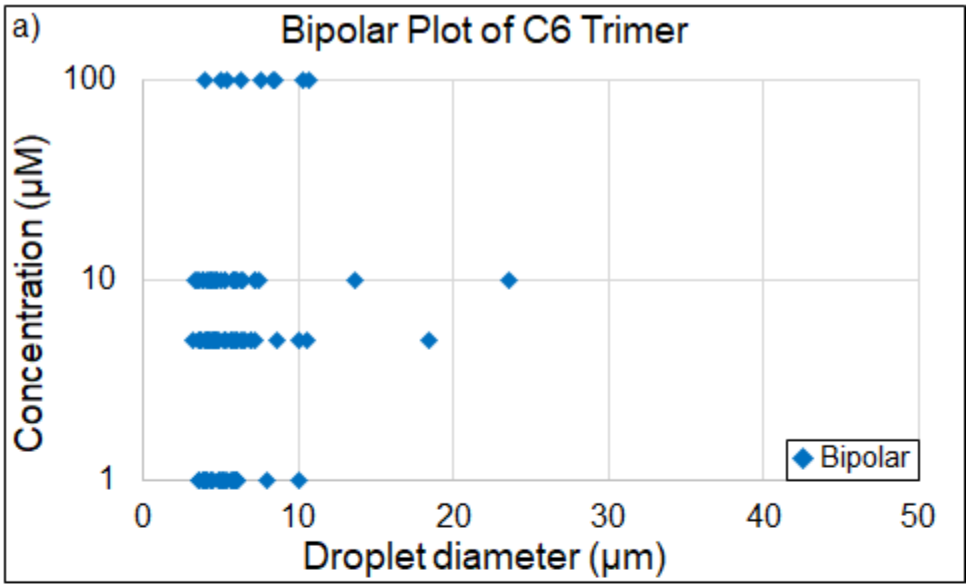
a)
Bipolar Plot of C6 Trimer
100
10
1
Concentration (µM)
0
10
20
30
40
50
Droplet diameter (µm)
Bipolar

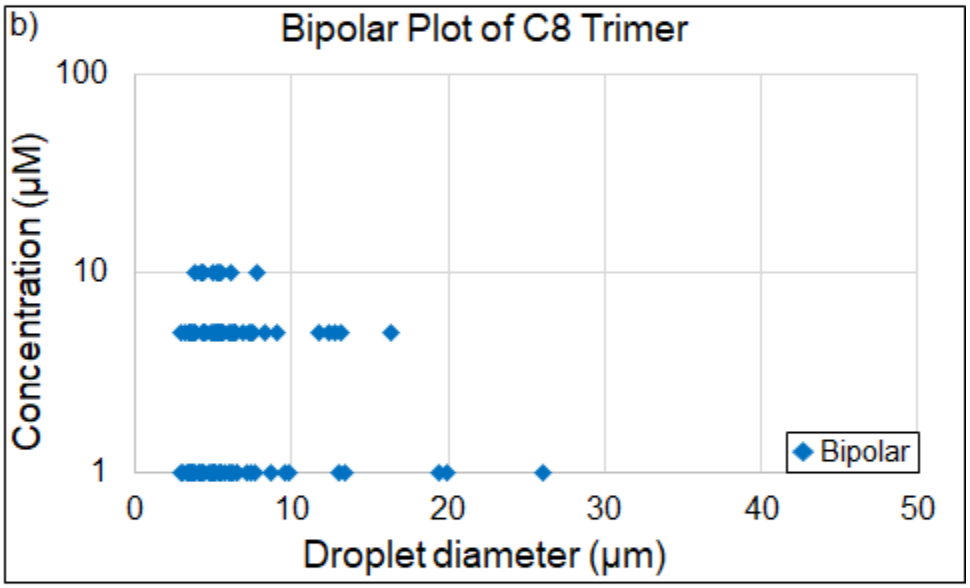
b)
Bipolar Plot of C8 Trimer
100
10
1
Concentration (µM)
0
10
20
30
40
50
Droplet diameter (µm)
Bipolar

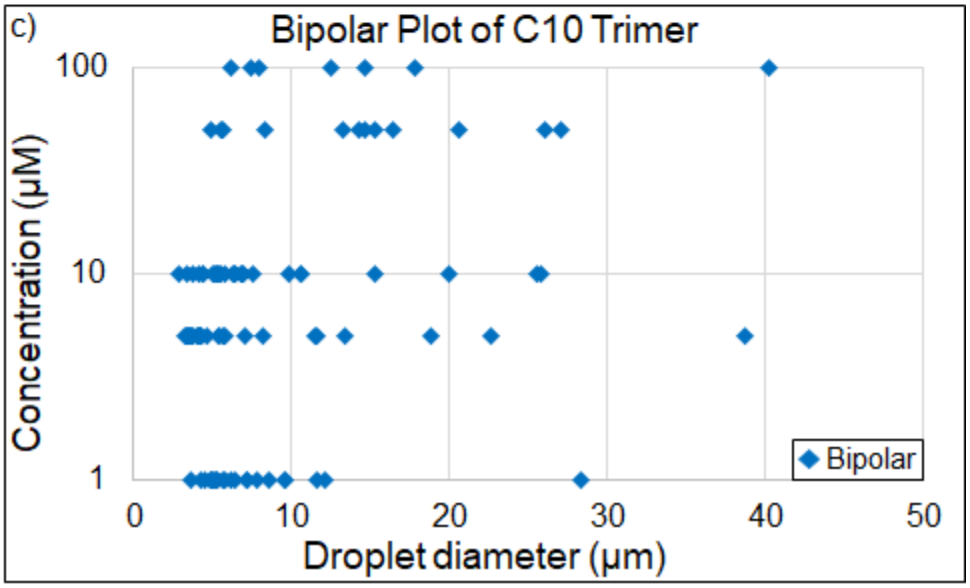
c)
Bipolar Plot of C10 Trimer
100
10
1
Concentration (µM)
0
10
20
30
40
50
Droplet diameter (µm)
Bipolar

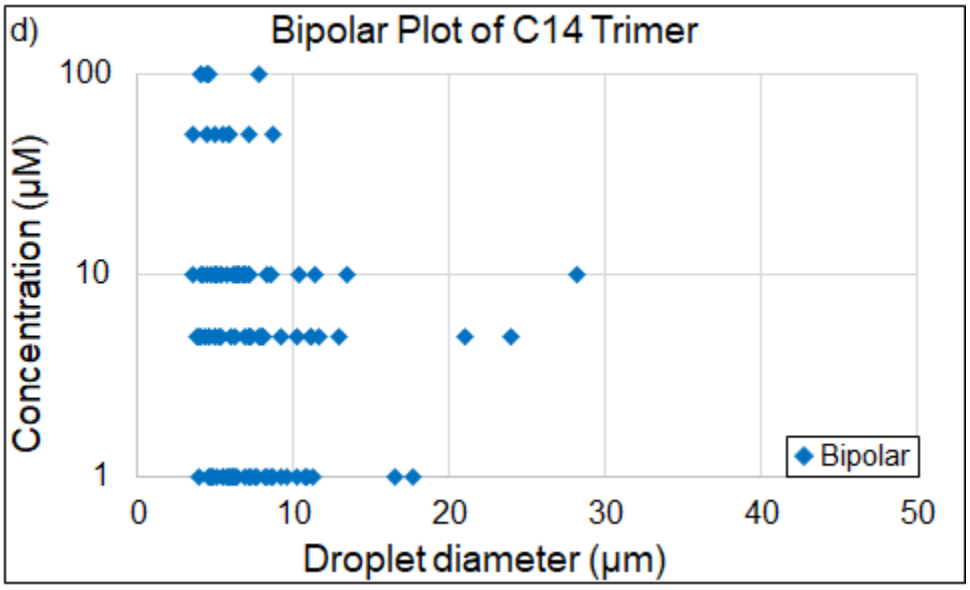

Figure 6.6. Concentration-diameter diagram of only bipolar 5CB liquid crystal droplets as a function of droplet diameter and Cx trimer concentration for all 4 Cx variations. (a) C6 trimer, (b) C8 trimer, (c) C10 trimer, and (d) C14 trimer.

6.3.5.2 Monopolar

Somewhat surprisingly, the distribution of monopolar droplets was qualitatively similar across all Cx trimers (figure 6.7). At 1 μM of each Cx variant there were very few monopolar droplets and the ones we saw were small (less than 15 μm diameter). At the 4 other concentrations there was a wide spread of diameters found at each concentration for each Cx variant.

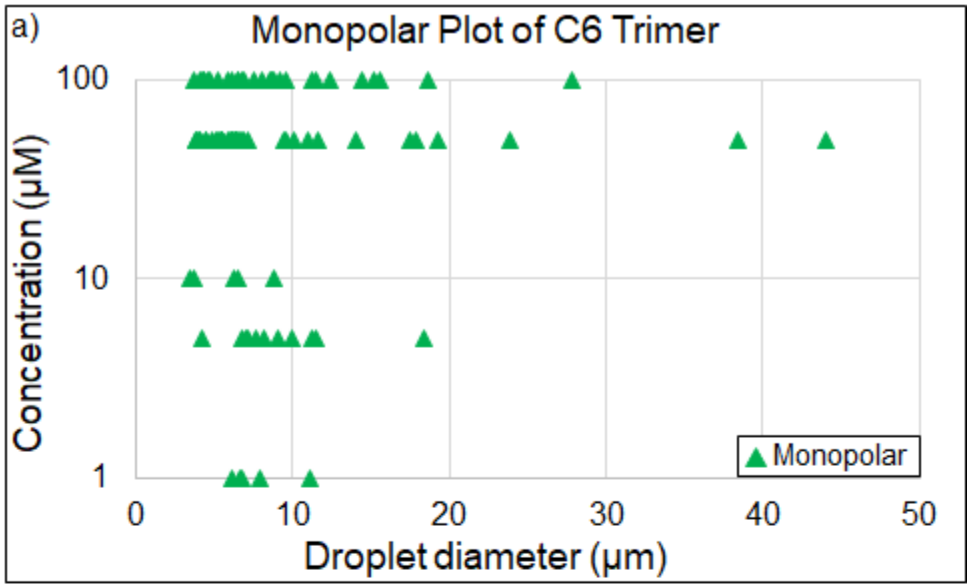
a)
Monopolar Plot of C6 Trimer
100
10
1
Concentration (µM)
0
10
20
30
40
50
Droplet diameter (µm)
Monopolar

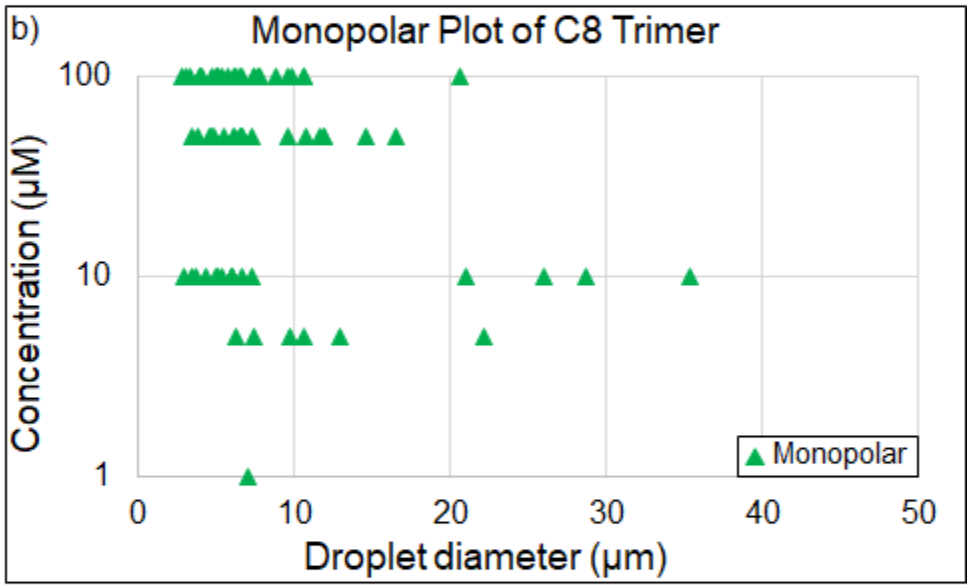
b)
Monopolar Plot of C8 Trimer
100
10
1
Concentration (µM)
0
10
20
30
40
50
Droplet diameter (µm)
Monopolar

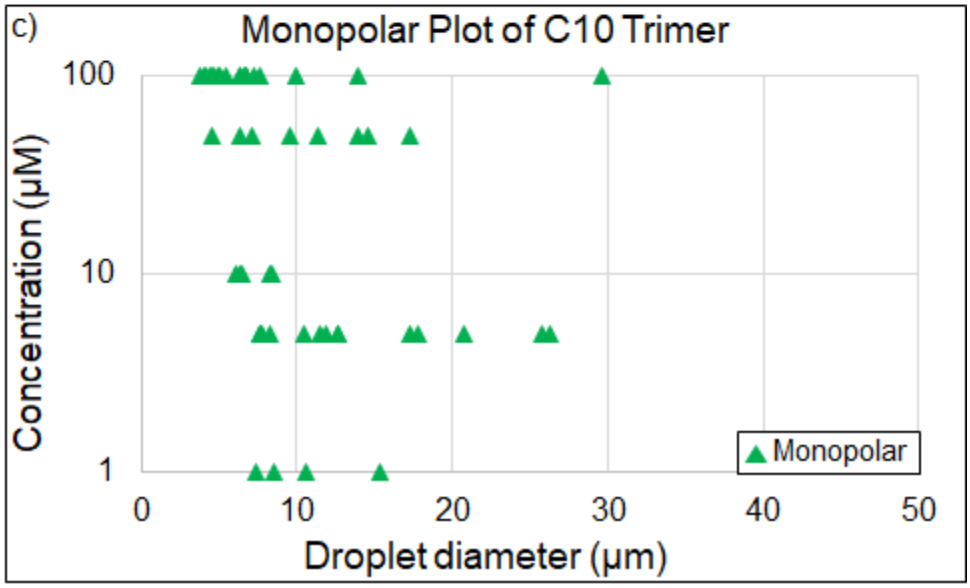
c)
Monopolar Plot of C10 Trimer
100
10
1
Concentration (µM)
0
10
20
30
40
50
Droplet diameter (µm)
Monopolar

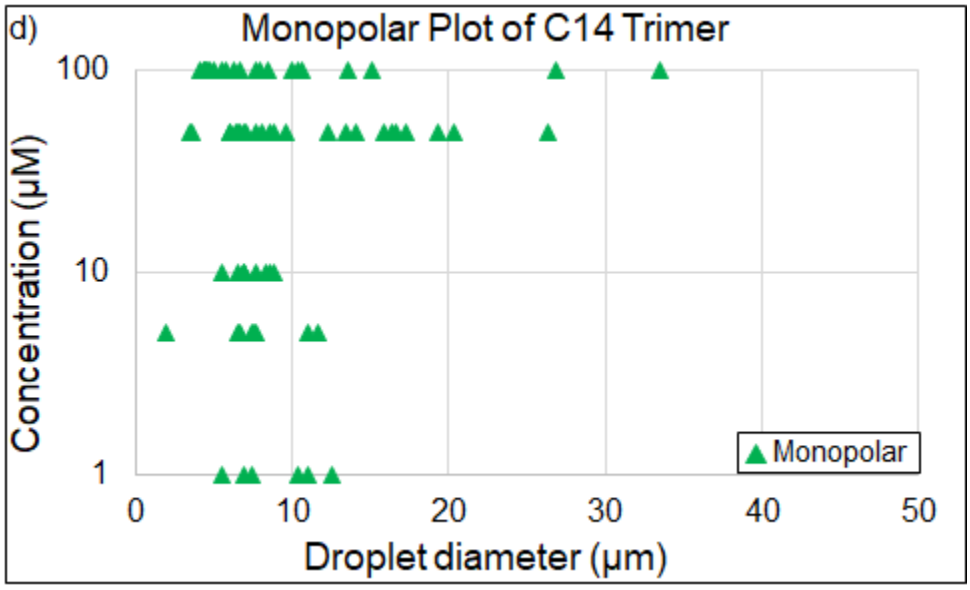

Figure 6.7. Concentration-diameter diagram of only monopolar 5CB liquid crystal droplets as a function of droplet diameter and Cx trimer concentration for all 4 Cx variations. (a) C6 trimer, (b) C8 trimer, (c) C10 trimer, and (d) C14 trimer.

6.3.5.3 Radial

As we previously discussed, the C8 trimer was the most proficient at forming radial droplets (figure 6.8 b). The number and percentage of radial droplets found at 50 μM and 100 μM exceeds that of the other Cx trimers.

6.4 Conclusions

Since these are all pure Cx trimer solutions, any transition we imagine based on the above results is assuming using the particular Cx trimer as the driving agent of the transition. We should think about each trimer independently from each other.

Based on the results of the C6 configuration plot (figure 6.2 a) it would appear that a possible bipolar to monopolar transition could happen if the C6 concentration was raised from 10 μM to 100 μM. This possible transition could be reproducible and result in a visual read-out. My intuition is that a bipolar to monopolar transition

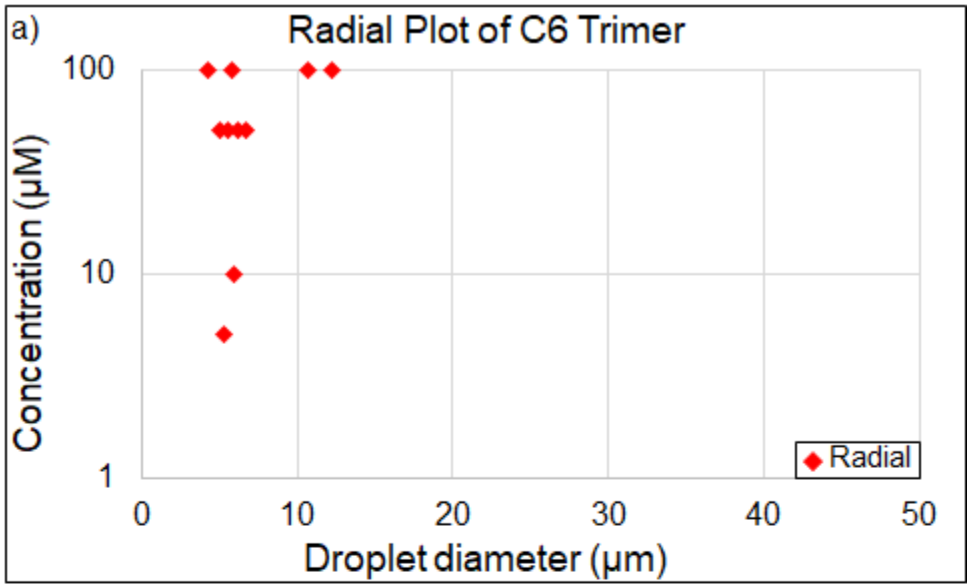
a)
Radial Plot of C6 Trimer
100
10
1
Concentration (µM)
0
10
20
30
40
50
Droplet diameter (µm)
Radial

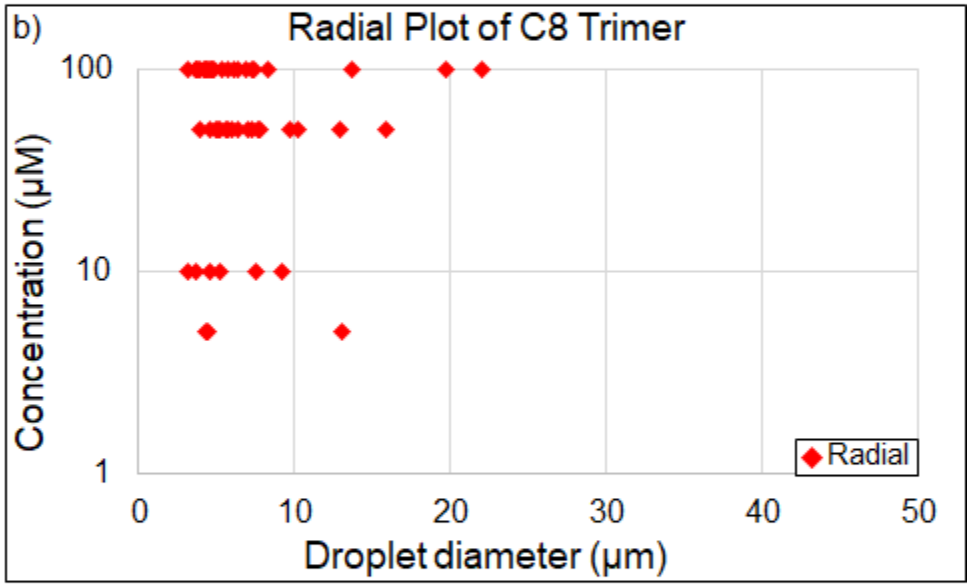
b)
Radial Plot of C8 Trimer
100
10
1
Concentration (µM)
0
10
20
30
40
50
Droplet diameter (µm)
Radial

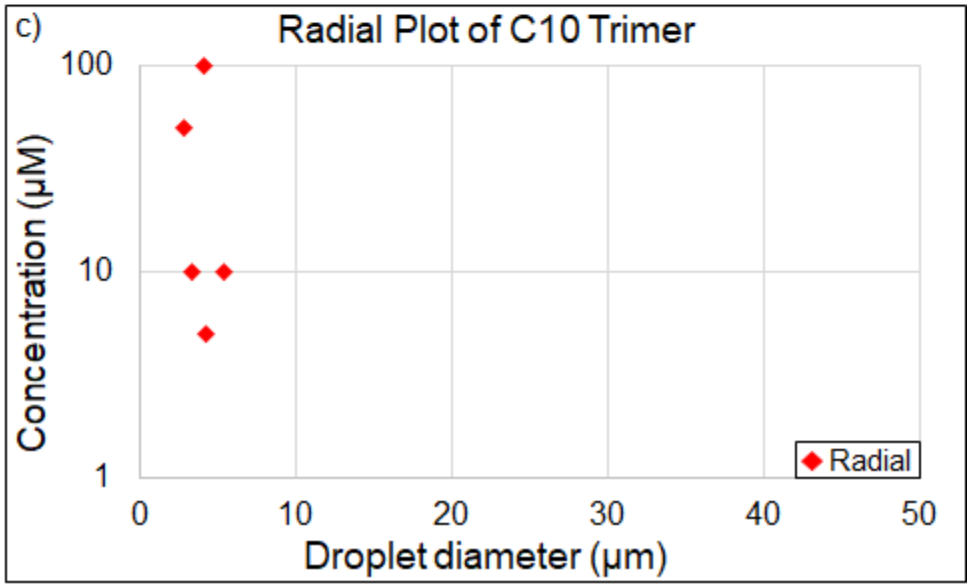
c)
Radial Plot of C10 Trimer
100
10
1
Concentration (µM)
0
10
20
30
40
50
Droplet diameter (µm)
Radial

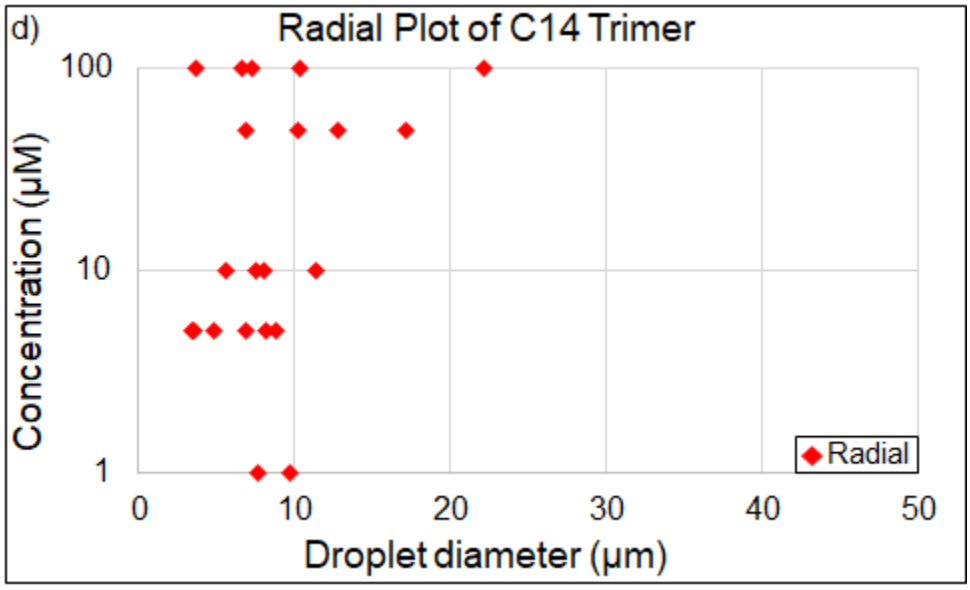

Figure 6.8. Concentration-diameter diagram of only radial 5CB liquid crystal droplets as a function of droplet diameter and Cx trimer concentration for all 4 Cx variations. (a) C6 trimer, (b) C8 trimer, (c) C10 trimer, and (d) C14 trimer.

would be less consistent than the bipolar to radial transition we saw in the SDS experiments.

The C8 trimer is more promising for dynamic transition experiments. The observation that there are about half radial droplets at 100 μM gives a little more hope for a bipolar to radial transition when going from 10 μM to 100 μM C8 trimer. Because of the mixed states found at 10 μM C8, we should start at a concentration of 5 μM where there are mostly bipolar droplets instead of 10 μM. This has a minimal affect on the execution of the transition, since it will only make the flowed in concentration to be very slightly higher.

Both the C10 and C14 trimers are not promising for triggered dynamic transitions. The fact that there is a decent mixture of bipolar and monopolar droplets at every concentration and only a handful of observed radial droplets, I predict no transition to be possible using a pure C10 or pure C14 surfactant system.

So, if I had to try a transition experiment using these surfactants, I would start with C8 trimer because there are the most radial droplets at higher concentration. It might be worth some time trying a bipolar to monopolar transition for the C6 trimer, but I wouldn't be surprised if 0 out of 10 experiments didn't show a transition.

CHAPTER 7

PROJECT 4: PROTEIN DRIVEN TRANSITION USING TPSL

The first three projects described above all use or propose to use the same mechanism, of a changing surfactant concentration, to cause a configurational change in a liquid crystal (LC) droplet. This project is different in that we tried to use the concentration of a protein, carbonic anhydrase (CA), instead of a surfactant to cause the transition between droplet configurations.

7.1 Motivation

Why the change in approach? Actually, *this* is the real deal. Projects 1, 2, and 3 were supporting projects that allowed us to build the skills and understanding necessary to attempt something like this. Changing the surfactant concentration is something that is really easy to do in a lab setting, but has limited real world applications. Being able to detect a protein by sensing a LC droplet transition is much more interesting. If the addition of a protein causes a configurational change, I can imagine having a medical test that uses this. The time scale of our transitions is on the order of magnitude of 1 minute. If you were tested for covid-19 recently, you would agree that a faster turn around on testing would be fantastic.

Let's say you start with a solution of bipolar droplets and the addition of a protein causes them to change to be radial. If the protein to be sensed is a specific product of a particular disease, and the surfactant is designed to only bind with that specific protein, then if you see the droplets become radial you know that protein was present and the person has the disease. Doesn't that sounds cool?!

7.2 Experimental Details

In this project we will again be using SDS (figure 7.1 a) as a supporting surfactant. We will also use a novel trimeric surfactant that was synthesized in the Thayumanavan lab. Like the trimer surfactants in Project 3, they have the same base structure (figure 7.1 b) but have the functional groups described in figure 7.1 c. Note that the triazole linker group (figure 7.1 d, left) is now on the hydrophilic (blue) tail instead of on the hydrophobic (red) tail like the trimers in Project 3. The functional group that binds to CA is shown in figure 7.1 d, right. I will refer to this trimeric surfactant with the protein sensitive ligand functional group as TPSL.

7.3 Results and Discussion

As with the other projects, we first begin by categorizing the equilibrium configuration of droplets at several surfactant concentrations. We first introduce TPSL to an SDS system to see what affect the TPSL has on the equilibrium configurations. We tested a fixed TPSL concentration of 1 μM and used the same 5 SDS concentrations as in project 1 (figure 7.2 a). We then tested the lowest 3 SDS concentrations, still with 1 μM TPSL, but with the addition of 2 μM CA (figure 7.2 b). We chose to focus on the lowest 3 SDS concentrations because that is where we found primarily bipolar droplets. We chose the TPSL and CA concentrations to be so relatively low because if we are using the TPSL to sense a protein in a system, we want the concentrations of both the TPSL and CA to be as low as possible. This is so that our system is sensitive to small signals.

The main difference between parts a and b of figure 7.2 is at the 100 and 300 μM SDS concentrations. At both of these SDS concentrations, without CA present, we have primarily bipolar droplets (96% and 88% for 100 and 300 μM SDS, respectively). At the same SDS and TPSL concentration, with the addition of CA there are still many (58% and 55%) bipolar droplets, but now there are many monopolar droplets

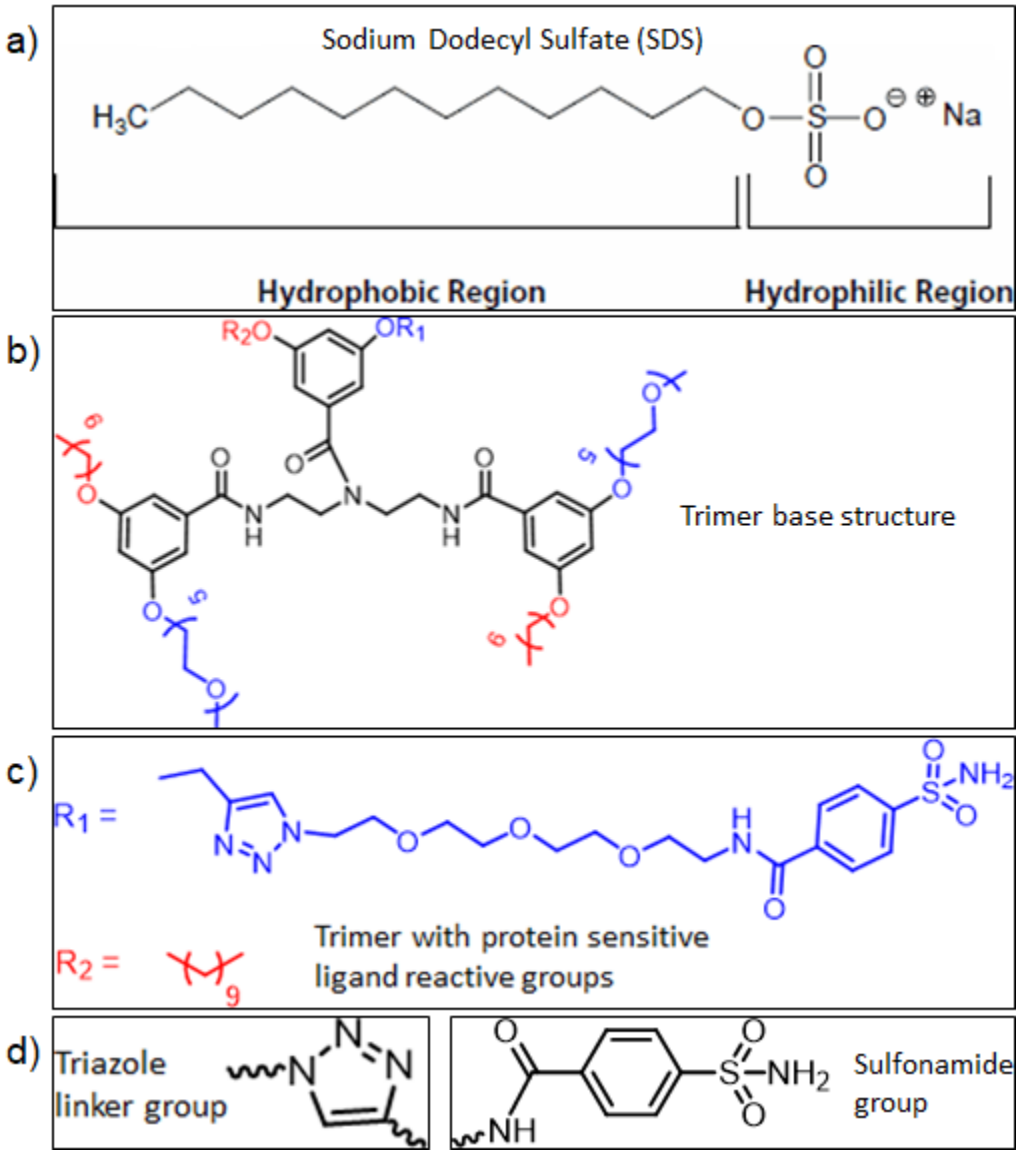

Figure 7.1. Chemical structures of all surfactants used in project 4, which are a subset of those shown in figure 2.1. (a) Sodium dodecyl sulfate (SDS). (b) Base structure of the novel trimeric surfactant with functional groups shown in (c). (d) Triazole sub unit (left) and sulfonamide ligand group (right).

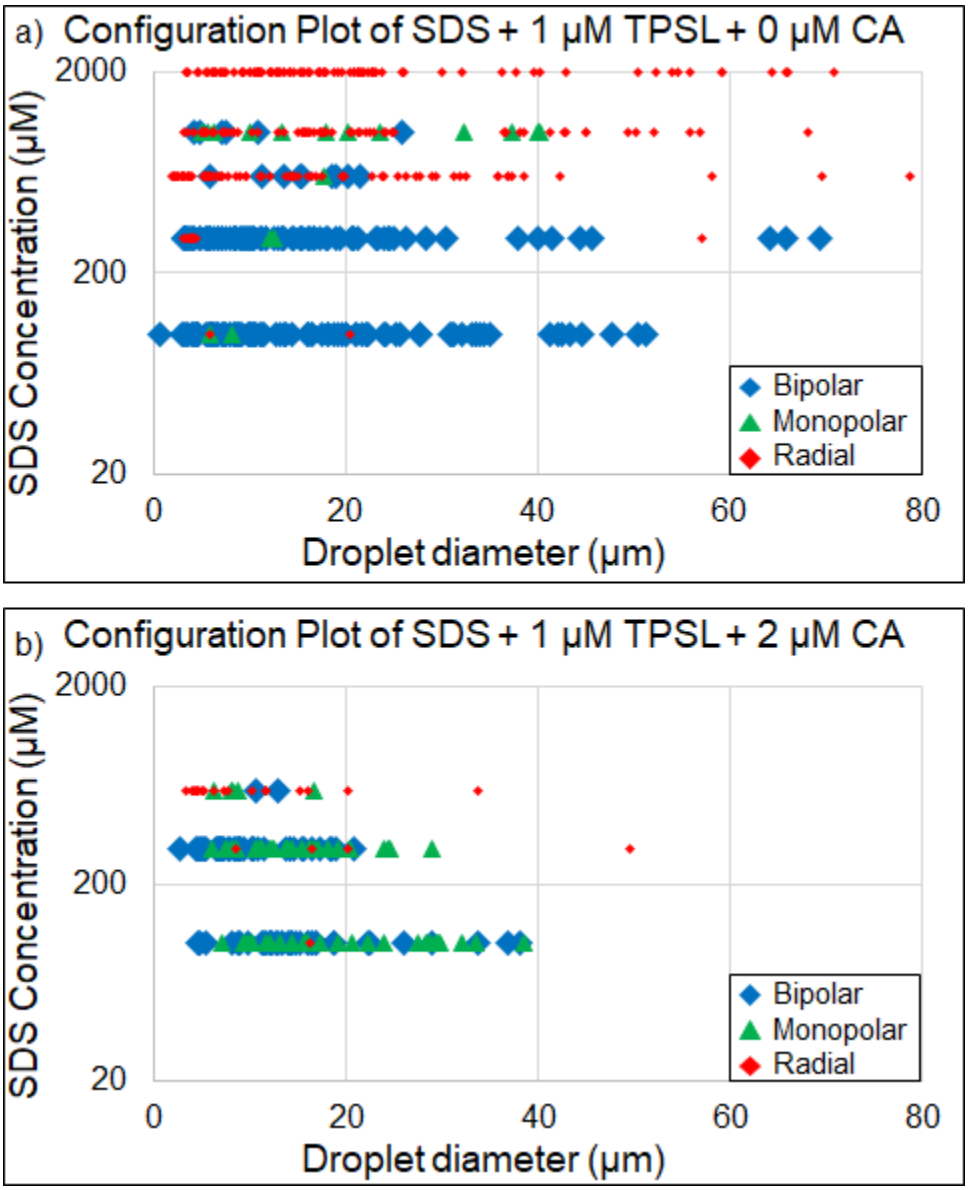

Figure 7.2. Concentration-diameter phase diagram of the 5CB liquid crystal droplets as a function of droplet diameter and SDS concentration. (a) A constant 1 μM TPSL is present in addition to the SDS. (b) In addition to the 1 μM TPSL and SDS, there is also 2 μM CA present.

too (40% and 40%). So, if we have an initial solution of 100 μM SDS and 1 μM TPSL and a bipolar droplet, we can introduce CA to the system and hopefully cause a transition from bipolar to monopolar.

Our first set of dynamic experiments started with an initial solution of 100 μM SDS and 1 μM TPSL (0 μM CA). Using a secondary solution of 100 μM SDS, 1 μM TPSL, and 6 μM CA, we increased the CA concentration over time to a final concentration of 2 μM to match our conditions of figure 7.2 b. At the end of the flowing, when the CA concentration was at 2 μM, we never saw a transition away from the bipolar configuration.

We decided to increase the CA concentration by an order of magnitude to see if more CA would cause the transition we expected from figure 7.2. In figure 7.3 left we are at the same initial surfactant conditions: 100 μM SDS and 1 μM TPSL with a CA concentration of 0 μM. We can see, based on the optical pattern, that the droplet is in the bipolar configuration. A little over 76 minutes later the CA concentration has increased all the way to 20 μM, but we still see the droplet in the bipolar configuration (figure 7.3 right). Shortly after the time shown in figure 7.3 right, an untrapped droplet collides with the trapped droplet and dislodges it from the optical trap. We did 4 total runs where the CA concentration was increased from 0 μM to 2 μM and 1 additional run where the CA concentration was increased from 0 μM to 20 μM.

So, what does this all mean? What reasons could there be for the transition experiments not causing a transition as we expected from the characterization results in figures 7.2?

First we asked if we are using enough CA. Maybe we would need to go even higher than 20 μM to see a transition. To answer this we looked up the dissociation constant, K_D, of the functional ligand group and CA. We used the information found in the article by Krishnamurthy 2008 [28]. Specifically, in Table 10 we used the value for the

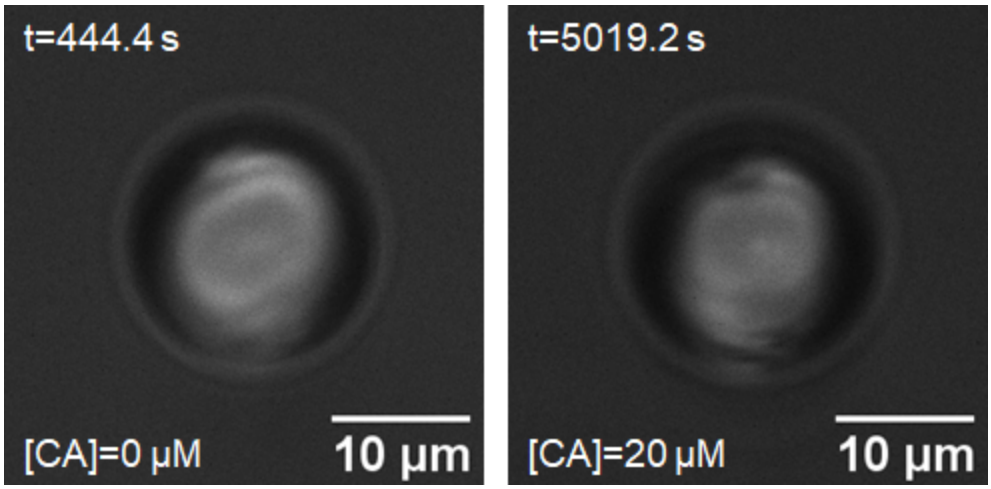

Figure 7.3. Before and after snapshot of a LC droplet at CA concentrations of 0 μM and 20 μM. The droplet stayed in the bipolar configuration and never transitioned to another configuration. Repeated 5 times, all with no transition.

second "type" of group (figure 7.1 d, right) with table entry **74** (figure 7.1 c), which lists a K_D of 160 nM. Using the definitions found in the "molecules with one binding site" on the wikipedia page for "Dissociation Constant" along with the definition of K_D, we can find an expression for the concentration of bound complex as a function of each component concentration and K_D value.

$$[AB] = \frac{1}{2}\left((A_0 + B_0 + k_D) - \sqrt{(A_0 + B_0 + k_D)^2 - 4A_0B_0}\right) \tag{7.1}$$

Where $[AB]$ is the concentration of bound TPSL-CA complex, A_0 is the concentration of TPSL in the system (a fixed 1 μM), and B_0 is the concentration of CA in the system. Since the concentration of CA is dynamic in the transition experiment, we can plot $[AB]$ as a function of B_0 (figure 7.4).

Plugging in values of $K_D = 0.16\mu M$, $A_0 = 1\mu M$, and $B_0 = 2\mu M$ or 20μM we calculate what percent of TPSL is bound to CA, with values of 87.5 % and 99.2 %. So, even if the first set of transition experiments that went up to 2 μM CA with 87.5 % of the TPSL bound, the experiment that went up to 20 μM CA with 99.2 % of the TPSL bound is about as good as you can get.

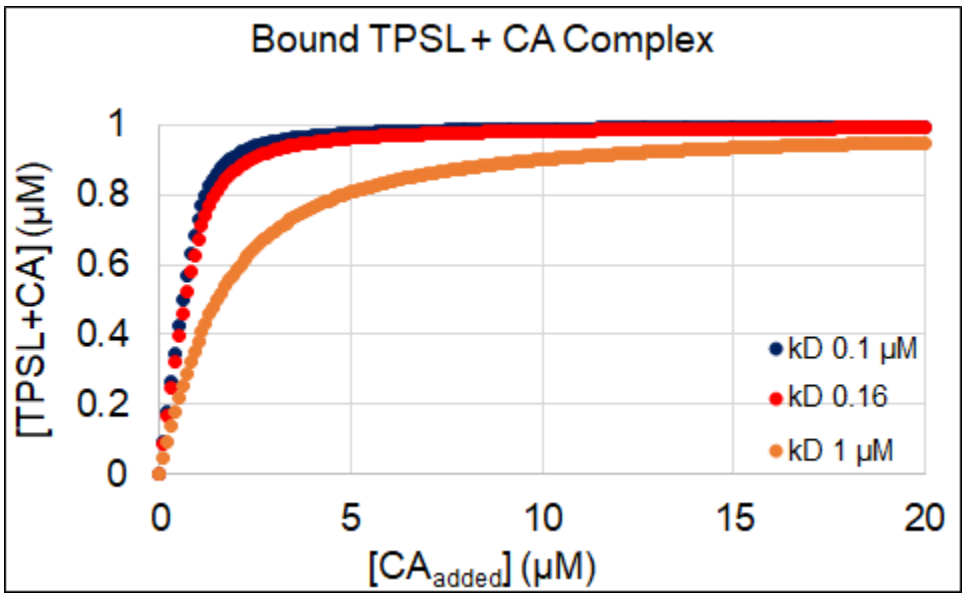

Figure 7.4. Simulated plot of concentration of bound TPSL-CA complex at k_D value of 0.16 μM (red) using equation 7.1. As a reference, we also simulated k_D values of 0.1 μM (blue) and 1 μM (orange).

Second we tested whether our CA was active and could actually bind to the sulfonamide ligand group of the TPSL surfactant. Using a carbonic anhydrase activity assay kit from BioVision (Catalog #: K472) and a Heλiosα UV visible spectrophotometer we ran a total of 7 samples and measured their activity. All samples include the substrate included in the kit and the following combinations of reagents. All TPSL concentrations are at 1 μM and CA concentrations are at 1 μM. The linear regime of the absorption plot is shown in figure 7.5. The first 5 samples listed are in blue and have a positive slope because the CA is reacting with the substrate. The concentration of SDS in the sample has a negligible affect on the slope. The last 2 samples are in red and have a slope of 0 because they either do not have CA at all or include an inhibitor as control experiments.

1. CA

2. CA + TPSL

3. CA + TPSL + 300 μM SDS

4. CA + TPSL + 600 μM SDS

5. CA + 600 μM SDS

6. TPSL + 600 μM SDS

7. CA + Inhibitor + TPSL + 600 μM SDS

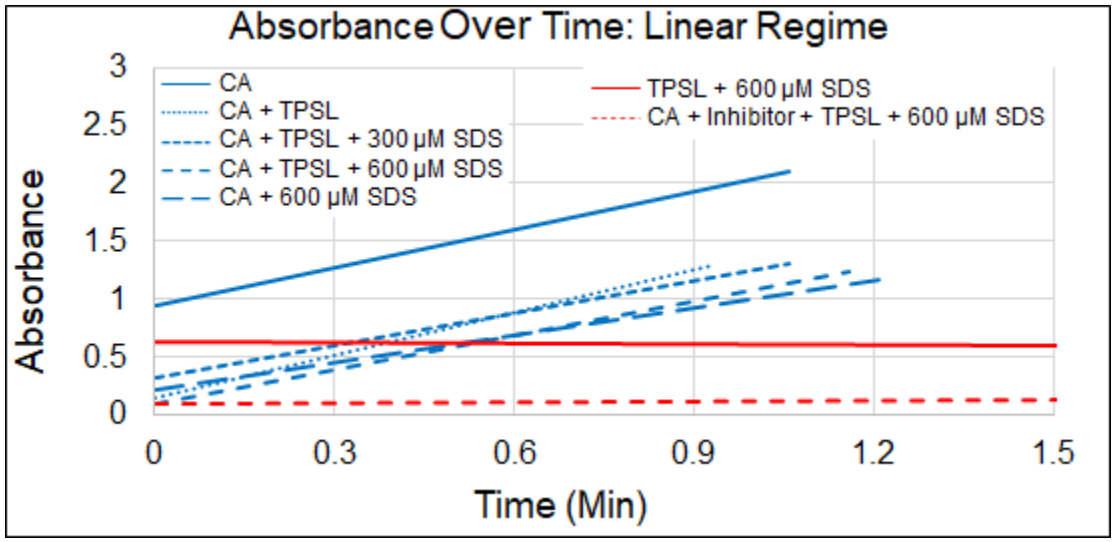

Figure 7.5. Absorption of the 7 samples listed on the plot over the first 1.5 min while the increase is still linear. The first 5 samples listed are in blue (left) and have a positive slope because the CA is reacting with the substrate. The last 2 samples are in red (right) and are negative controls.

Figure 7.5 shows that our CA is indeed active and binds to the substrate, even in the presence of TPSL and/or CA.

7.4 Conclusions

Unfortunately, based on the experiments we have done so far, it appears that TPSL and CA are not a surfactant-protein pair that will work as a protein sensing system. Do not abandon hope! There are nearly limitless combinations that could be

tested and the ineffectiveness of this system does not mean that other systems will also be ineffective. Too often in science we focus on what "works", but this data show that this TPSL-CA system "does not work" (yet) and that is still a valuable lesson.

OUTLOOK AND FUTURE DIRECTIONS

There are three main restrictions on the objectives and methods described above. Perhaps the largest difficulty with this work is in method 2. I can only trap a single droplet at a time, and so to get many data points I need to make many samples. At best, I can run four experiments of method 2 in a day, and typically one or two of them will not be useable. With the technique described in Curtis 2002 [8] it would be possible to have several trapping locations in the frame. Even if two or three droplets could be trapped and seen transition simultaneously, that would increase the data collection rate by a factor of the same amount. As an approximation using the average droplet diameter and the field of view of the camera, a maximum number of about 25 droplets could be observed simultaneously. This has the potential of making a day's worth of work equal to over a month's work using the current optical tweezer set-up.

The second piece of the project that could be modified is the method of making the LC emulsion. Currently, all the LC emulsion samples I make are polydisperse. While this has the benefit of being able to observe the phase transitions over a wide range of droplet diameters, it has the drawback of low repeatability for specific diameters. If microfluidic devices were used to create a monodisperse LC emulsion, then specific droplet diameters could be measured in a systematic way. Microfluidics is a growing but already strong field and using them for this work is feasible.

Lastly, the most obvious way to expand this work is to test more novel surfactants. Specifically, surfactants that are designed with triggerable groups sensitive to stimuli besides protein binding would be ideal. By exploring the dynamics of phase transitions in the presence of other novel surfactants and the triggering of the transition with different triggers, the scope of the applications grows quickly.

The results of these 4 projects is a step forward toward making responsive materials inspired by nature. Characterizing the transitions between the bipolar and radial phases, which have different light scattering patterns, will allow for a more targeted and precise configuration change. The use of novel sufactants and various triggers unlocks the potential for several different avenues of triggering the bipolar to radial configuration transitions. These different mechanisms allow responsive materials to be realized in equally as many different ways. The flexibility and customization depth of responsive materials is what I find to be most exciting.

APPENDIX A

DROPLET CATALOGUE

This appendix has a four page figure that shows many example droplets of each configuration that we classify. This is intended to be used by a new student on the project as a reference to help them categorize their own data. There are several examples of the three main internal configurations, radial, bipolar, and monopolar, as these are the most important (figure A.1 a, b, and c). I've also included a handful of "other" droplets that I do not know how to classify and "unknown" droplets that are narrowed down to two configurations, but can't decide which one (figure A.1 d and e). Penultimately, there is an example of a droplet to *not* measure because in this case it is not circular (spherical)! The reason why this happens is because the LC is not actually in a droplet and is instead wetting on the coverslip or slide (figure A.1 f). Lastly, there are two examples of droplets, circled in yellow, that are in focus while the other droplets in the field of view are out of focus. These droplets are the ones you're looking for. The out of focus droplets are possibly wetting the surface, so it is safe to go higher in the z-direction to look for droplets (figure A.1 g).

All data shown here are using SDS as the only surfactant molecule and are all at the same concentration.

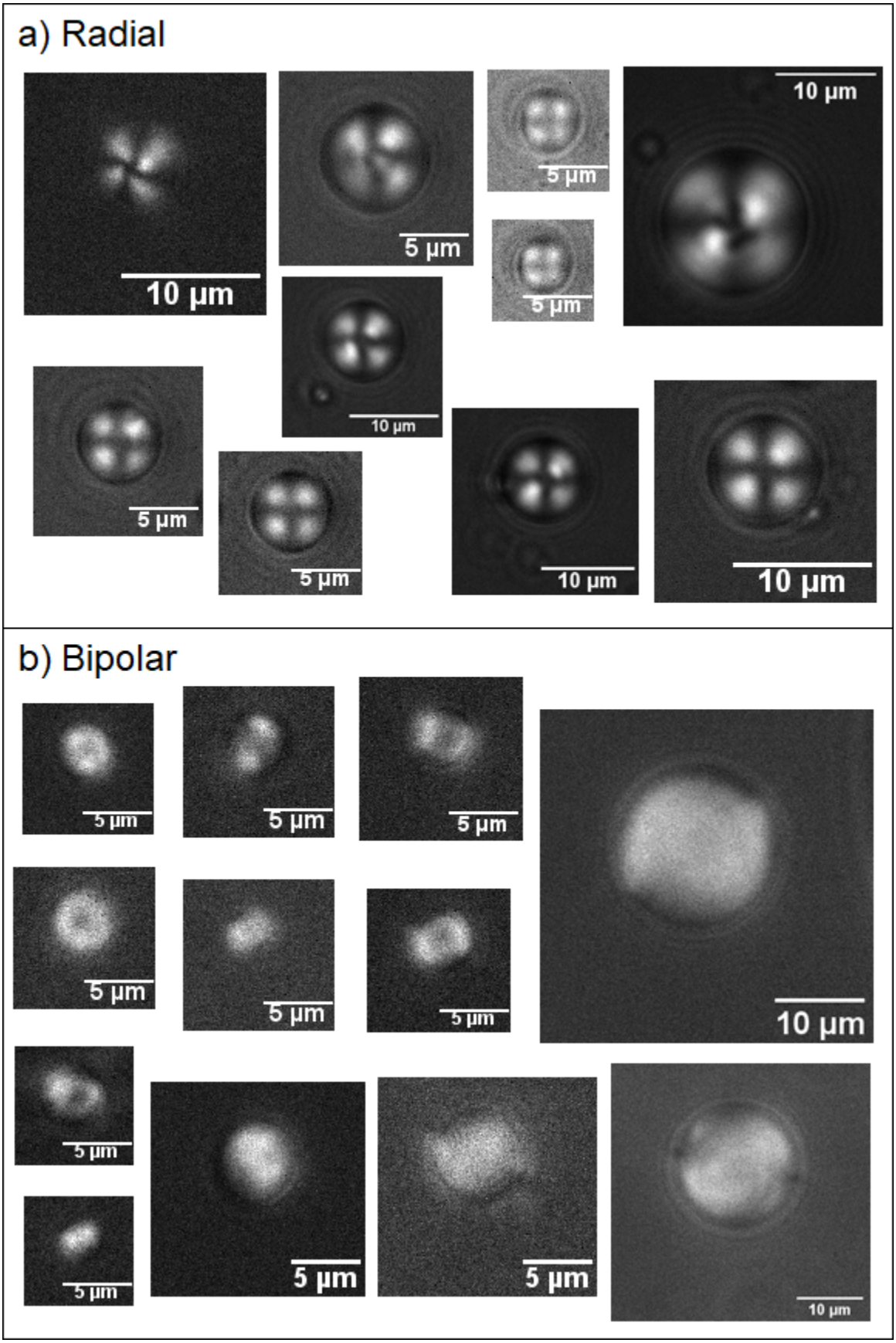
a) Radial
10 µm
5 µm
5 µm
10 µm
5 µm
10 µm
5 µm
5 µm
10 µm
10 µm
b) Bipolar
5 µm
5 µm
5 µm
10 µm
5 µm
5 µm
5 µm
5 µm
5 µm
5 µm
10 µm

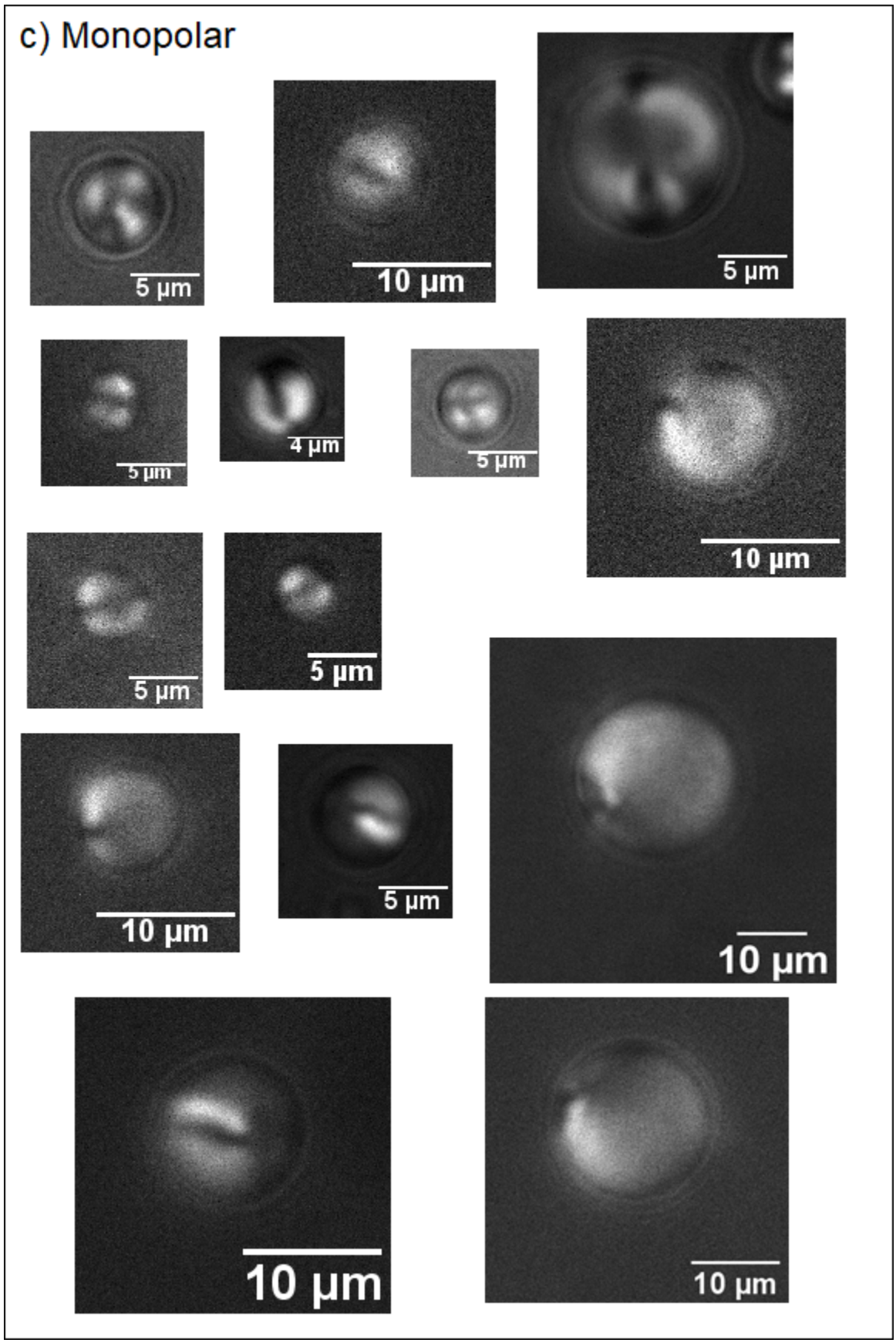
c) Monopolar
5 µm
10 µm
5 µm
5 µm
4 µm
5 µm
10 µm
5 µm
5 µm
10 µm
5 µm
10 µm
10 µm

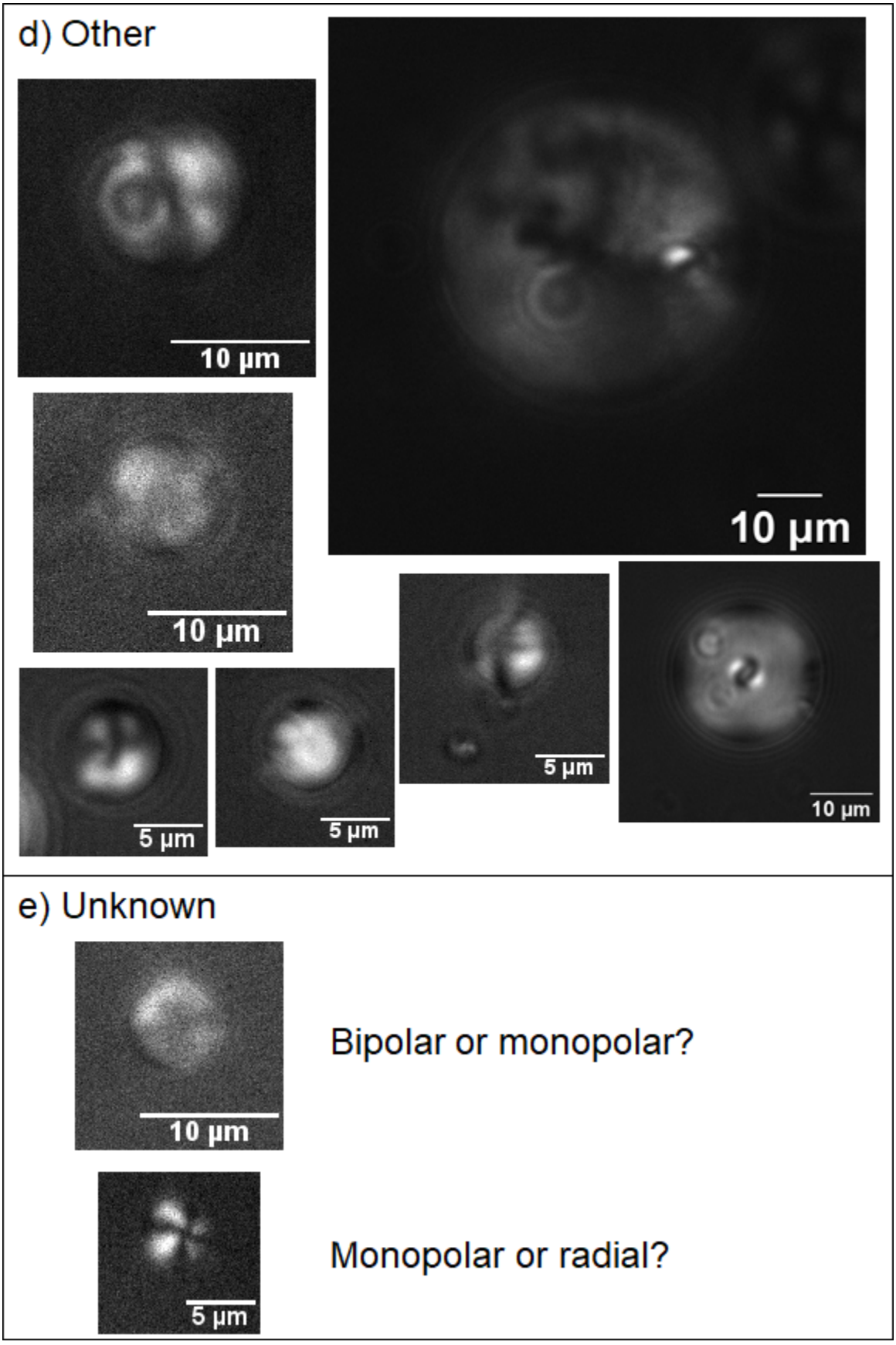
d) Other
10 µm
10 µm
10 µm
5 µm
5 µm
5 µm
10 µm
e) Unknown
10 µm
Bipolar or monopolar?
5 µm
Monopolar or radial?

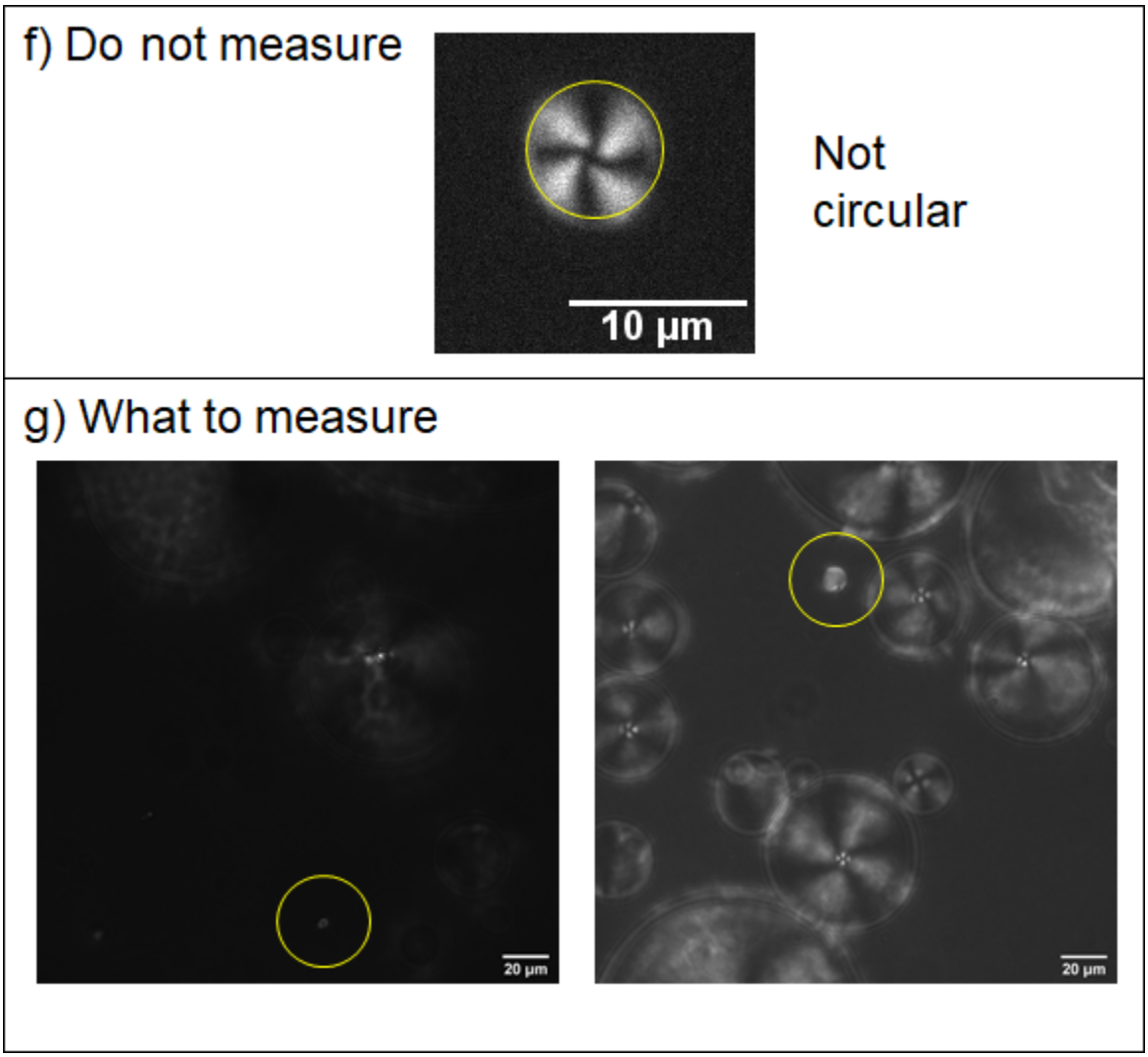

Figure A.1. Many example droplets of internal configuration (a) radial, (b) bipolar, (c) monopolar, (d) Other, and (e) Unknown. Also included are (f) what droplets to not measure and (g) what droplet to measure.

APPENDIX B

DROPLET CONFIGURATION CHEAT SHEET

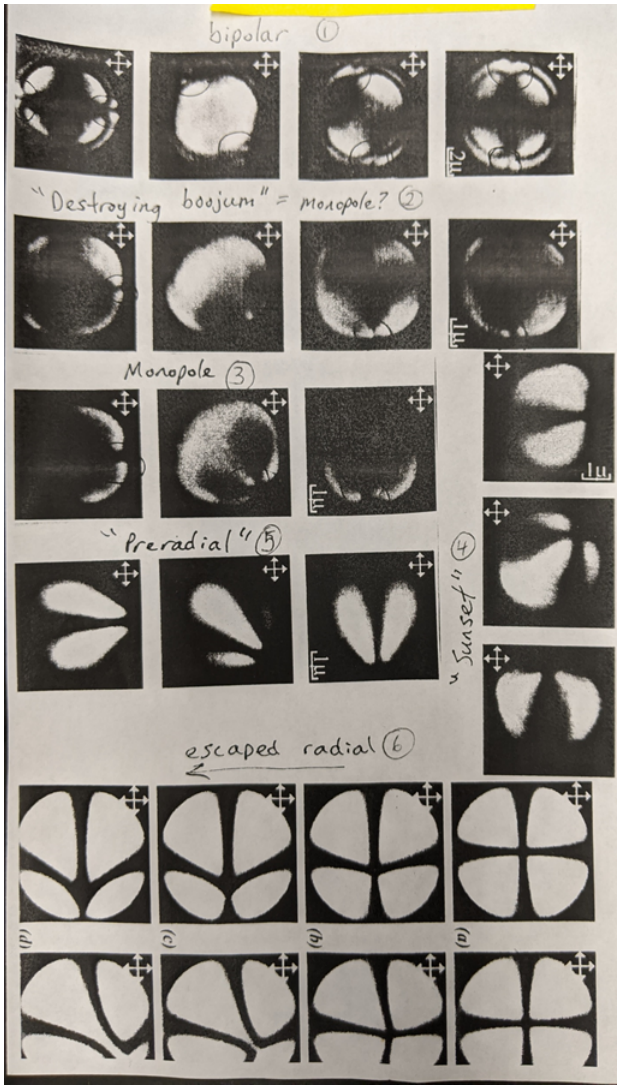

Figure B.1. Experimental images taken from Prischepa 2005 [40] and compiled into a 1 page cheat sheet. Ben, Linda, and I used this as a reference when classifying the droplets shown in Appendix A.

APPENDIX C

DROPLET PRACTICE CATEGORIZATION

Use appendices A and B as resources while trying to assign a configuration to each of these droplets. The "solutions" are given on the page after the quiz, so no peeking until you're done!

Note that you are not limited to classifying these droplets as only radial, bipolar, or monopolar. If you're not sure, call it unknown. If you don't think it's anything, call it other.

All data shown here are using SDS as the only surfactant molecule and are all at the same concentration as in figure A.1.

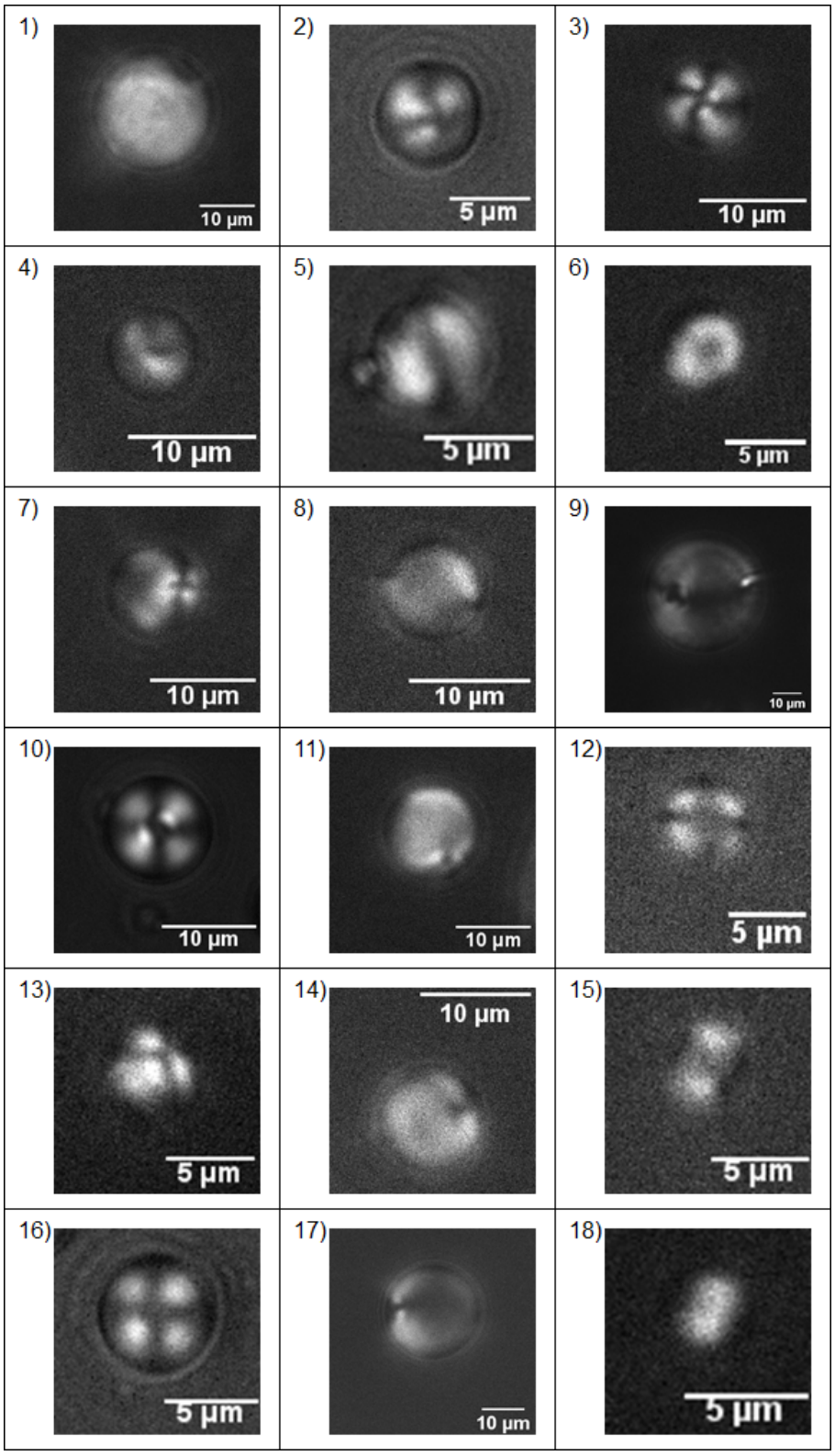

Figure C.1. This 18 droplet quiz is to give a student new to the project some practice on classifying LC droplets with "answers" provided.

C.1 Solutions to Droplet Practice

These are what I would have classified them as. If you disagree, that doesn't necessarily mean that you're wrong. If you can justify why yours is correct and mine is incorrect, then you're probably right!

1. Bipolar
2. Monopolar
3. Radial
4. Other
5. Monopolar
6. Bipolar
7. Unknown: might be radial or monopolar
8. Bipolar
9. Other
10. Radial
11. Monopolar
12. Bipolar
13. Monopolar
14. Monopolar
15. Bipolar
16. Radial
17. Monopolar
18. Bipolar

APPENDIX D

EXPERIMENTAL TECHNIQUES AND PROTOCOLS

In this appendix I provide a list of reagents used in the projects and include experimental protocols that can be used to reproduce the experiments described in this work.

D.1 Reagents

A complete list of all reagents used for the experiments detailed in the following sections are listed below. Each item has a catalog number or CAS number where appropriate and manufacturer in parenthesis.

- Culture tubes: Cat no 14-961-27 (Fisher)
- 10 uL Hamilton syringe: Cemented needle, point style 2 (Hamilton Company)
- Chloroform: CAS 67-66-3 (Fisher)
- Sodium Dodecyl Sulfate: Cat no 71725-50g (Sigma)
- 4'-Pentyl-4-biphenylcarbonitrile (5CB): CAS no 40817-08-1, Cat no 328510 (Sigma)
- (Zap) Z-poxy 5 minute set (Pacer Technology)
- 1,1'-Dioctadecyl-3,3,3',3'-Tetramethylindocarbocyanine Perchlorate (DiI): Catalog number D282 (Fisher)
- 22x30 – 1.5 glass coverslips: 12-544 (Fisher Scientific)
- 1 cm cloning cylinders: CLS316610 (Sigma Aldrich)
- PTFE #30 AWG thin wall tubing (Cole Parmer)
- 1 mL plastic syringe with Luer-Lok tip 30G tip x1/2 (0.3 mm x 13 mm) Precision glide (Becton, Dickinson and Company)
- Syringe pump: SP200i (World Precision Instruments)
- 22x22 – 1.5 glass coverslips: 12-541-B (Fisher)
- 75x25x1 mm glass slide: Cat no 16004-422 (VWR microscope slides)

- NIS Elements AR 4.30.02 64-bit software
- Microscope
  - Nikon Eclipse Ti microscope
  - Nikon Plan Apo 60x WI objective, 1.20 NA, WD 0.31-0.28, ∞ / 0.15-0.18 DIC N2
  - Andor Zyla sCMOS camera
  - Crossed polarizers
  - Optical trap

D.2 Protocols for Experiments

This section includes fours sets of protocols. These protocols get you and your LC droplets all the way to the microscope. Appendix E teaches you how to measure, analyze, and plot the data. As with any protocol, read all steps before starting and complete each step before starting the next one. I've included some comments to help clarify some steps.

The transition experiments described in this work used a specific experimental setup to meet the demands on the experiment. We needed to use a chamber that we could dynamically adjust the surfactant concentration inside and we did this by using a cylindrical chamber that was open to the air and connected to a syringe pump.

For characterization experiments you can use the same type of chamber used in the transition experiments but without the tubing. To make a characterization chamber, stop after step 4. We used to do these experiments using a more traditional flow chamber, but found that the height restriction of the chamber was not ideal.

D.2.1 10 mM Phosphate Buffered Saline (PBS)

D.2.2 Cylindrical chamber construction

Figure D.1 shows a completed chamber. This is like the picture on the front of the puzzle box so you know what you're going for.

Figure D.2 is the 3D printed tool described in step 4 below.

1. Clean a coverslip by blowing both sides with air. Prepare a number of coverslips equal to the number of experiments you plan on doing and one backup.

   I used normal air passed through a 0.2 μm pore filter. Using N2 gas is supposedly better.

2. Clean an equal number of cloning cylinder by blowing it with air. Focus on the inside, top and bottom.

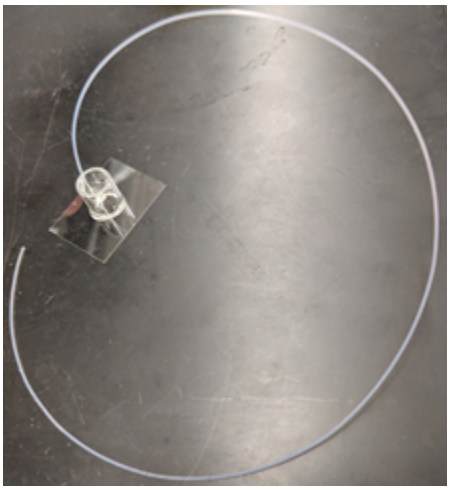

Figure D.1. Example chamber used for transition experiments, fully constructed but empty.

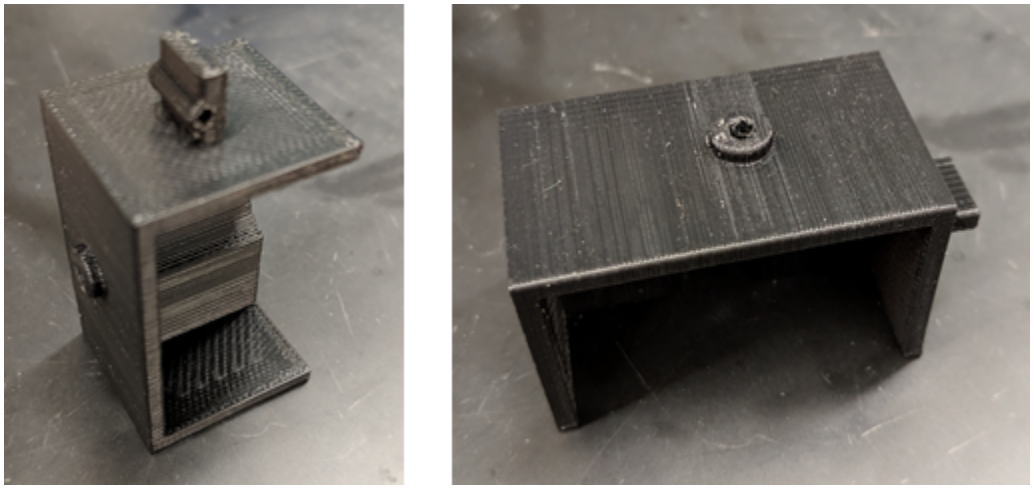

Figure D.2. 3D printed tool as seen from the side (left) and above (right). The device is printed on the side so that the holes do not get clogged with scaffolding material during printing.

3. Mix some 5-min epoxy and use it to attach the cylinders to the coverslips in a 1:1 ratio. Use a toothpick to smear a thin layer of epoxy on the bottom of the cylinder. If you're preparing more than five experiments, it may need a second mix of epoxy.

4. Wait for the epoxy to dry completely. Use this time to turn on the optics and cut however many lengths of tubing you need.

   If you're making a chamber for characterization experiments, stop after this step, but skip the tubing.

   For my specific optical set up, 330 mm of tubing was sufficient. This length was enough to comfortably reach from the chamber to the syringe pump while not having lots of slack. You may need more or can get away with less using another set up. **It is critical to calculate the internal volume of the tubing.**

5. Attach the tubing using epoxy to the inside of the cylinder. Keeping the tubing in place while the epoxy hardens is best done by using the 3D printed tools. I prefer the ones labeled "1" and "3" and only doing two at a time.

   This step is the most likely to go wrong. You need to mix the epoxy and let it sit for 2-3 minutes and become thick before applying it to the cylinder. During this 2-3 minutes, feed the tubing through the 3D printed tools. If you use the epoxy too early, it will run down the inside of the cylinder and pool at the bottom, blocking the inlet tube. If you use the epoxy too late, it will not be soft enough to mold around the inlet tube and the inlet tube will not be secure.

   I've found three little things that help. The first is that during the 2-3 minute wait, try to see how the tubing that was fed through the tool's hole will sit in the chamber and where under the tool the chamber should sit. This will help position the tubing into the chamber once the epoxy has been added. The window of time to secure the epoxy is pretty small, and if you're slow getting the first one aligned, the epoxy may be too solid to complete the second chamber. The second is that while mixing the epoxy and during the 2-3 minute wait, use the toothpick to pick up some epoxy and see how it runs off. There is a point where it will bead up on the toothpick and very slowly drip off, or maybe not at all. This is when you want to apply it to the cylinder. The third tip is about how to apply the epoxy to the cylinder. Get a small gloop on the toothpick and scrape it off into the cylinder from the top. As you're scraping, spread it over a width of a couple toothpick diameters so that it isn't one big gloop.

6. Quickly place the cylinder under the 3D printed tool in such a way that the tubing doesn't immediately contact the epoxy. With the cylinder in place, reposition the device to move the tubing into the epoxy. Wait until the epoxy is completely solid before removing the 3D tool or moving the chamber.

   To see if the epoxy is solid on the chamber, poke the epoxy mix that you used. Once that epoxy you took from is solid, the epoxy used in the chamber is solid. Wait another minute anyway.

D.2.3 LC Emulsion Sample Preparation

1. Prepare all solutions for the experiments. Think ahead about what volumes you'll need based on the syringes and needles available.

2. Label one syringe with a piece of tape for the "initial solution", which is the same surfactant concentration that the emulsion was made at. Draw into the syringe however much volume is needed for the day's experiments.

3. Label a second syringe with a piece of tape for the "secondary solution", which is calculated in such a way that after the flowing the sample will be at a specified final concentration.

   Be aware of how long each needle is. For long needles it is easy to draw into the syringe from the bottom of the eppendorf tube. If the needle is short, then you can only draw from above the 1 mL mark on the eppendorf tube (using 2mL tubes). So, with short needles, even if you need 500 μL, you should make 1.5 mL.

   If the secondary flow needs 124.1 μL, and I was doing 5 experiments that day, I would fill 150 x 5 = 750 μL into the syringe. The initial flow through needs 100 μL per run, so I would fill at least 500 μL.

4. Get a number of culture tubes equal to the number of experiments you plan to run that day.

5. Using air, blow out any dust that may be inside the culture tube.

   Again, I used normal air passed through a 0.2 μm pore filter. Using N2 gas is supposedly better.

6. Add 250 μL of initial solution (from what is left in the eppendorf tube) to the cleaned culture tubes.

7. Clean the 10 μL Hamilton syringe by drawing and expelling chloroform ten times. Blow through with filtered air (or N2 gas).

8. Use the 10 μL Hamilton syringe to draw up 0.5 μL of 5CB for each experiment that day.

9. Add 0.5 μL of 5CB to each culture tube.

   This 0.5 μL is small enough that if you expel it gently and carefully, it will bead up on the end of the syringe. Lower the syringe into the 250 μL of initial solution and the 5CB will go into the solution and leave the syringe tip. Remove the syringe, expel another 0.5 μL, and lower into the next culture tube. Repeat until done. Note that this is only allowed because each solution is the same surfactant concentration, so there is no risk of messing up the concentration in a later tube.

10. Cover each tube with a small square of parafilm.

11. Clean the 10 μL Hamilton syringe by drawing and expelling chloroform ten times. Blow through with filtered air (or N2 gas).

12. Flick the culture tube to break up the 5CB into small droplets.

    How hard you flick the tube will (loosely) determine the size of the droplets. If you can see the droplets macroscopically, they're too big and you should flick more or harder.

D.2.4 Getting the sample on the microscope

Now that you have filled syringes, several LC emulsion samples, and fully constructed chambers, take everything to the microscope room.

1. Mount the empty cylindrical chamber with tubing on the microscope.

2. Place the initial solution syringe on the syringe pump and focus the chamber on the microscope.

3. Flow 70 μL of initial solution from the syringe into the chamber. I flowed at a rate of 70 μL/min. Check the chamber to see if liquid has gotten into the chamber. If not, either the end of the tube in the chamber is blocked by epoxy, or the end attached to the syringe pump is loose. Check for a small puddle under the connection. Either way, that chamber is no longer usable, so restart this protocol with a new chamber.

4. Disconnect the initial solution syringe

5. Replace the initial solution syringe with the secondary solution syringe. Connect the tubing.

6. Re-flick a culture tube and then pipette 30 μL of 5CB emulsion to the chamber.

   This 100 μL total should be enough to cover the bottom the chamber. If it doesn't appear covered, use the pipettor to draw up 20 μL from somewhere in the chamber and expel it where the chamber is still dry.

7. Find a droplet and trap it. Move the droplet to the opposite side of the chamber from where the inlet tube is attached.

   I did this while recording, but there is no analysis done on these videos. I did three minute videos and would end them early if I found a droplet quickly or run multiple short videos if I couldn't find a droplet quickly. I record these videos mostly as back-up evidence that the droplet is trapped. I trap it on the opposite side of the chamber so that the inlet flow doesn't disrupt the trapped droplet.

8. Double check that Elements is set up to run a long movie during the transition and is no longer recording for three minutes as you were while finding a droplet.

9. Place a finger over the "run" or "start" button on the syringe pump. Start the movie recording, and about 1 second later when the window pops up with the start of the recording, hit the button on the syringe pump.

   My videos had a time step between frames of 200 ms or 300 ms. A video at that frame rate for almost two hours is a **huge** file. Elements won't let you start recording if the whole video won't fit, which is good, but you should also check that you have enough room on a hard drive for all the videos.

D.2.5 Using the Syringe Pump

Since the syringe pumps I used were actually borrowed from the Dinsmore lab, I'm going to write this part for a generic syringe pump.

First, explore the settings and options on the syringe pump you're using. The important settings are: volume, (flow) rate, and (syringe inner) diameter. Some pumps have a built in database of common syringes and have the diameter saved, but you can always just look it up from the manufacturer and input it manually.

The way the syringe pump works is that the syringe is secured on the device with some clamp and when you turn it on there is a movable blocky piece that moves in one direction that will push the plunger. A couple things to check before starting any flow from the syringe pump. 1) Check that the lock on the block is set so that it actually moves when you turn on the pump. If the block is not locked, then there will be no flow. 2) Check that the block is snugly against the syringe's plunger so that when the block starts moving liquid starts getting expelled from the syringe. If you don't do this then the machine will think it pushed the plunger 10 cm and really it only pushed it 9.9 cm, which is enough to make your calculations wrong.

Given the inner diameter of the syringe, the total volume you want to flow, and the flow rate, the device will calculate what speed to move the block at and for how long to match those parameters.

Something else to keep in mind is that if you tell the syringe pump to flow 100 μL not all of it will make it to the chamber. Some will still be left in the inlet tube! That is why it is important to look up the inner diameter of the tubing you use, measure the length, and calculate the internal volume of your tubing. I always used a length of 330 mm which has an internal volume of 24.1 μL. If I want to flow 100 μL into the chamber, I tell the pump to flow 124.1 μL.

If you're replacing the syringe but using the same tubing as in the transition experiments, the second flow through will first add 24.1 μL of the previous solution into the chamber and then the remaining volume as secondary solution. Because there is no air in the tubing to start, if you tell the pump to add 124.1 μL it will add 24.1 μL of initial solution and then 100 μL of secondary solution.

D.2.6 How to take data

If you use the recommended cylindrical cup, the only thing you have to keep in mind is to not directly pipette your LC sample to the dry chamber. I advise that you add 100 μL of your surfactant concentration to the chamber first to wet the bottom.

Then, add 50 μL of sample to the chamber. The reason for doing this is that when you expel the emulsion from the pipette tip into a dry chamber you actually splatter most of the LC droplets onto the coverslip. If you have a little bit of volume already in the chamber when you pipette, then this happens much less or not at all.

There are two strategies used to take data that Ben, Linda, and I have used. Method 1: Record continuously as you scan through the chamber in a snaking pattern to observe each droplet. When you get to a droplet, move up and down in the z-direction being sure that you pass through the plane where the droplet is focused. I would use 3-min movies so that analyzing them was more bite-sized.

Method 2: Move through the chamber in the same snaking pattern, but do not continuously record. Instead, when you get to an area with droplets, start recording and do the same z-direction sweep to pass through the plane where the droplet is in focus.

Method 2 is better when the chamber is very sparse. That way the "dead time" of no droplets in method 1 isn't recorded. Method 2 is also arguably better when the chamber is very dense. You can make a tile-like pattern to get all the data. For a tile-like pattern, record a z-sweep for a field of view, move in the x-y plane so that no droplets you just recorded are still visible, and do another z sweep. The concern with method 2 is that you may choose not to record a droplet because there is only one or two in the field of view and instead find a field of view with more droplets in it.

Regardless of the method you choose to use, I suggest that you hover around the z-plane that is about one average droplet radius above the bottom of the chamber. At this level most droplets will be almost in focus, but probably not exactly. When doing the z-sweep, go down so that the droplet is definitely out of focus, then back up slowly until you're well above the droplet, then back down to roughly wherever you started.

APPENDIX E

DATA ANALYSIS TECHNIQUES AND PROTOCOLS

E.1 Measuring Droplet Diameter

We use Fiji, a free image analysis software, to make all of our measurements. You can download it yourself for free at this link: (https://imagej.net/Fiji). When you open Fiji you can select "File" → "Open" to open a .nd2 data file. You will see the window shown in figure E.1 and the setting that I typically use. Opening large files first as a virtual stack will allow you to find which frames of the movie have the transition. For the characterization experiments, you should always use a virtual stack because you only have to record droplet diameter, position, and frame of focus.

The other option is to open the video by specifying stacks (figure E.2) which will give you the window shown in figure E.3.

If there are too many frames in the video, or the RAM on your computer is small, then you may get an error opening all of the frames. If you get a RAM error, I suggest opening the video as a virtual stack. If you already opened the video and know what frames are of interest, you can use this window to open only the ones you care about. You can also change T step which you can use to not open every frame, but every third frame, for example, by entering 3.

When you open a movie (with metadata) you'll have two windows open like in figure E.4. I repositioned the windows so the movie is on the left and metadata is on the right (figure E.4.) Near the bottom of the metadata window you will find the timestamp information when exactly each frame was recorded, which is needed in the transition experiments to calculate the concentration of the flowed in surfactant solution.

When you first open a movie it will appear all black (figure E.4 left). If you navigate to "Image" → "Adjust" → "Brightness/Contrast" (figure E.5) you will open another window named "B&C" (figure E.6, left).

Notice the histogram in the "B&C" window is the full 0 to 65535 range for a 16 bit image with a sharp peak that doesn't show in the video. If you press the "Reset" button (figure E.7) the look up table will return to what it was when the video was recorded. Now the histogram is between 195 and 9512, and we can actually see things in the video (figure E.7 center).

Next, I suggest checking the scale of the video by navigating to "Analyze" → "Set Scale" (figure E.8) which will open the "Set Scale" window shown in figure E.9. I prefer to make my measurements with no scale and convert pixel measurements to real distances using a known conversion factor. For the microscope I used with 60x magnification, this was 1000 pixels = 110 μm.

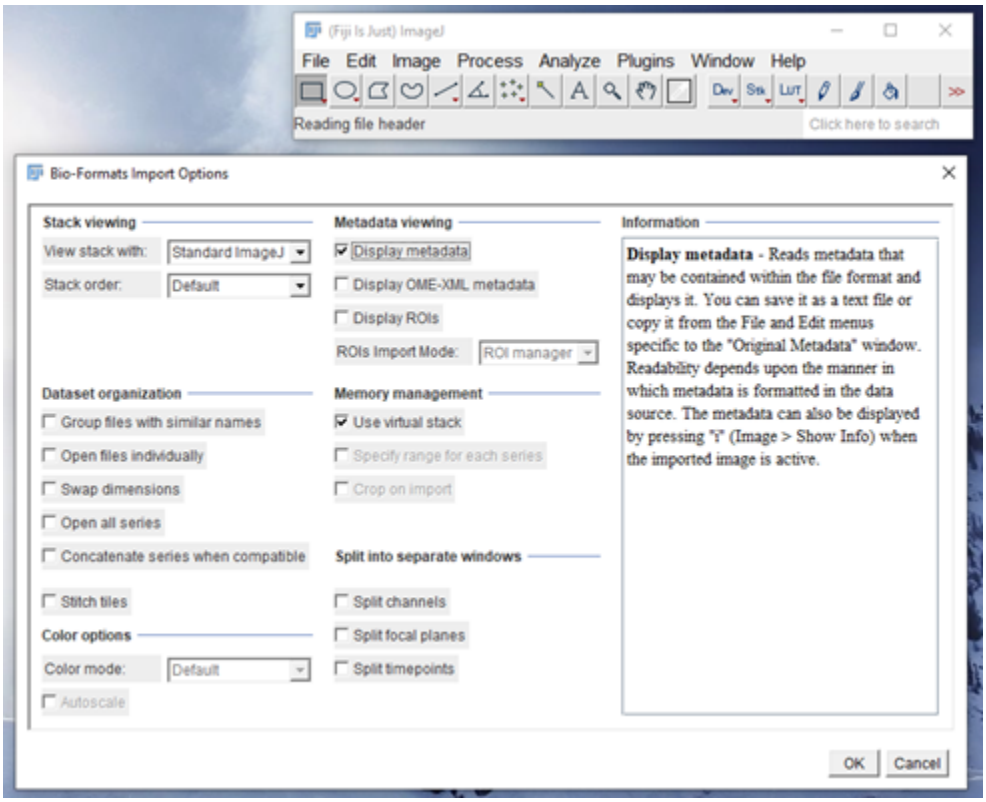

Figure E.1. Screen shot of Fiji toolbar (top right) and the "Bio-Formats Import Options" window when opening a new .nd2 file. The drop down menu for "view stack with" is set to "Standard ImageJ" and the menu for "stack order" is "Default". The only two boxes check are "display metadata" and "use virtual stack".

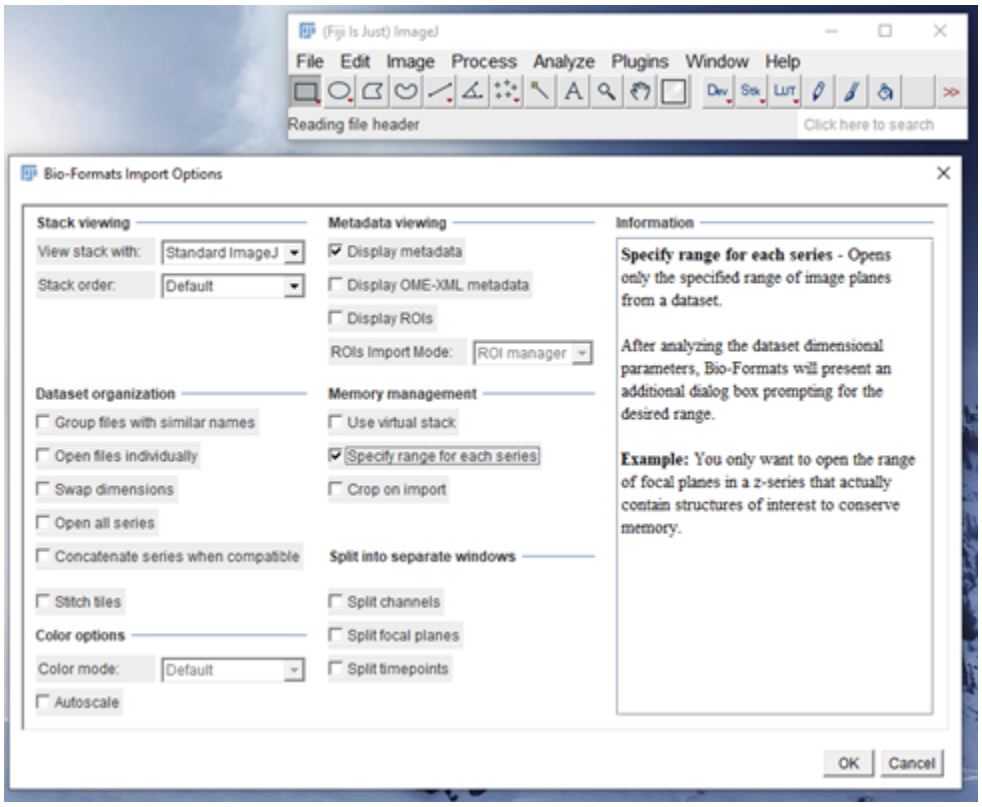

Figure E.2. Screen shot of Fiji toolbar (top right) and the "Bio-Formats Import Options" window when opening a new .nd2 file. The drop down menu for "view stack with" is set to "Standard ImageJ" and the menu for "stack order" is "Default". The only two boxes check are "display metadata" and "specify range for each series".

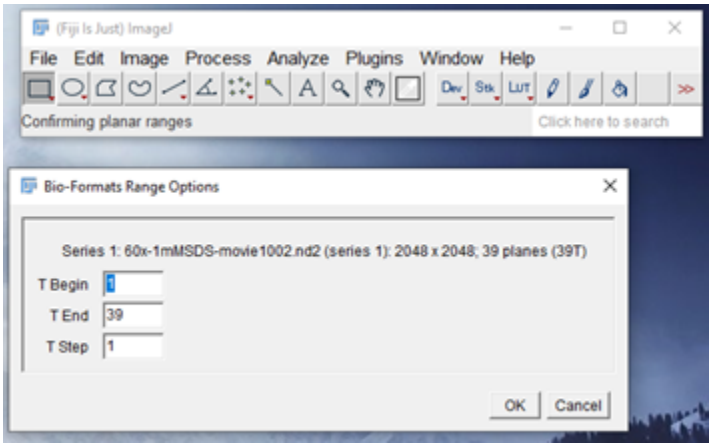

Figure E.3. Screen shot of Fiji toolbar (top right) and the "Bio-Formats Import Options" window after hitting the "ok" button in figure E.2.

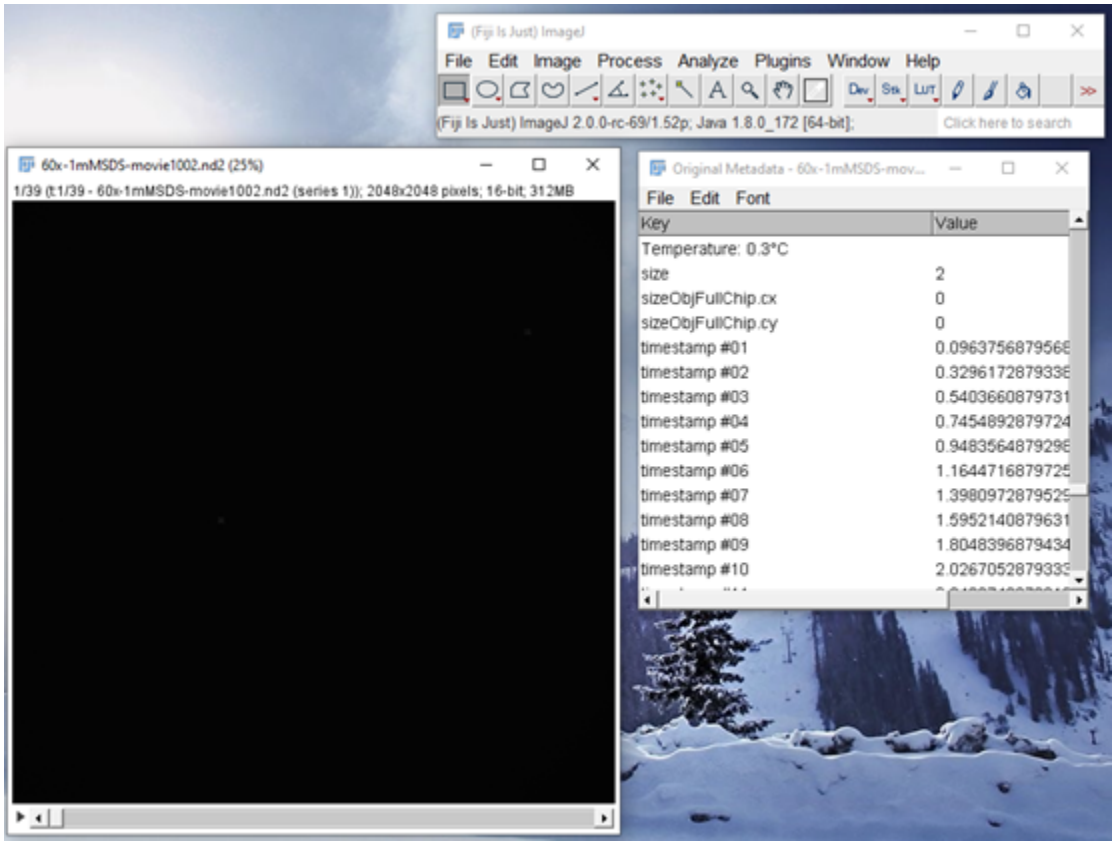

Figure E.4. Screen shot of Fiji toolbar (top right), the movie video (left), and metadata (right) after hitting the "ok" button in figure E.3.

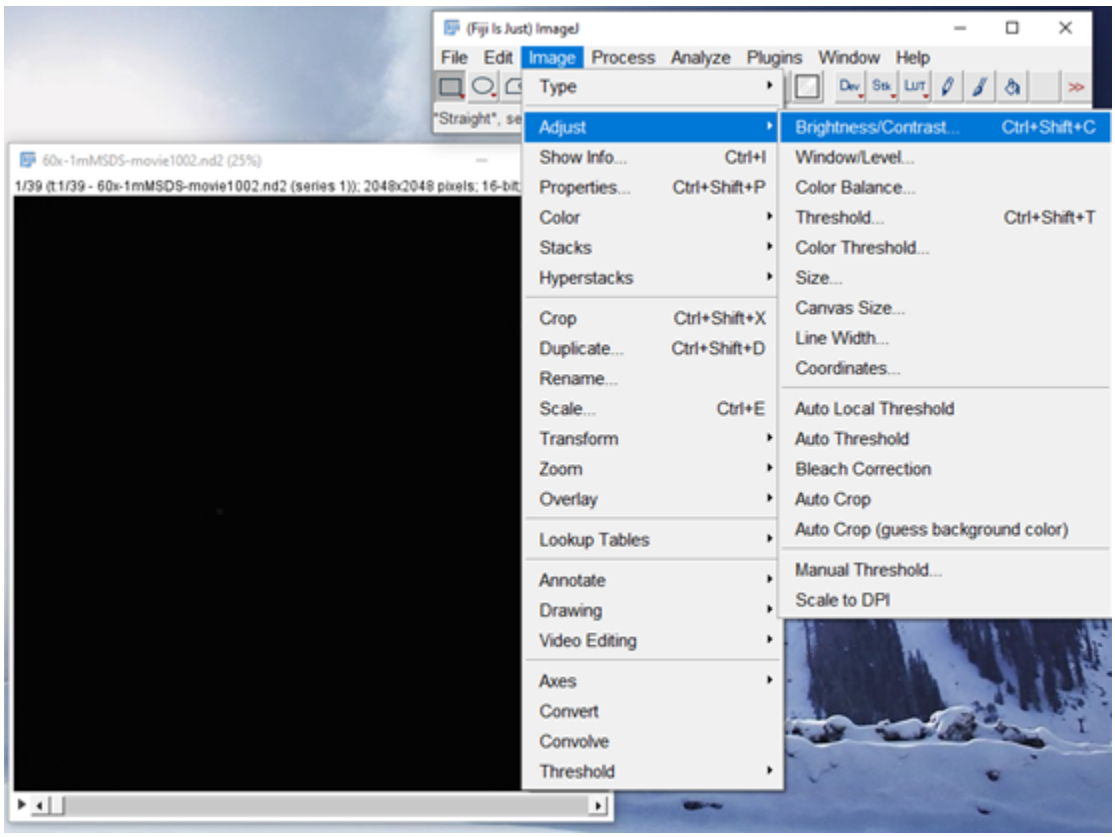

Figure E.5. Screen shot of Fiji toolbar (top right), the movie video (left), and metadata (right) after hitting the "ok" button in figure E.3. Navigation path to adjust the look up table shown as blue highlighted options.

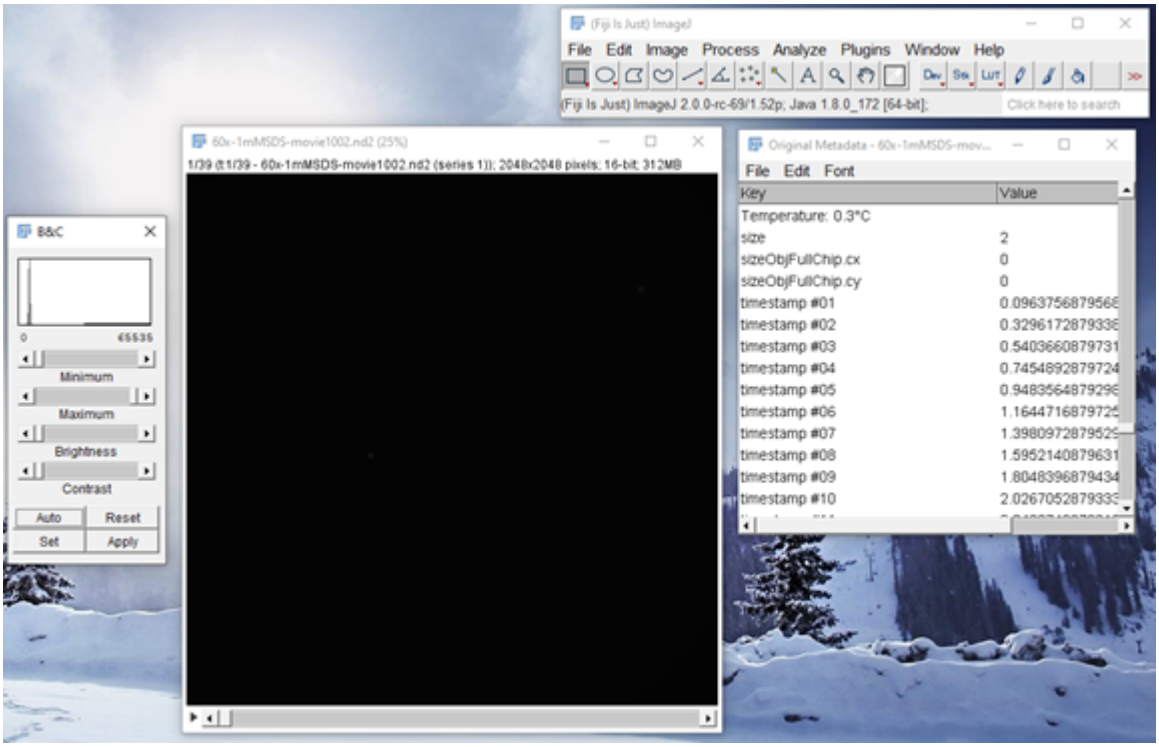

Figure E.6. Screen shot of Fiji toolbar (top right), the movie video (center), and metadata (right) after hitting the "ok" button in figure E.3. The "B&C" window (left) is a result of following the path shown in figure E.5.

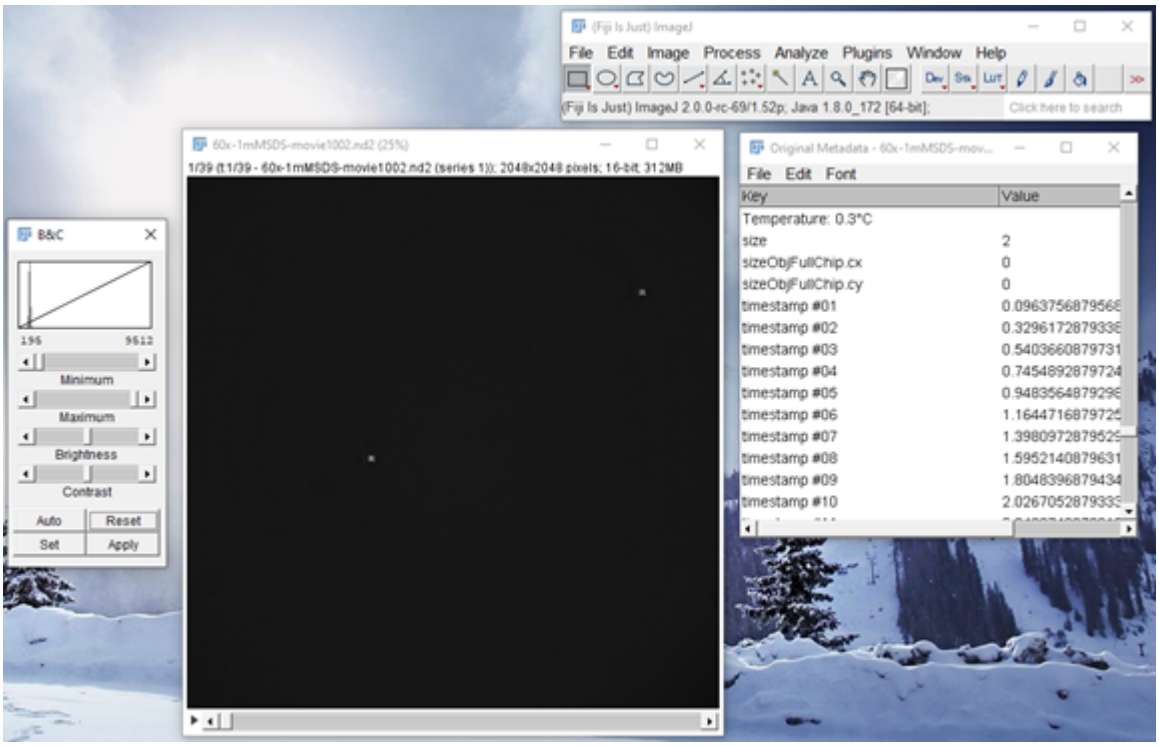

Figure E.7. Screen shot of Fiji toolbar (top right), the movie video (center), and metadata (right) after hitting the "ok" button in figure E.3. The "B&C" window (left) has been "reset", which is why we can now see droplets in the movie.

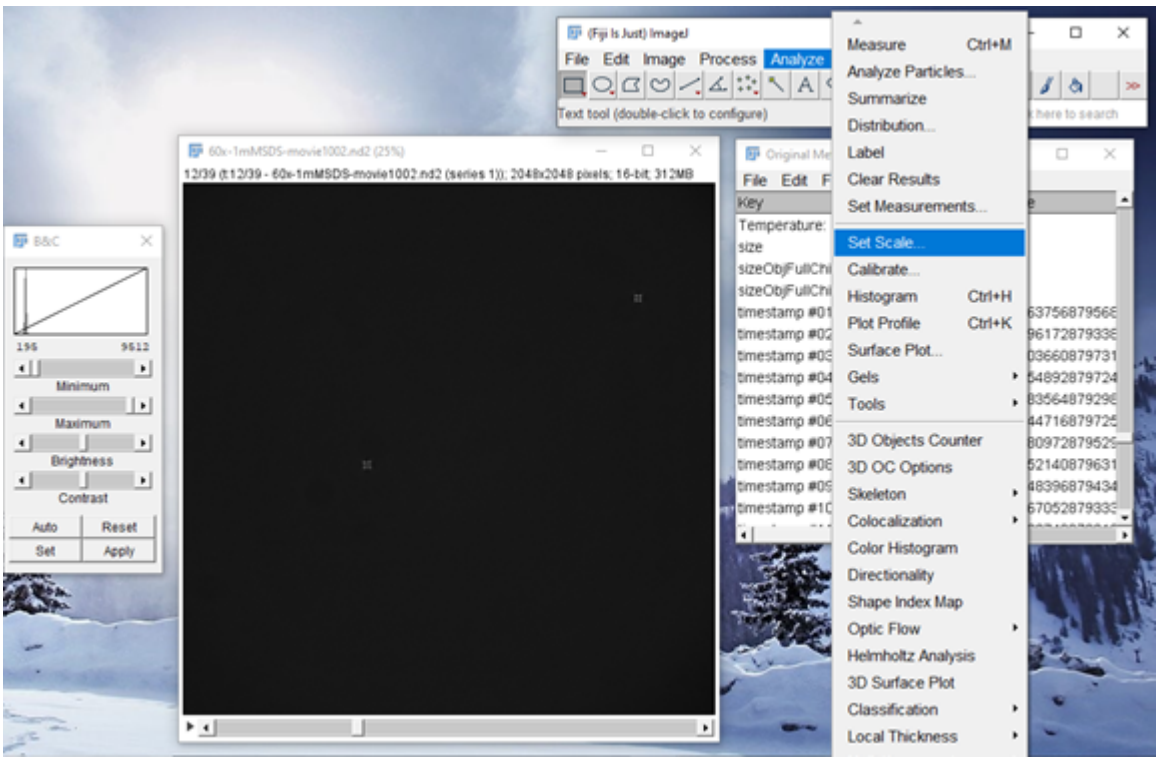

Figure E.8. Screen shot of Fiji toolbar (top right), the "B&C" window (left), the movie video (center), and metadata (right) as seen in figure E.7. Navigation path to set the video scale shown as blue highlighted options.

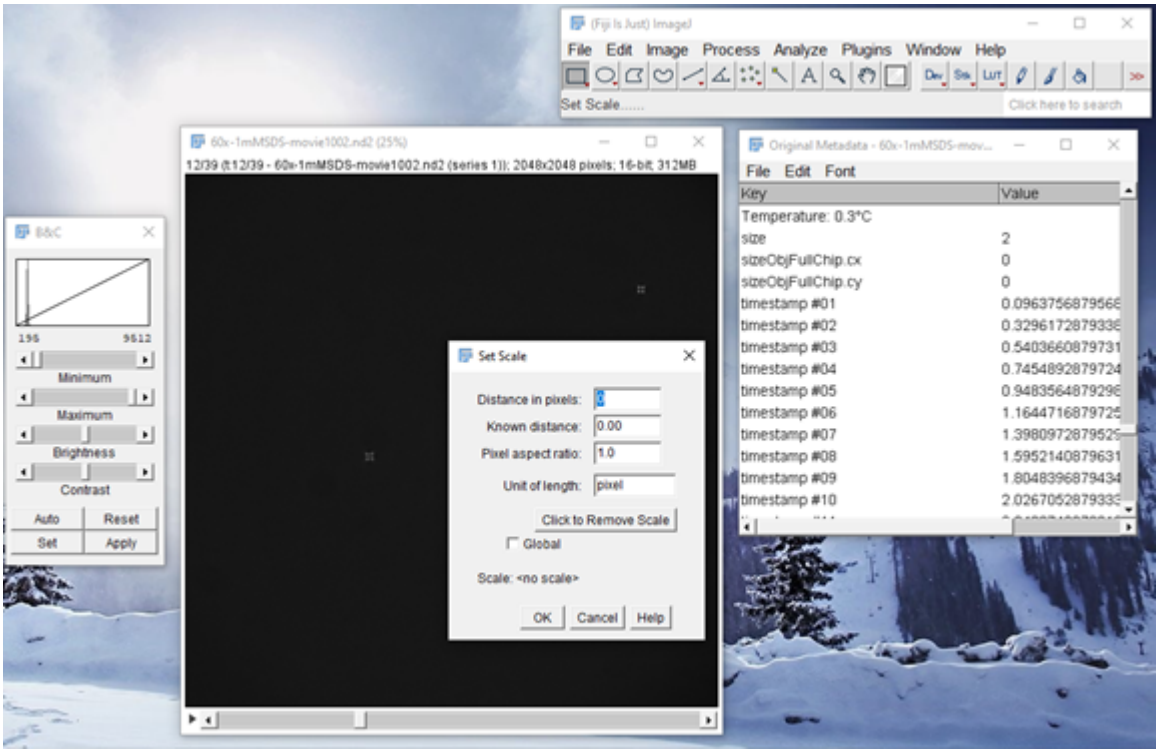

Figure E.9. Screen shot of Fiji toolbar (top right), the "B&C" window (left), the movie video (center), and metadata (right) as seen in figure E.7. Shows the "Set scale" window that opens after following the navigation path in figure E.8.

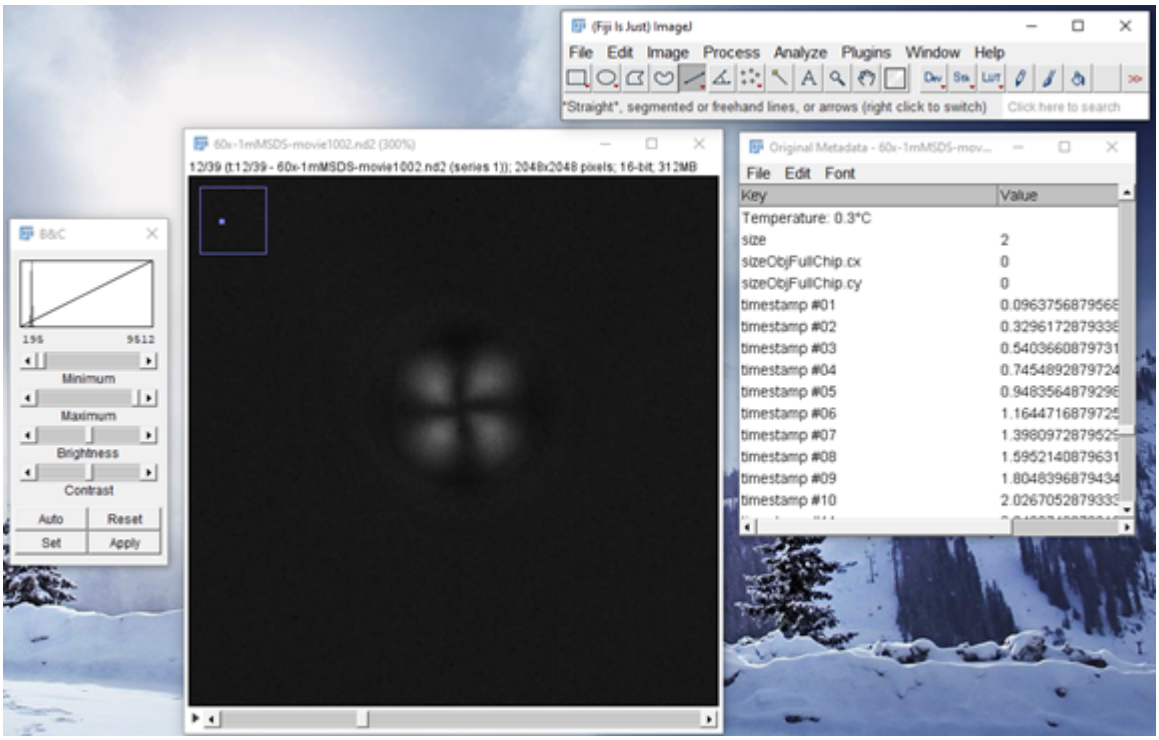

Figure E.10. Screen shot of Fiji toolbar (top right), the "B&C" window (left), the movie video (center), and metadata (right). Here, the movie has been zoomed in on a droplet and moved to a frame where it is in focus.

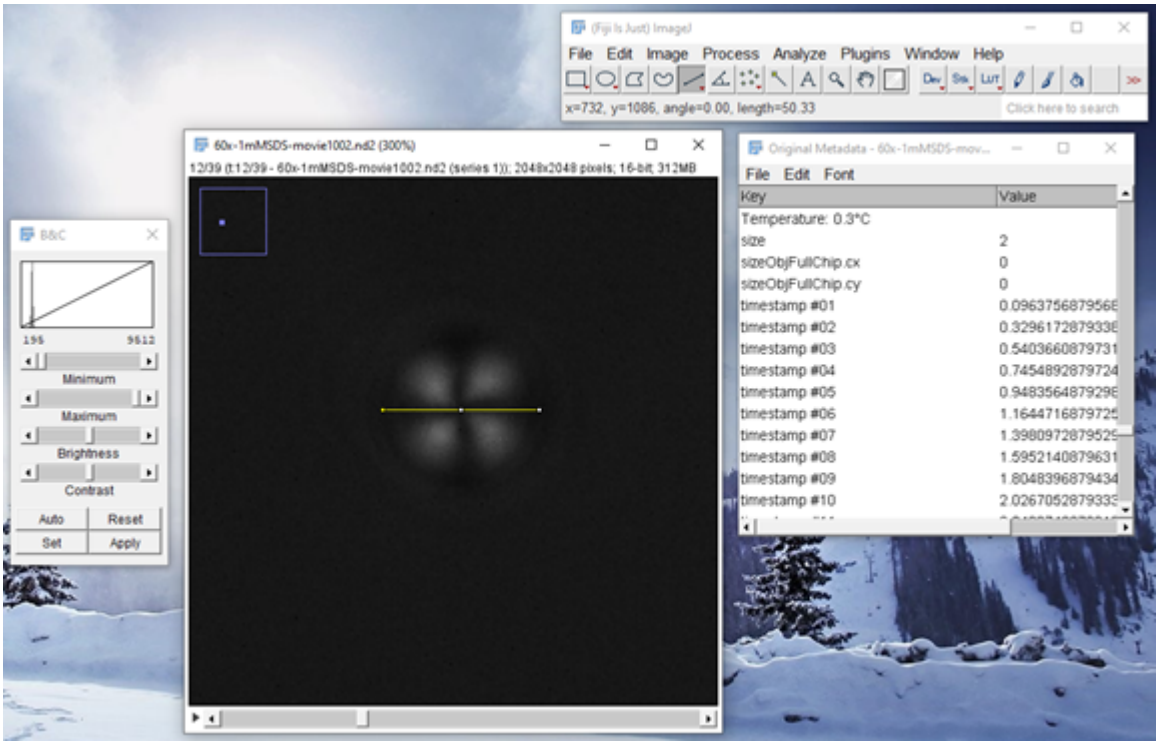

Figure E.11. Screen shot of Fiji toolbar (top right), the "B&C" window (left), the movie video (center), and metadata (right). Here, a horizontal line is drawn across the width of the diameter and measured to be 50.33 pixels.

Once the brightness/contrast has been adjusted and the scale of the movie set, you can begin making measurements! In figure E.10 I have zoomed in (using the "+" key on my keyboard or the magnifying glass tool and left click on mouse) on a droplet and played the movie until the droplet came into focus. As an exercise to the reader, identify the configuration of the droplet.

To measure the droplet's diameter I take two measurements and average them. I measure both the "width" of the droplet and the "height" of the droplet. If you hold down the "Shift" key while drawing a line (figure E.11) you can make one perfectly horizontal or vertical (figure E.12).

In this case I measured 50.33 with the horizontal line and 48.33 with the vertical line and would record 49 as the droplet diameter. These numbers appear in the Fiji main toolbar as the "length", referring to the length of the line drawn. I always recorded integer values for the diameter because I can't confidently measure 0.3 pixels.

To record the position of the droplet I put my mouse at the approximate center of the droplet and record the "x" and "y" values that appear on the Fiji toolbar. To record the frame that the droplet is in, we actually record the frame number from the movie's window and not the "z" value in the Fiji toolbar, which is 1 less than the number in the movie's window. The reason for this is that the very first frame of a

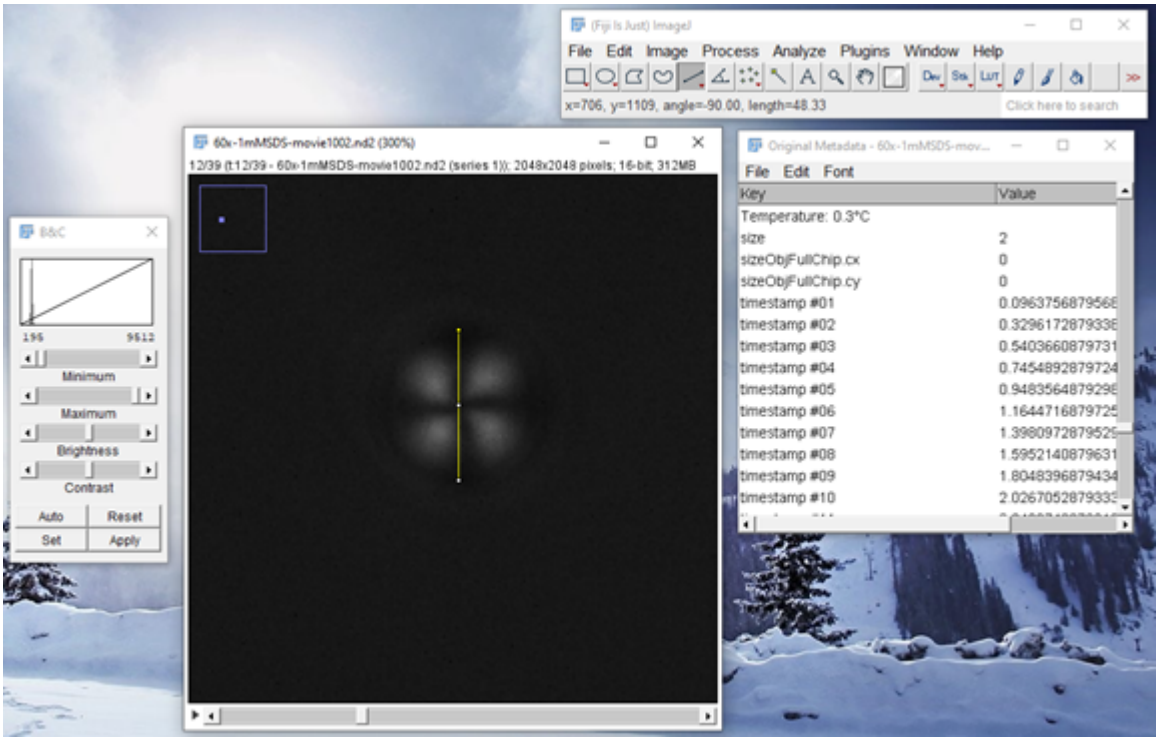

Figure E.12. Screen shot of Fiji toolbar (top right), the "B&C" window (left), the movie video (center), and metadata (right). Here, a vertical line is drawn across the width of the diameter and measured to be 48.33 pixels.

movie is z=0, but frame 1. If I wanted to open a single frame of a movie, using the technique of figure E.3, I would input 1 and 1 to open the first frame, not 0 and 0.

E.2 Measuring Transition Concentration

To figure out the concentration that a transition happens, we really need to find the *time* in the video it happens by finding the frame that the transition starts. Then we can use 4.1 and the other experimental parameters to calculate the surfactant concentration.

Recall the definitions of what I consider to be the transition. The bipolar to radial transition starts as soon as the ring defect appears, and ends when the defect finishes moving to the center of the droplet. Reversing these, we get the reverse transition. The radial to bipolar transition starts as soon as the defect in the center begins moving toward the edge of the droplet and ends with ring defect fully disappears.

These transitions aren't sharp, so there is some uncertainty in the measurement. The general strategy is to open the whole movie as a virtual stack with metadata (figure E.1) and find the approximate time range the transition happens. This has to be done twice, once for the start of the transition and once for the end of the transition. Since the process is symmetric with respect to start or end and also between bipolar to radial or radial to bipolar, I'll only explain in detail how one would do this for the start of a bipolar to radial transition.

First, find a frame where you're confident the ring hasn't formed yet, the droplet is definitely bipolar, and use this as your lower limit. Do the same and find a frame after the transition started where there is definitely a ring defect visible, this will be your upper limit. The goal is to make this difference in frames as small as possible and ultimately choose the middle value between the bounds. Ask yourself if the frame immediately after the lower limit or the frame immediately before the upper limit show the start or end of the transition. Iterate until you get to the narrowest frame range possible, ideally single digits.

BIBLIOGRAPHY

[1] 328510, Sigma-Aldrich. *5CB MSDS*, 2020 (accessed July 12, 2020).

[2] Armas-Pérez, J. C., Londono-Hurtado, A., Guzmán, O., Hernández-Ortiz, J. P., and de Pablo, J. J. Theoretically informed Monte Carlo simulation of liquid crystals by sampling of alignment-tensor fields. *Journal of Chemical Physics 143* (2015), 044107.

[3] Atzin, N., Guzmán, O., Gutiérrez, O., Hirst, L. S., and Ghosh, S. Free-energy model for nanoparticle self-assembly by liquid crystal sorting. *Physical Review E 97*, 6 (jun 2018), 062704.

[4] Barhoumi, Aoune, Liu, Qian, and Kohane, Daniel S. Ultraviolet light-mediated drug delivery: Principles, applications, and challenges. *Journal of Controlled Release 219* (2015), 31–42.

[5] Bogi, A., and Faetti, S. Elastic, dielectric and optical constants of 4'-pentyl-4-cyanobiphenyl. *Liquid Crystals 28*, 5 (2001), 729–739.

[6] Carlton, Rebecca J., Gupta, Jugal K., Swift, Candice L., and Abbott, Nicholas L. Influence of simple electrolytes on the orientational ordering of thermotropic liquid crystals at aqueous interfaces. *Langmuir 28*, 1 (2012), 31–36.

[7] Chaikin, P. M., and Lubensky, T. C. *Principles of Condensed Matter Physics*. Cambridge University Press, 1995.

[8] Curtis, Jennifer E, Koss, Brian A, and Grier, David G. Dynamic holographic optical tweezers. 169–175.

[9] Dark, M. L., Moore, M. H., Shenoy, D. K., and Shashidhar, R. Rotational viscosity and molecular structure of nematic liquid crystals. *Liquid Crystals 33*, 1 (2006), 67–73.

[10] de Gennes, P. G., and Prost, J. *The Physics of Liquid Crystals*. Clarendon Press, Oxford, 1993.

[11] Eimura, Hiroki, Miller, Daniel S., Wang, Xiaoguang, Abbott, Nicholas L., and Kato, Takashi. Self-Assembly of Bioconjugated Amphiphilic Mesogens Having Specific Binding Moieties at Aqueous-Liquid Crystal Interfaces. *Chemistry of Materials 28*, 4 (2016), 1170–1178.

[12] Fang, JP, and Joos, P. The dynamic surface tension of sds—dodecanol mixtures: 1. the submicellarsystems. *Colloids and surfaces 65*, 2-3 (1992), 113–120.

[13] Fournier, J. B., and Galatola, P. Modeling planar degenerate wetting and anchoring in nematic liquid crystals. *Europhysics Letters 72*, 3 (nov 2005), 403–409.

[14] Frank, F. C. Liquid crystals. On the theory of liquid crystals. *Discussions of the Faraday Society 25*, I (1958), 19.

[15] Frey, E, Nelson, D R, and Fisher, D S. Observation of a single - beam gradient force optical trap for dielectric particles. *Phys . Rev . B Phys . Rev . B Phys . Rev . E 43*, 179 (1991), 623–629.

[16] Ganta, Srinivas, Devalapally, Harikrishna, Shahiwala, Aliasgar, and Amiji, Mansoor. A review of stimuli-responsive nanocarriers for drug and gene delivery. *Journal of Controlled Release 126*, 3 (2008), 187–204.

[17] Gao, Jingjing, Liu, Xiaochi, Secinti, Hatice, Jiang, Ziwen, Munkhbat, Oyuntuya, Xu, Yisheng, Guo, Xuhong, and Thayumanavan, S. Photoactivation of Ligands for Extrinsically and Intrinsically Triggered Disassembly of Amphiphilic Nanoassemblies. *Chemistry - A European Journal 24*, 8 (2018), 1789–1794.

[18] Gelebart, Anne Helene, Jan Mulder, Dirk, Varga, Michael, Konya, Andrew, Vantomme, Ghislaine, Meijer, E. W., Selinger, Robin L.B., and Broer, Dirk J. Making waves in a photoactive polymer film. *Nature 546*, 7660 (2017), 632–636.

[19] Gupta, Jugal K, Sivakumar, Sri, Caruso, Frank, and Abbott, Nicholas L. Size-dependent ordering of liquid crystals observed in polymeric capsules with micrometer and smaller diameters. *Angewandte Chemie International Edition 48*, 9 (2009), 1652–1655.

[20] Gupta, Jugal K, Zimmerman, Jacob S, de Pablo, Juan J, Caruso, Frank, and Abbott, Nicholas L. Characterization of adsorbate-induced ordering transitions of liquid crystals within monodisperse droplets. *Langmuir 25*, 16 (2009), 9016–9024.

[21] Heppke, Gerd, and Moro, Dirk. Chiral order from achiral molecules. *Science 279*, 5358 (1998), 1872–1873.

[22] Hernández, J., Provenzano, C., Pagliusi, P., and Cipparrone, G. Optical manipulation of liquid crystal droplets through holographic polarized tweezers: Magnus effect. *Molecular Crystals and Liquid Crystals 558*, April 2014 (2012), 72–83.

[23] Jones, Richard A.L. Soft_Condensed_Matter_Jones_Oup_2002.Pdf, 2002.

[24] Kim, Young Ki, Raghupathi, Krishna R., Pendery, Joel S., Khomein, Piyachai, Sridhar, Uma, De Pablo, Juan J., Thayumanavan, S., and Abbott, Nicholas L. Oligomers as Triggers for Responsive Liquid Crystals. *Langmuir 34*, 34 (2018), 10092–10101.

[25] Kim, Young-Ki, Senyuk, Bohdan, and Lavrentovich, Oleg D. Molecular reorientation of a nematic liquid crystal by thermal expansion. *Nature Communications 3*, May (2012), 1133.

[26] Kim, Young Ki, Wang, Xiaoguang, Mondkar, Pranati, Bukusoglu, Emre, and Abbott, Nicholas L. Self-reporting and self-regulating liquid crystals. *Nature 557*, 7706 (2018), 539–544.

[27] Klaikherd, Akamol, Nagamani, Chikkannagari, and Thayumanavan, S. Multi-stimuli sensitive amphiphilic block copolymer assemblies. *Journal of the American Chemical Society 131*, 13 (2009), 4830–4838.

[28] Krishnamurthy, Vijay M, Kaufman, George K, Urbach, Adam R, Gitlin, Irina, Gudiksen, Katherine L, Weibel, Douglas B, and Whitesides, George M. Carbonic anhydrase as a model for biophysical and physical-organic studies of proteins and protein- ligand binding. *Chemical reviews 108*, 3 (2008), 946–1051.

[29] Kwon, Jung Yeon, Khan, Mashooq, and Park, Soo Young. PH-Responsive liquid crystal double emulsion droplets prepared using microfluidics. *RSC Advances 6*, 61 (2016), 55976–55983.

[30] Liu, Xiaochi, Hu, Ding, Jiang, Ziwen, Zhuang, Jiaming, Xu, Yisheng, Guo, Xuhong, and Thayumanavan, S. Multi-Stimuli-Responsive Amphiphilic Assemblies through Simple Postpolymerization Modifications. *Macromolecules 49*, 17 (2016), 6186–6192.

[31] Londoño-Hurtado, Alejandro, Armas-Pérez, Julio C, Hernández-Ortiz, Juan P, and de Pablo, Juan J. Homeotropic nano-particle assembly on degenerate planar nematic interfaces: films and droplets. *Soft matter 11*, 25 (2015), 5067–5076.

[32] Lopez-Leon, Teresa, and Fernandez-Nieves, Alberto. Drops and shells of liquid crystal. *Colloid and Polymer Science 289*, 4 (2011), 345–359.

[33] Manouras, Theodore, and Vamvakaki, Maria. Field responsive materials: Photo-, electro-, magnetic- and ultrasound-sensitive polymers. *Polymer Chemistry 8*, 1 (2017), 74–96.

[34] Miller, Daniel S, and Abbott, Nicholas L. Soft Matter crystalline droplets †. 374–382.

[35] Molla, Mijanur Rahaman, Rangadurai, Poornima, Pavan, Giovanni M., and Thayumanavan, S. Experimental and theoretical investigations in stimuli responsive dendrimer-based assemblies. *Nanoscale 7*, 9 (2015), 3817–3837.

[36] Mori, H., Gartland, E. C., Kelly, J. R., and Bos, P. J. Multidimensional Director Modeling Using the Q Tensor Representation in a Liquid Crystal Cell and Its Application to the π Cell with Patterned Electrodes. *Japanese Journal of Applied Physics 38*, 1 (1999), 135–146.

[37] Mura, Simona, Nicolas, Julien, and Couvreur, Patrick. Stimuli-responsive nanocarriers for drug delivery. *Nature Materials 12*, 11 (2013), 991–1003.

[38] Mysels, Karol J. Surface tension of solutions of pure sodium dodecyl sulfate. *Langmuir 2*, 4 (1986), 423–428.

[39] Price, Andrew D, and Schwartz, Daniel K. DNA Hybridization-Induced Reorientation of Liquid Crystal Anchoring at the Nematic Liquid Crystal / Aqueous Interface. 8188–8194.

[40] Prishchepa, OO, Shabanov, AV, and Zyryanov, V Ya. Director configurations in nematic droplets with inhomogeneous boundary conditions. *Physical Review E 72*, 3 (2005), 031712.

[41] Raghupathi, Krishna R., Sridhar, Uma, Byrne, Kevin, Raghupathi, Kishore, and Thayumanavan, S. Influence of backbone conformational rigidity in temperature-sensitive amphiphilic supramolecular assemblies. *Journal of the American Chemical Society 137*, 16 (2015), 5308–5311.

[42] Ramezani-dakhel, Authors Hadi, Rahimi, Mohammad, Pendery, Joel, and Kim, Young-ki. Title : Amphiphile Induced Phase Transition of Liquid Crystals at Aqueous Interfaces. 1–17.

[43] Rapini, A., and Papoular, M. Distorsion D'une lamelle nematique sous champ magnetique conditions d'ancrage aux parois. *Journal de Physique Colloques 30* (1969), C4–54–C4–56.

[44] Roy, Debashish, Cambre, Jennifer N., and Sumerlin, Brent S. Future perspectives and recent advances in stimuli-responsive materials. *Progress in Polymer Science (Oxford) 35*, 1-2 (2010), 278–301.

[45] Sagara, Yoshimitsu, and Kato, Takashi. Mechanically induced luminescence changes in molecular assemblies. *Nature Chemistry 1*, 8 (2009), 605–610.

[46] Selinger, Jonathan V. Interpretation of saddle-splay and the Oseen-Frank free energy in liquid crystals.

[47] Shechter, Jake, Atzin, Noe, Mozaffari, Ali, Zhang, Rui, Zhou, Ye, Strain, Benjamin, Oster, Linda M, De Pablo, Juan J, and Ross, Jennifer L. Direct observation of liquid crystal droplet configurational transitions using optical tweezers. *Langmuir* (2020).

[48] Stuart, Martien A.Cohen, Huck, Wilhelm T.S., Genzer, Jan, Müller, Marcus, Ober, Christopher, Stamm, Manfred, Sukhorukov, Gleb B., Szleifer, Igal, Tsukruk, Vladimir V., Urban, Marek, Winnik, Françoise, Zauscher, Stefan, Luzinov, Igor, and Minko, Sergiy. Emerging applications of stimuli-responsive polymer materials. *Nature Materials 9*, 2 (2010), 101–113.

[49] Takashima, Yoshinori, Hatanaka, Shogo, Otsubo, Miyuki, Nakahata, Masaki, Kakuta, Takahiro, Hashidzume, Akihito, Yamaguchi, Hiroyasu, and Harada, Akira. Expansion-contraction of photoresponsive artificial muscle regulated by host-guest interactions. *Nature Communications 3* (2012), 1270–1278.

[50] Tjipto, Elvira, Cadwell, Katie D, Quinn, John F, Johnston, Angus P R, Abbott, Nicholas L, and Caruso, Frank. Tailoring the Interfaces between Nematic Liquid Crystal Emulsions and Aqueous Phases via Layer-by-Layer Assembly.

[51] Tran, Lisa, Lavrentovich, Maxim O., Durey, Guillaume, Darmon, Alexandre, Haase, Martin F., Li, Ningwei, Lee, Daeyeon, Stebe, Kathleen J., Kamien, Randall D., and Lopez-Leon, Teresa. Change in stripes for cholesteric shells via anchoring in moderation. *Physical Review X 7*, 4 (2017), 1–14.

[52] Wang, Xiaoguang, Miller, Daniel S., Bukusoglu, Emre, de Pablo, Juan J., and Abbott, Nicholas L. Topological defects in liquid crystals as templates for molecular self-assembly. *Nature Materials 15*, 1 (2015), 106–112.

[53] Xia, Fan, and Jiang, Lei. Bio-inspired, smart, multiscale interfacial materials. *Advanced Materials 20*, 15 (2008), 2842–2858.

[54] Yamada, Munenori, Kondo, Mizuho, Mamiya, Jun Ichi, Yu, Yanlei, Kinoshita, Motoi, Barrett, Christopher J., and Ikeda, Tomiki. Photomobile polymer materials: Towards light-driven plastic motors. *Angewandte Chemie - International Edition 47*, 27 (2008), 4986–4988.

[55] Zhuang, Jiaming, Gordon, Mallory R., Ventura, Judy, Li, Longyu, and Thayumanavan, S. Multi-stimuli responsive macromolecules and their assemblies. *Chemical Society Reviews 42*, 17 (2013), 7421–7435.